MEASUREMENT OF FINNED-TUBE HEAT EXCHANGER PERFORMANCE

A Thesis
Presented to
The Academic Faculty

By

Creed Taylor

In Partial Fulfillment
of the Requirements for the Degree
Master of Science in Mechanical Engineering

Georgia Institute of Technology
December 2004

MEASUREMENT OF FINNED-TUBE HEAT EXCHANGER PERFORMANCE

Approved by:

Sam V. Shelton, Chairman

Sheldon M. Jeter

Srinivas Garimella

Date Approved: November 19th 2004

Dedicated to William E. Thompson

ACKNOWLEDGMENTS

Foremost, I would like to thank Dr. Shelton for the freedom and backing to learn how to think and research. He has been a mentor and an inspiration. His encouragement and support made this work possible. I especially appreciate the many opportunities that he has given me as well as his faith in my abilities.

I would also like to thank to my fellow graduate students for their support and friendship: Steven Tillery, Ramiro Rivera-Rivera, Laura Cole, Kirk Martin, and Logan McLeod. In particular, a special thanks to Susan Stewart whose constant encouragement and assistance has been invaluable.

I would like to thank my family, who have continually given me their love and encouraged me to reach my dreams. I could not have done this without you. I would also like to thank Staci who has been my constant sounding board and my biggest fan during the experimental and writing phases of this work.

Most importantly I would like to thank God. Thank you for all of these blessings.

TABLE OF CONTENTS

LIST OF TABLES

LIST OF FIGURES

NOMENCLATURE

Symbols

A	Area
a	Ratio of transverse tube spacing to tube diameter
A_{fin}	Surface area of the fins
A_i	Heat transfer area on the water side ($\pi D_i L_{tot}$)
A_{min}	Minimum free flow area
A_o	Total heat transfer area on the air side ($A_{fin}+A_t$)
A_t	Surface area of the tubes
B	Geometry parameter for hexagon
b	Ratio of longitudinal tube spacing to tube diameter
C	The inverse of the modified Wilson plot slope
C_z	Average row correction factor
c_z	Individual row correction factor
C_r	Ratio of heat capacities rates ($C_{\min}/C_{\max}$)
c_p	Specific heat at constant pressure
C_{max}	Maximum heat capacity rate
C_{min}	Minimum heat capacity rate
D	Diameter
D_c	Collar diameter (D_o+2t_{fin})
D_h	Hydraulic diameter ($4A_{min}D_{depc}/A_o$)
$D_{h.W}$	Hydraulic diameter for Wang 1999b ($4A_{min}/L$)

D_i	Inside tube diameter
DP	Pressure drop [inH_2O]
Eu	Euler number
Eu_{cor}	Corrected Euler number
$F1$-$F3$	Plain fin correlation parameters (Wang)
$F5$-$F9$	Louvered fin correlation parameters (Wang)
f	Fanning friction factor
FP	F.C. McQuiston Fanning friction factor correlation parameter
F_p	Fin pitch (C.C. Wang) [mm]
F_s	Fin spacing (present study) [fpi]
G_{max}	Mass velocity through minimum air flow area
H	Geometry parameter for hexagon
h_c	Contact conductance heat transfer coefficient
h_i	Water-side average convective heat transfer coefficient
h_o	Air-side average convective heat transfer coefficient
$J5$-$J8$	Louvered fin correlation parameters (Wang)
j	Colburn j-factor ($StPr^{2/3}$)
j_4	j-factor for 4 row coil
j_n	j-factor for fewer than 4 rows (n = number of rows)
JP	F.C. McQuiston Colburn j factor correlation parameter
k	Thermal conductivity
k_1	Staggered array geometry factor
k_c	Contraction coefficient for row inlet

k_e	Expansion coefficient for row exit
L_h	Louver height
L_p	Louver pitch
$\dot{m}$	Mass flow rate [lbm/hr]
M	Number of data points
m	standard extended surface parameter
N	Number of tube rows (R.L. Webb & Grey, C.C. Wang)
N_f	Fin Spacing (D.G. Rich) [fpi]
ncirc	Number of parallel refrigerant flow circuits
N_r	Number of tube rows (F.C. McQuiston)
N_{row}	Number of tube rows (present study, R.L. Webb & Kang)
NTU	Number of transfer units
Nu	Nusselt number
P	Pressure
P3-P6	Plain fin correlation parameters (Wang)
P_f	Fin Pitch (R.L. Webb & Kang) [m]
P_{hex}	Perimeter of hexagon
P_l	Longitudinal Tube Spacing (C.C. Wang) [mm]
P_l	Longitudinal Tube Spacing (R.L. Webb & Kang) [m]
P_s	Fin Spacing (F.C. McQuiston) [fpf]
P_t	Transverse Tube Spacing (C.C. Wang) [mm]
P_t	Transverse Tube Spacing (R.L. Webb & Kang) [m]
ΔP	Pressure drop

Pr	Prandtl Number (ν/α)
q_{cst}	Euler number inverse power series coefficient
$\dot{Q}$	Heat transfer rate
R	Radius of a circular fin
r_{cst}	Euler number inverse power series coefficient
r_t	Outside tube radius
R_e	Equivalent circular fin radius
R^*	Hydraulic Fin Radius
Re	Reynolds number
$\mathrm{Re}_{\mathrm{Dc}}$	Reynolds number based on collar diameter
$\mathrm{Re}_{\mathrm{Di}}$	Reynolds number based on inside tube diameter
$\mathrm{Re}_{\mathrm{Do}}$	Reynolds number based on outside tube diameter
Re_l	Reynolds number based on longitudinal tube spacing, X_l
Re_{ls}	Reynolds number based on louver strip length or louver pitch, L_p
R_a	Air side Thermal Resistance
$R_{c,cond}$	Contact Conduction Thermal Resistance
R_o	Overall Thermal Resistance
$R_{t,cond}$	Tube Conduction Thermal Resistance
R_w	Water side Thermal Resistance
s	Fin Pitch (R.L. Webb & Grey) [m]
s_{cst}	Euler number inverse power series coefficient
S_{l}	Longitudinal Tube Spacing (R.L. Webb & Grey) [m]
S_{t}	Transverse Tube Spacing (R.L. Webb & Grey) [m]

St	Stanton Number (Nu/RePr)
T	Temperature [°F]
t_{cst}	Euler number inverse power series coefficient
ΔT	Temperature Difference
ΔT_{lm}	Log Mean Temperature Difference
t	Fin thickness (present study) [in]
t	Fin thickness (R.L. Webb & Gray, R.L. Webb & Kang) [m]
$\overline{t}_{m,w}$	Mean Water Temperature
tpr	Tubes per row
tprc	Tubes per row in a circuit
TR UA	Ten minute Trailing Average *UA*
u_{cst}	Euler number inverse power series coefficient
UA	Overall heat transfer coefficient
V	Air velocity through the minimum free flow area
V_i	Water velocity through one tube
X	Wilson abscissa $\left(\frac{1}{A_i}\right)\left(\frac{D_i^{0.2}}{\left(1+.001\cdot\overline{t}_w\right)V_w^{0.8}}\right)$
X_{diag}	Diagonal spacing between tubes (present study) [in]
X_a	Transverse tube spacing (F.C. McQuiston) [ft]
X_b	Longitudinal tube spacing (F.C. McQuiston) [ft]
X_l	Longitudinal tube spacing (present study) [in]
X_t	Transverse tube spacing (present study) [in]
y	Fin Thickness (F.C. McQuiston) [ft]

z	Number of Tube Rows (present study)
z_n	Geometry parameters of hexagon (n = 1,2,3,4)

Greek Characters

δ_t	Tube thickness
δ_f	Fin thickness (C.C. Wang) [mm]
ρ	Density
μ	Dynamic viscosity
η_{fin}	Circular fin efficiency
η_o	Fin surface efficiency
ε	Heat exchanger effectiveness
ϕ	Fin efficiency parameter for a circular fin
σ	Ratio of frontal to minimum free flow areas

Subscripts

1	Inlet
2	Outlet
4	4-row (McQuiston)
A	Air
air	Air
avg	Average
c	Cold fluid
c,i	Cold fluid inlet
c,o	Cold fluid outlet
exp	Experimental data

fin	Fin
h	Hot fluid
h,i	Hot fluid inlet
h,o	Hot fluid outlet
lou	Louver
Ls	Louver strip length, or louver pitch
m	McQuiston
n	n-row (McQuiston)
r	Rich
tot	Total
tub	Tube
water	Water
wg	Webb & Grey
wk	Webb & Kang
wl	Wang (louvered fin)
wl,m	Modified Wang (louvered fin)
wp	Wang (plain fin)
wp,m	Modified Wang (plain fin)

SUMMARY

Finned-tube heat exchangers are predominantly used in space conditioning systems, as well as other applications requiring heat exchange between two fluids. One important widespread use is in residential air conditioning systems. These residential cooling systems influence the peak demand on the U.S. national electrical system, which occurs on the hot summer afternoons, and thereby sets the requirement for the expensive infrastructure requirement of the nation's power plant and electrical distribution system. In addition to this peak demand, these residential air conditioners are major energy users that dominate residential electrical costs and environmental impact.

The design of finned-tube condenser coils, (heat exchangers), requires the selection of over a dozen design parameters by the designer. The refrigerant side flow and heat transfer characteristics inside the tubes depend mostly on the tube diameter design parameter and have been thoroughly studied. However, the air side flow around the tube bundle and through the fin gaps is much more complex and depends on over a dozen design parameters. Therefore, experimental measurement of the air side performance is needed. Because of the complex nature of the flow and the number of possible heat exchanger designs the air side performance has not been addressed in a comprehensive manner.

First this study built an experimental system and developed methodology for measuring the air side heat transfer and pressure drop characteristics of fin tube heat exchangers. This capability was then used to continue the goal of expanding and clarifying the present knowledge and understanding of air side performance to enable the air conditioner system designer in verifying an optimum fin tube condenser design.

In this study eight fin tube heat exchangers were tested over an air flow face velocity range of 5 – 12 ft/s (675-1600cfm). The raw data were reduced to the desired heat transfer and friction data, *j* and *f* factors. This reduced heat transfer and friction data was plotted versus Reynolds number and compared. The effect of fin spacing, the number of rows and fin enhancement were all investigated.

The following Colburn *j* factor trends were noted: 1) the *j* factor for 4-row coils was generally lower than the *j* factor for 2-row coils at low Reynolds number (with all other parameters being equal), and the *j* factor for 2-row coils was linear when plotted on a log-log scale versus Reynolds number while that from 4-row coils was non-linear, 2) the *j* factor for 2-row coils shows no dependence on fin spacing, while the *j* factor for 4-row coils shows an increase in the heat transfer coefficient for an increase in the number of fins per inch, 3) the *j* factor for a louvered coil was 1.75 times higher than the *j* factor for a plain coil (with all other parameters being equal).

The following friction factor trends were noted: 1) the friction factor for a 4-row 21fpi coil was significantly higher than the friction factor for a 4-row 12fpi coil at low Reynolds number (with all other parameters being equal), 2) the friction factor for a louvered coil was 1.7 – 2.2 times higher than the friction factor for a plain coil, with all other parameters being equal.

The heat transfer and friction data were also plotted and compared with various correlations available from open literature. The overall accuracy of each correlation to predict experimental data was calculated. Correlations by C.C. Wang (1998b, 1999) showed the best agreement with the data. A notable difference in the friction data - the present study's data are higher than any of the correlations investigated – it is

hypothesized to be due to the fact that all of the coils tested had a rippled fin edge, whereas none of the coils used to develop the investigated correlations had this ripple. At present, this geometric difference has an unknown effect on the experimental data. Wang's correlations (1998b, 1999) were modified to fit the current study's data.

CHAPTER I

INTRODUCTION

I.A: Background

Fin-tube heat exchangers are essential components in residential heat pump and air-conditioning systems. These systems are thermodynamically modeled as the vapor compression refrigeration cycle, shown in Figure 1.1. The working fluid used in these systems is most commonly a synthetic refrigerant.

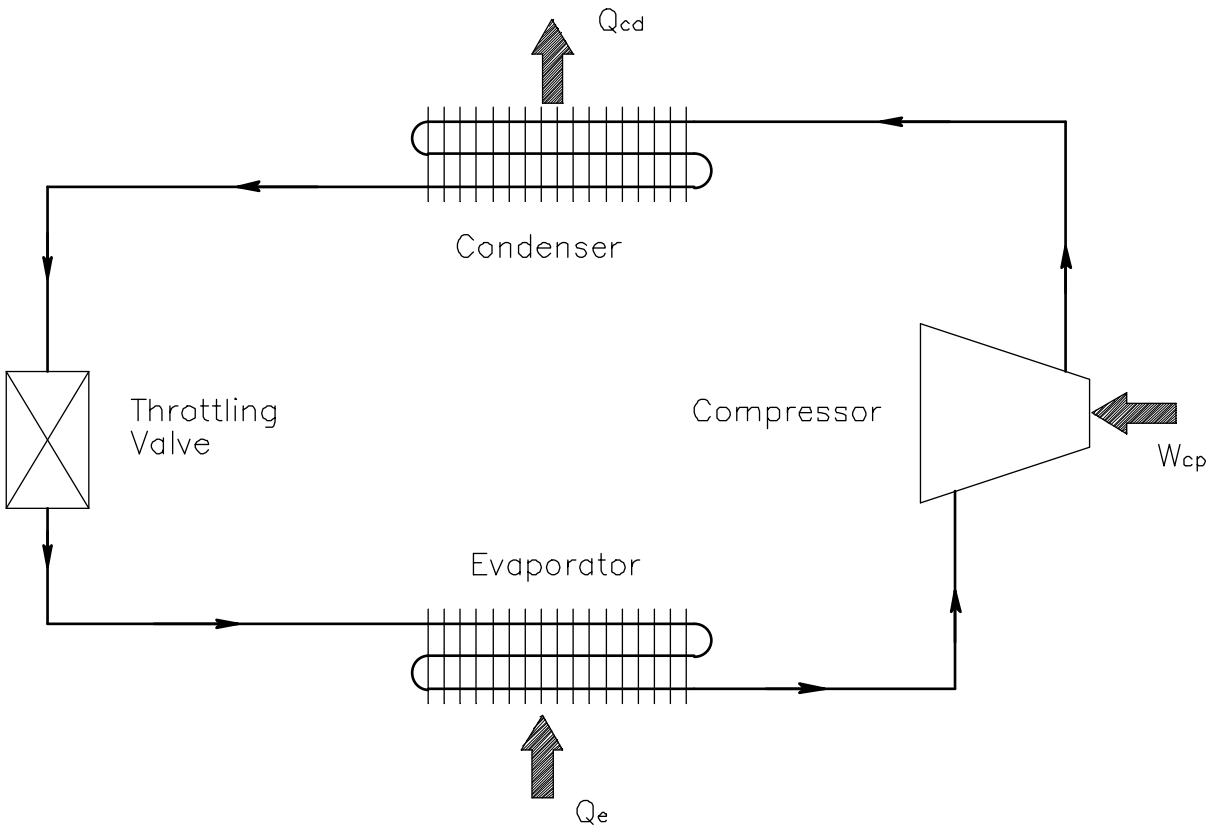

Figure 1.1. Vapor Compression Cycle

Figure 1.2 shows a typical outdoor condensing unit for a residential air-conditioning system. This package includes the compressor, the condenser and the throttling valve. The evaporator is located inside the residence. Typically the condenser occupies three of the four sides of a condensing unit. Air is pulled through the condenser by a fan mounted at the top of the condensing unit.

Figure 1.2. A Typical Outdoor Air-Conditioning System Condensing Unit

Finned-tube heat exchangers, or coils, consist of mechanically or hydraulically expanded round tubes in a block of parallel continuous fins. An example is shown in Figure 1.3. Fin-tube heat exchangers are designed for maximum heat transfer between two fluids with a minimum pressure drop associated with each fluid. In this study the working fluid is water instead of refrigerant. There are several practical reasons for this

decision: the air-side performance is the subject of this study not the refrigerant-side, the use of refrigerant would have been expensive and would have resulted in lengthy procedures for the common task of changing coils. Hereafter inside the tubes or the refrigerant side will be referred to as the water side.

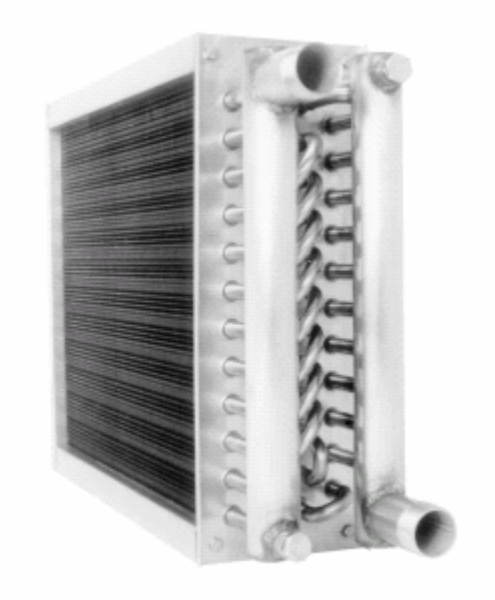

Figure 1.3. Heat exchanger

The design of finned-tube heat exchangers requires specification of more than a dozen parameters, including but not limited to the following: transverse tube spacing, longitudinal tube spacing, tube diameter, number of tube rows, fin spacing, fin thickness, and fin type (plain or enhanced). A schematic of a 4-row coil, along with some of the nomenclature used in this study is shown in Figure 1.4. The broken lines indicate the separation of parallel flow paths on the water-side, herein called circuits. Circuiting is another important specification that will affect performance of a finned-tube heat exchanger.

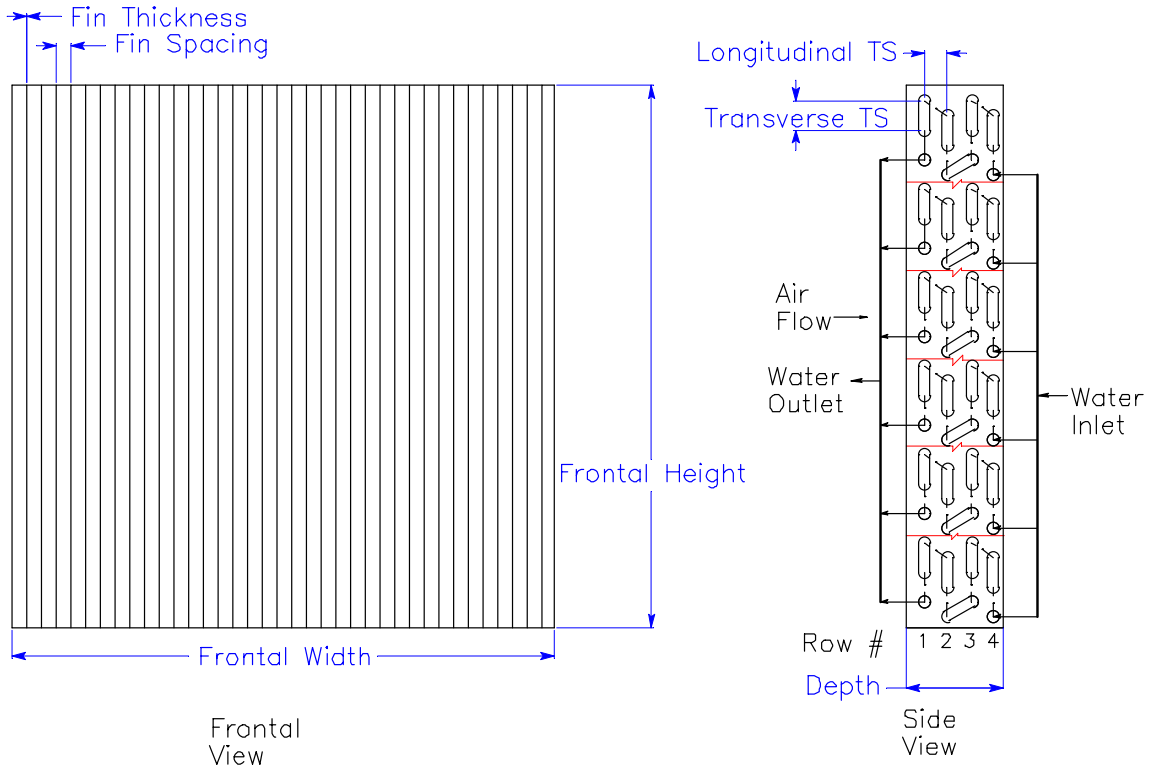

Figure 1.4. Schematic of a 4-row coil

The coils in this study have flat fins with a rippled edge at the air entrance and exit. Figure 1.5 shows an enlarged cutaway view of a 4-row coil, including the ripples. The air flow direction is indicated along with the row numbers for reference.

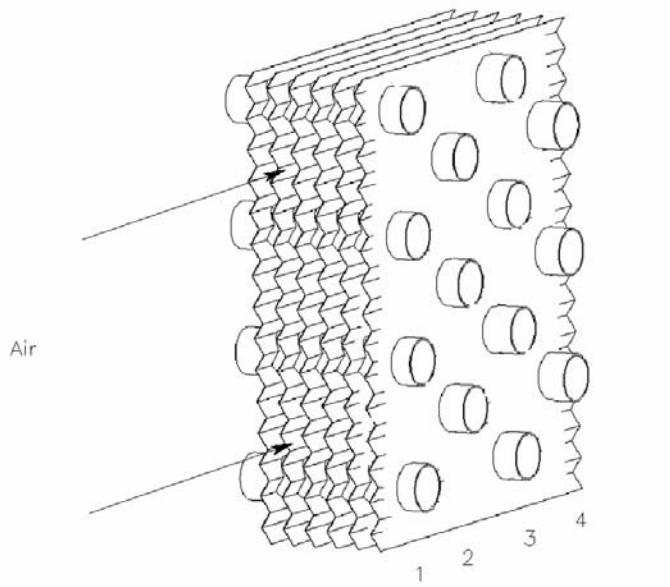

Figure 1.5. An enlarged cutaway view of a plain 4-row coil

The addition of louvers adds another level of sophistication to the design of a finned-tube heat exchanger. A schematic of the louvers in this study along with pertinent nomenclature are shown for a 2-row coil in Figure 1.6. Section B-B shows two fins in the air flow direction. Louver height and major louver pitch are important defining parameters used in this study.

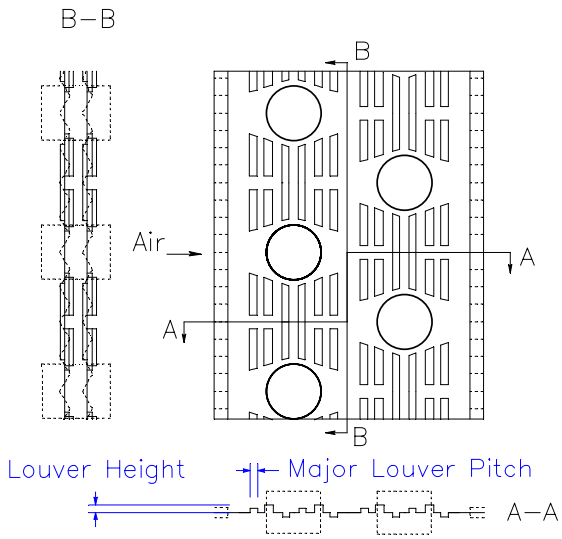

Figure 1.6: Louvered fin geometry in the present work

I.B: Motivation

Finned-tube heat exchangers are common and vital components in many energy systems. One primary application affecting a large fraction of U.S. peak electrical power usage is residential air conditioning outdoor refrigerant-to-air condensers. According to the Annual Energy Outlook 2004 (AEO2004) report by the Energy Information Administration (EIA), a part of the U.S. Department of Energy, residential electricity consumption is expected to grow at a rate of 1.4% over the next 20 years. Residential demand varies by season, day and time of day. The EIA further states that: "Driven by summer peaks, the periodicity of residential demand increases the peak-to-average load ratio for load-serving entities, which must rely on quick-starting turbines or internal combustion units to meet peak demand." With CO_2, NO_X, and particulate emissions directly tied to energy production and use, the need for further HVAC equipment efficiency improvements will continue to grow in the coming decades. Heat exchangers have the largest margin for improvement of all of the components of a residential central

air conditioner. C.C. Wang (2000a), states that for typical applications of air-cooled heat exchangers, the air-side resistance is generally the controlling total thermal resistance. In recognition of the need for continual efficiency improvement, the federal efficiency standard for residential central air conditioners will be increased from SEER 10 to SEER 13, where SEER stands for Seasonal Energy Efficiency Ratio. This change will be put in effect in January 2006. The current federal efficiency standard is SEER 10 and was put in effect in 1992. Under the new standard, energy use by new air conditioners will be reduced by 23% relative to the current standard. According to an ACEEE (American Council for an Energy-Efficient Economy) analysis, this will reduce the peak demand for electric power by 41,500 Megawatts by 2020 (equivalent to 138 typical new power plants of 300 MW each) and save consumers approximately $5 billion over the 2006-2030 period. It will also reduce air pollutant and greenhouse gas emissions, saving 7.2 million metric tons of carbon in 2020, which is equivalent to taking more than 3 million vehicles off the road.

Due to the complex nature of the air flow between the fins and over the tubes, design optimization of finned-tube heat exchangers requires experimental correlations of airside heat transfer and pressure drop characteristics. This design optimization is characterized by a trade off between heat transfer and pressure drop, which is evident for both plain and louvered fin tube heat exchangers. While some experimental data is available for finned tube heat exchangers of interest in air conditioning condensers, the data covers a very limited range of design parameters. This prevents considering heat exchanger designs outside the limited range of the data correlations. As is typically the case, optimization analysis has shown optimum designs to lie on the bounds of the

existing data. Stewart (2003) performed a design optimization, maximizing overall system efficiency for a fixed cost and frontal area, of an enhanced finned-tube condenser. Her conclusions were that the design optimum for a given optimization was often limited by the bounds of the correlations used. This present study is a necessary step to validate the testing procedures on several typical coils so that future data can be used to develop correlations with a wider range of defining parameters and also to experimentally confirm numerical design optimizations.

This experimental study tested eight heat exchangers, whose defining parameters have been systematically varied to facilitate comparison. The heat transfer and friction characteristics are presented in the form of Colburn j and Fanning friction factors. The details of the experimental methods and data reduction are given. The dependence of heat transfer and friction on the number of rows, fin spacing and fin enhancement were investigated. Also, several correlations were compared with experimental data. The experiments demonstrate the complex behavior of air side heat transfer and friction characteristics of fin tube heat exchangers. There is need for further study to widen the parametric range and improve the accuracy of correlations as well as to develop more robust/ effective fin enhancements.

CHAPTER II

LITERATURE REVIEW

Finned-tube heat exchangers are common devices; however, their performance characteristics are complicated. As previously mentioned this study focuses on the air-side performance of fin tube heat exchangers. The working fluid was chosen to be water to reduce the cost and time to change coils. The water side heat transfer and pressure drop behavior inside the tubes is well established and fairly straight forward. In contrast, the air side heat transfer and pressure drop behavior is the subject of countless research studies and is quite complicated. Designers must rely on experimental measurement of these characteristics. Often, air side performance is proprietary. Finned-tube heat exchangers have been tested for at least the last 90 years (Wilson 1915). During that time, advances in technology as well as the efforts of many research engineers has increased the knowledge and availability of air side performance data. The endeavors of D.G. Rich (1973, 1975), F.C. McQuiston (1978, 1981), R.L. Webb (1986, 1998), and C.C. Wang (1998a, 1998b, 1998c, 1999, 2000a, 200b) serve as milestones in the road of experimental performance measurement and correlation of the air-side performance. This literature review will address a number of experimental studies, experimental correlations, and data reduction publications which focused on the airside performance of fin tube heat exchangers.

There is a wealth of heat transfer coefficient and friction factor data for finned-tube heat exchangers, which is often presented in correlation equation form. However, there are also an infinite number of configurations for heat exchangers: e.g. transverse

tube spacing, longitudinal tube spacing, tube diameter, number of tube rows, fin spacing, fin thickness, and fins type (plain, louvered, or other enhancement), to name a just few defining parameters. To further confuse the matter, experimental techniques and methods of data reduction vary from one experimenter to the next. For instance, the equilibrium criteria or the appropriate ε-*NTU* relationship for the given geometry are not standardized. Also, nomenclature is not standardized and definitions for some parameters are not readily available. Table 2.1 summarizes and compares the different nomenclatures used by other researchers with those used in the present study. Although this information is included in the nomenclature section on page vii, that format is cumbersome to use for an in depth discussion.

Table 2.1. Nomenclature Summary

	Present Study		Rich		McQuiston		Webb and Grey		Webb and Kang		Wang	
Fin Spacing	F_s	[fpi]	N_f	[fpi]	P_s	[fpf]						
Fin Pitch							s	[m]	P_f	[m]	F_p	[mm]
Fin Thickness	t	[in]		[in]	y	[ft]	t	[m]	t	[m]	δ_f	[mm]
Longitudinal Tube Spacing	X_l	[in]		[in]	X_b	[ft]	S_l	[m]	P_l	[m]	P_l	[mm]
Transverse Tube Spacing	X_t	[in]		[in]	X_a	[ft]	S_t	[m]	P_t	[m]	P_t	[mm]
Number of Tube Rows	N_{row}, z	[-]		[-]	N_r	[-]	N	[-]	N_{row}	[-]	N	[-]

II.A: Experimental Heat Exchanger Studies

Wilson (1915) performed an experimental work in which he developed a graphical method of calculating the water-side heat transfer coefficient as a function of water velocity. This method was included in McAdams (1954); it was also incorporated in the study by Rich (1973). A modified form of Wilson's graphical method was used in this present study.

Rich published two experimental studies. The first (1973) study focused on the effect of fin spacing on heat transfer and friction performance of four-row finned-tube heat exchangers, is discussed in section B because it contains heat transfer coefficient and friction factor correlations. The second (1975) study focused on the effect of the number of tube rows on heat transfer performance of heat exchangers, was a continuation of his previous experimental work. In it Rich tested six coils which were geometrically identical to his previous research with two exceptions: the number of tube rows was varied from 1 to 6 and all of the coils had a fin pitch of 14.5 fins/in. The coils were labeled on the basis of the number of tube rows. The tube diameter was 0.525 in. after expansion. The data trends are shown in Figure 2.1. Rich also performed a separate test on the four row coil, measuring the temperature of the inlet and outlet of each row. The circuiting for this test was such that the tubes of each row were connected to form a separate circuit. This allowed Rich to calculate the heat transfer coefficient for each row. Data trends are shown in Figure 2.2. Rich concluded the following:

1. The average heat transfer coefficient for a deep coil can be higher or lower than that of a shallow coil, depending on Reynolds number. Similarly the heat transfer coefficients for a down stream row can be higher or lower than for an upstream row depending on Reynolds number.
2. The addition of downstream rows has a negligible effect on heat transfer from upstream rows.
3. At high Reynolds number, heat transfer coefficients of downstream rows are higher than those of upstream rows; similarly average coefficients for deep coils are higher than for shallow coils, at high Reynolds number.

4. At low Reynolds number, heat transfer coefficients for deep coils are significantly lower than for shallow coils.

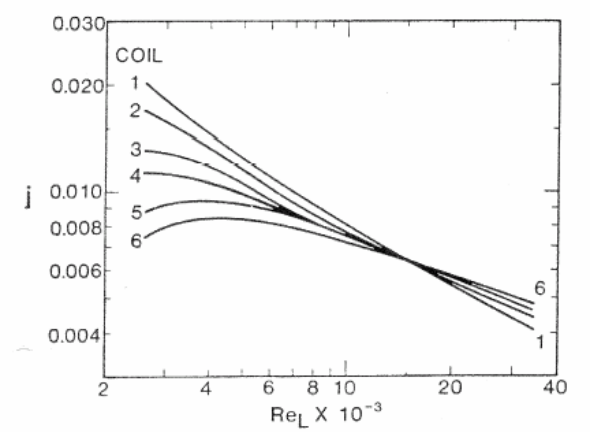

Figure 2.1. Effect of number of rows on the overall *j* factor (Rich 1975)

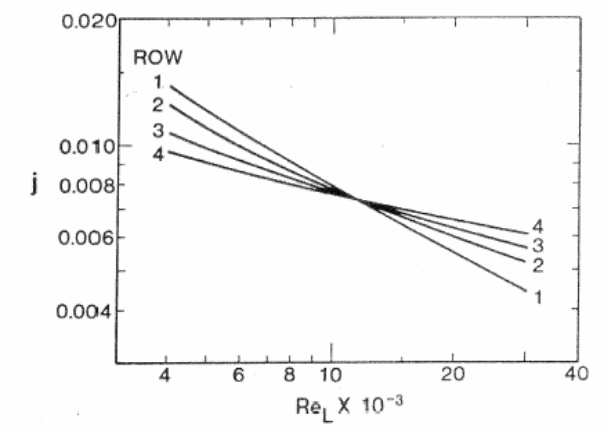

Figure 2.2. Effect of number of rows on the local *j* factor (Rich 1975)

Wang et al. (1998c) performed a comparison study of eight finned-tube heat exchangers. Table 2.2 shows the systematic variation of parameters that define the heat exchangers studied. This study is similar to the variation of parameters in the present study. The louver height and major louver pitch are not known. Wang et al. concluded

that the effect of fin pitch on heat transfer performance is negligible for four-row coils having Re_{Dc} > 1,000 and that for Re_{Dc} < 1,000 heat transfer performance is highly dependent on fin pitch. The upper Reynolds number range result is supported by experimental data from Rich (1973), and from several studies performed by Wang et al. Wang et al. also concluded that the heat transfer performance of two-row configuration increases with decrease of fin pitch. This publication discusses the choice of minimum equilibrium criterion used as well as the method of data reduction. The minimum equilibrium criterion chosen by Wang states that the heat transfer rate as calculated from the tube-side and from the air-side should be within 3%, and that the tube-side resistance (evaluated as $\frac{1}{h_i A_i}$) was less than 15% of the overall thermal resistance in all cases. The data reduction methods include: the use of the unmixed-unmixed cross-flow ε-NTU relationship, the incorporation of the contact resistance (which was stated to be less than 4%) into the air-side resistance, and the inclusion of entrance and exit pressure losses in the calculation of friction factor.

Table 2.2. Wang (1998c): Parametric Range

No	Fin Pattern	Fin Pitch (mm) [fins/in]	Nominal Tube OD (mm) [in]	P_t (mm) [in]	P_l (mm) [in]	Number of Rows
1	Plain	1.78 [14.26]	7.0 [0.273]	21 [0.826]	12.7 [0.5]	2
2	Plain	1.22 [20.8]	7.0 [0.273]	21 [0.826]	12.7 [0.5]	2
3	Plain	1.78 [14.26]	7.0 [0.273]	21 [0.826]	12.7 [0.5]	4
4	Plain	1.22 [20.8]	7.0 [0.273]	21 [0.826]	12.7 [0.5]	4
5	Louver	1.78 [14.26]	7.0 [0.273]	21 [0.826]	12.7 [0.5]	2
6	Louver	1.22 [20.8]	7.0 [0.273]	21 [0.826]	12.7 [0.5]	2
7	Louver	1.78 [14.26]	7.0 [0.273]	21 [0.826]	12.7 [0.5]	4
8	Louver	1.22 [20.8]	7.0 [0.273]	21 [0.826]	12.7 [0.5]	4

II.B: Experimental Heat Exchanger Correlations

Rich (1973) performed experimental work to determine the effect of fin spacing on heat transfer and friction performance of multi-row fin-and-tube heat exchangers. Except for the fin spacing all of the physical dimensions of the nine coils tested were identical. Each coil had 4 rows of staggered tubes in the air flow direction. The tube diameter was 0.525 in. after expansion. The fin spacing varied from 0 to 20.6 fins per inch. Rich developed a correlation for both heat transfer coefficient and friction factor using row spacing as a basis for the Reynolds number. It should be noted that Rich's correlations are only valid for his geometry: there is only one tube spacing configuration and one tube diameter. Rich concluded the following:

1. The heat transfer coefficient is essentially independent of fin spacing between 3-21 fins per inch at a given mass velocity.
2. The pressure drop can be broken into two additive components, one due to the tubes, form drag, and one due to the fins, skin drag.
3. The friction factor for the fins is independent of fin spacing for 3-14 fins per inch at a given mass velocity.
4. For fin spacing of less than 14 fins per inch the friction factor for the fins varies similar to that of developing flow over a plate where the boundary layer is retriggered at each tube row rather than flow in a channel with fully developed flow over the length of the coil width.

Zukauskas and Ulinskas (1998) developed correlations for the pressure drop of a staggered bank of bare tubes (no fins) in cross flow. These correlations give pressure

drop as a function of geometry over a range of Reynolds numbers. Geometric parameters included in the analysis are: tube diameter, transverse tube spacing, longitudinal tube spacing, and number of tube rows. Zukauskas and Ulinskas discuss several possible variations that influence the pressure drop, including:

1. Wall to bulk viscosity.
2. Property variations through the bank of tubes.
3. Acceleration pressure drop arising from temperature rise.

McQuiston (1979) developed correlations for both Colburn *j* and Fanning friction factors based on several sources of data. McQuiston's goal was to make correlations for wet-surface mass transport. In order to do this, he first correlated dry surface sensible heat transfer and friction data, which are the correlations investigated in this present study. The *j* factors were correlated within ± 10% while the *f* factors were correlated within ± 35%. The parametric range of McQuiston's correlation is shown in Table 2.3. The application of this correlation to compare with the coils in the present study stretches the limits of the correlation; the tube spacing in the present study is 0.77 in. in the flow direction, compared to the 1 - 1.5 in. parametric range. All other parameters are within their respective ranges.

Table 2.3. McQuiston (1979) Plain Fin Correlations: Parametric Range

Fin Pattern	Plain
Number of Rows	1 - 4
Diameter OD (ft) [in]	0.031 - 0.052 [0.375 - 0.625]
Fin Pitch (fins/ft) [fins/in]	96 - 168 [8 - 14]
Tube Spacing (ft) [in]	0.083 - 0.125 [1 - 1.5]

Webb and Gray (1986) developed heat transfer coefficient and fin friction factor correlations based on their own experimental data as well as other sources. Data from 16 heat exchanger configurations were used to develop the heat transfer coefficient correlation; the resulting RMS error is 7.3%. Similarly, data from 18 heat exchanger configurations were used to develop the fin friction factor correlation; the resulting RMS error is 7.8%. A multiple regression technique was used with inputs being geometric quantities: transverse tube spacing, longitudinal tube spacing, tube diameter, number of tube rows, and fin spacing. Entrance and exit pressure drops were not included in the fin friction factor. The parametric range of Webb and Grey's correlation is shown in Table 2.4. The application of this correlation to compare with the coils in the present study stretches the limits of this correlation; the S_t/D parameter is 2.63 in the present study compared to the applicable 1.97 – 2.55 range. All other parameters are within their respective ranges.

Table 2.4. Webb (1986) Plain Fin Correlations: Parametric Range

Fin Pattern	Plain
Number of Rows	1 - 8
S_t/D	1.97 - 2.55
S_l/D	1.7 - 2.58
s/D	0.08 - 0.64

Wang et al. (1999) performed a correlation for plain fin geometry based on several sources of experimental data. Data from a total of 74 coil configurations were used to develop the correlation. The heat transfer correlation can correlate 88.6% of the database within ±15%, and the friction correlation can correlate 85.1% of the database

within ±15%. The parametric range of Wang's correlation is shown in Table 2.5. The application of this correlation to compare with the coils in the present study is appropriate; all of the parameters are within their respective ranges.

Table 2.5. Wang (1999) Plain Fin Correlations: Parametric Range

Fin Pattern	Plain
Number of Rows	1 - 6
Diameter OD (mm) [in]	0.635 - 12.7 [0.25 - 0.5]
Fin Pitch (mm) [fins/in]	1.19 - 8.7 [2.9 - 21.5]
P_t (mm) [in]	17.7 - 31.75 [0.694 - 1.25]
P_l (mm) [in]	12.4 - 27.5 [0.488 - 1.08]

Webb and Kang (1998) performed experimental work on eight enhanced fin shapes. Nine different coil configurations were tested and used to develop the heat transfer coefficient correlation. The heat transfer coefficient correlation can correlate 63% of this database within ±15%. The parametric range of Webb and Kang's correlation is shown in Table 2.6. The application of this correlation to compare with the coils in the present study stretches the limits of this correlation; the four-row coils in this study are outside of the 1 – 2 row range, P_l/D parameter is 2.053 which is outside of the 1.59 – 1.89 range, and the P_f/D parameter is 0.127(for the 21 fpi coils in the present study) which is outside the 0.134 - 0.252 range.

Table 2.6. Webb (1998) Louvered Fin Correlations: Parametric Range

Fin Pattern	Louvered
Number of Rows	1 - 2
P_t/D	2.32 - 2.80
P_l/D	1.59 - 1.89
P_f/D	0.134 - 0.252

Wang et al. (1998b) performed a correlation for louvered fins based on several sources of experimental data. Data from a total of 49 coil configurations were used to develop the correlation. The heat transfer correlation can correlate 95.5% of the database within ±15%, and the friction correlation can correlate 90.8% of the database within ±15%. The parametric range of Wang's correlation is shown in Table 2.7. The application of this correlation to compare with the coils in the present study stretches the limits of this correlation: the P_l parameter is 0.77 in. which is outside the 0.5 – 0.75 in. range and the major louver pitch is 0.064 in. in the present study which is outside the 0.067 – 0.147 in. range. All other parameters are within their respective ranges.

Table 2.7. Wang (1998b) Louvered Fin Correlations: Parametric Range

Fin Pattern	Louvered
Number of Rows	1 - 6
Diameter OD (mm) [in]	6.93 - 10.42 [0.27 - 0.41]
Fin Pitch (mm) [fins/in]	1.21 - 2.49 [10.2 - 21.2]
P_t (mm) [in]	17.7 - 25.4 [0.694 - 1]
P_l (mm) [in]	12.7 - 22 [0.5 - 0.75]
Louver height (mm) [in]	0.9 - 1.4 [0.03 - 0.055]
Major Louver Pitch (mm) [in]	1.7 - 3.75 [0.067 - 0.147]

II.C: Air-side Data Reduction

Wang et al. (2000b) published a paper detailing data reduction for air side performance of fin-and-tube heat exchangers. This paper discusses the importance of the correct choice of ε-NTU relationship, calculation of fin efficiency, and whether entrance and exit pressure losses should be included in reduction of friction factors. Wang et al. states that the thermal contact resistance is a source of uncertainty and that generally this effect is included in the air-side resistance.

II.D: Application to the present study

This experimental study will incorporate and discuss methods and evaluate correlations presented in this literature review. The discussion of the application of the reviewed literature will progress from heat transfer to friction factor and finally to an overview of the parametric ranges of the presented correlations.

The present study incorporates several methods and practices from the literature reviewed to help calculate the heat transfer characteristics of heat exchangers, as the following will detail. A modified Wilson method was used to determine the water side thermal resistance. This method was also used by Rich (1973). Wang (1998c) opted for Gnielinski's (1976) correlation to determine the waterside heat transfer coefficient. The use of Gnielinski's correlation would eliminate the need for the modified Wilson test and therefore reduce the time to acquire a full data set for a coil. However, an experimental method was preferred to a correlation, because it more accurately characterizes the water side heat transfer behavior. Thermal contact conductance between the fins and the tubes is not calculated, and is indirectly included in the air side heat transfer results. According to Wang (1999) it is very difficult to accurately predict the contact resistance and hence, most of the published works on the airside performance absorbed contact resistance into the airside performance. Tubes in this study are mechanically expanded to an interference fit of 0.004 in. to ensure minimal contact resistance. The present study uses Schmidt's (1949) approximation method to calculate the fin efficiency. This is consistent with Wang's experimental methods.

Wang et al. (2000b) discuss the proper choice of ε-*NTU* correlation for a given geometry. In the present study since the circuiting was serpentine each row was analyzed independently and furthermore when *NTU* is less than 1.5 the effect of the number of rows is insignificant and therefore all available ε-*NTU* correlations are essentially equivalent and the cross-flow unmixed-unmixed ε-*NTU* correlation was used.

The present study incorporates several methods and practices from the literature reviewed to help calculate the friction characteristics of heat exchangers, as the following will detail. The work of Rich (1973) was used as a guide to separate the pressure drop into two additive superimposed components, one component due to the tubes and one component due to the fins. All literature reviewed followed this convention when calculating the fanning friction factor for the fins. Rich performed a tube bundle pressure drop test. Wang opted to use a correlation from Kays and London (1984) to approximate the pressure drop due to the bare tubes. Correlations from a more recent study, Zukauskas and Ulinskas (1998), were used to approximate the pressure drop due to the bare tubes in the present study. Webb also used Zukauskas' correlations to calculate the pressure drop due to the bare tubes. Kays and London (1984) states that when the core pressure drop is calculated this takes into account the tube row contraction and expansion (entrance, K_c , and exit, K_e) loss coefficients, thus K_c and K_e will be zero. The flow acceleration due to the contraction ratio, σ, and the density change is included in the fin friction factor formula.

Each correlation discussed in Section B was compared with applicable experimental data in Chapter VI. As mentioned in Section B, the present study's parameters fall outside of some of the correlations parametric ranges. Some researchers

have used dimensionless groups to define the parametric range for their correlations. This makes the task of comparing correlations more difficult. Figure 2.3 summarizes the present study's parametric range along with the parametric range for each correlation.

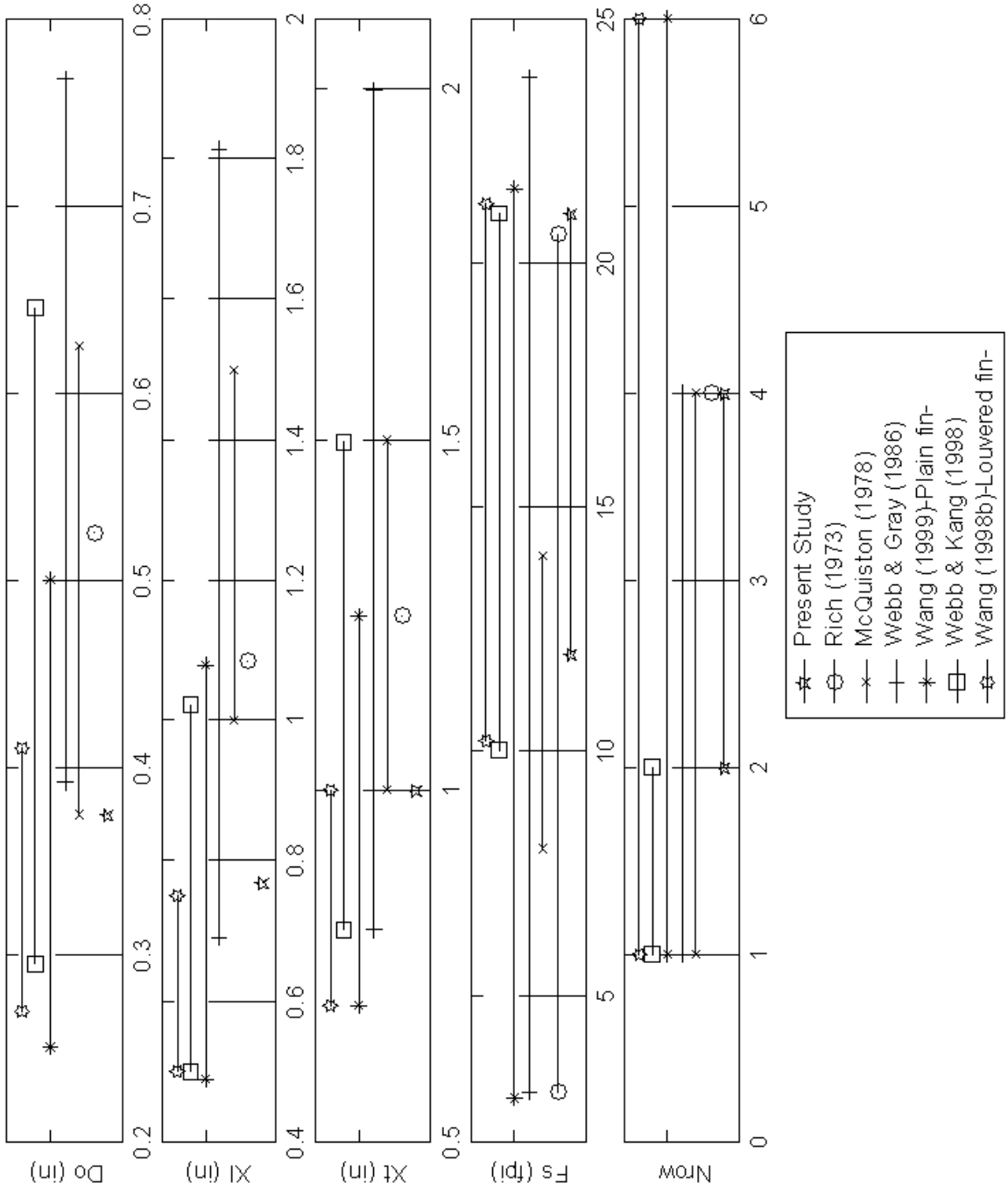

Figure 2.3: Parametric range comparison

CHAPTER III

Experimental System and Methodology

III.A Experimental System

III.A.1 Heat Exchanger Description

Eight Heat Exchangers were tested (labeled A-H). Table 3.1 shows the systematic variation of parameters for the coils tested. This present study is similar to the study performed by Wang et al. (1998c). Wang's study consisted of eight heat exchangers with varying parameters as shown in Table 2.2.

Table 3.1. Systematic Variation of Parameters

Coil	Number of Rows	Fins per inch	Fin Type	Major Louver Pitch [in]	Louver Height [in]
A	4	21	Plain	-	-
B	4	12	Plain	-	-
C	2	21	Plain	-	-
D	2	12	Plain	-	-
E	4	21	Louvered	0.064	0.043
F	4	12	Louvered	0.064	0.043
G	2	21	Louvered	0.064	0.043
H	2	12	Louvered	0.064	0.043

A 3D CAD model of a four row coil is shown in Figure 3.1.

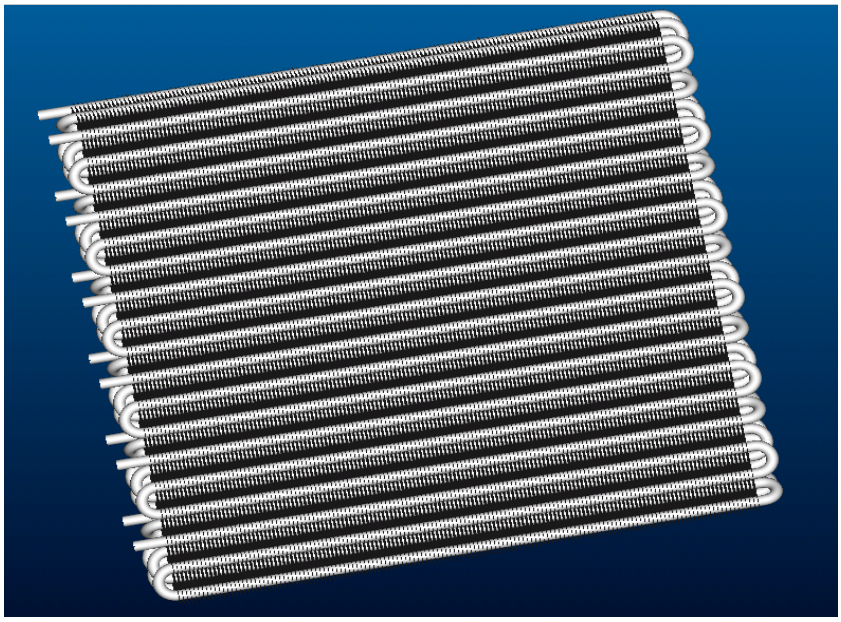

Figure 3.1. CAD model of a 4-Row Coil

Figures in Chapter I show a more detailed look at finned tube heat exchangers. Specifically, Figure 1.4 shows a schematic of a 4-row coil with the defining parameters labeled, Figure 1.5 shows an enlarged cutaway view of a plain 4-row coil including the rippled edge geometry, and Figure 1.6 shows an orthographic representation of the louvered fin geometry in this study. Table 3.2 shows the parameters common to all of the coils. All of the fins are 0.005 in. thick and have a rippled leading and trailing edge profile. The rippling increases the mechanical durability of the fins.

Table 3.2. Common Coil Parameters

Frontal Height [in.]	18	Number of Circuits	6
Frontal Width [in.]	18	Tubes per Row per Circuit	3
Face Attitude	Vertical	Outer Tube Diameter [in.]	0.375
Tube Attitude	Vertical	Row Arrangement	Staggered
Fin Thickness [in.]	0.005	Transverse Tube Spacing [in.]	1
Fin Geometry	Flat-Rippled Edges	Longitudinal Tube Spacing [in.]	0.77

The orientation of the coils is stated in Table 3.2. Figure 3.2 shows the three most common testing orientations. All of the tests in this study correspond to option C, vertical tubes flow and horizontal airflow.

A	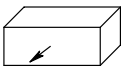	Horizontal Air Flow, Horizontal Tubes	Level with the y-axis and x-axis.
B		Vertical Air Flow, Horizontal Tubes	Level with the z-axis and x-axis.
C		Horizontal Air Flow, Vertical Tubes	Level with the y-axis and x-axis.

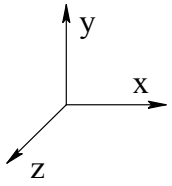

Figure 3.2. Testing Orientation

III.A.2 Apparatus

III.A.2.i Equipment

A photograph of the test apparatus is shown in Figure 3.3 and a schematic of the test apparatus is shown in Figure 3.4. The system was designed to draw room air over the finned side of the coils while circulating hot water through the tubes. Following the air path after leaving the test section air passes through a diffusion baffle and a flow metering section before being exhausted through a blower into the plenum of the laboratory room. The diffusion baffle is comprised of a perforated sheet of metal. The flow metering section is comprised of a calibrated elliptical nozzle and differential pressure ports. Nozzle loss coefficients were obtained from ASHRAE (1987) Standard 41.2-1987. A frequency controller (0-60Hz) was used to modulate the power to the blower. The exhaust air is ducted into the ceiling plenum before it returns back into the room. Following the water path, the water leaves the pump and goes through the flow control valve, the heater, and then enters the test coil. The water inlet temperature was measured with an RTD temperature sensor and controlled using a PID controller. The PID controller was connected to a solid state relay which was connected to the water heating elements. After leaving the test coil the water travels through a water flow meter with a voltage pulse output and returns to the reservoir for the submersible pump.

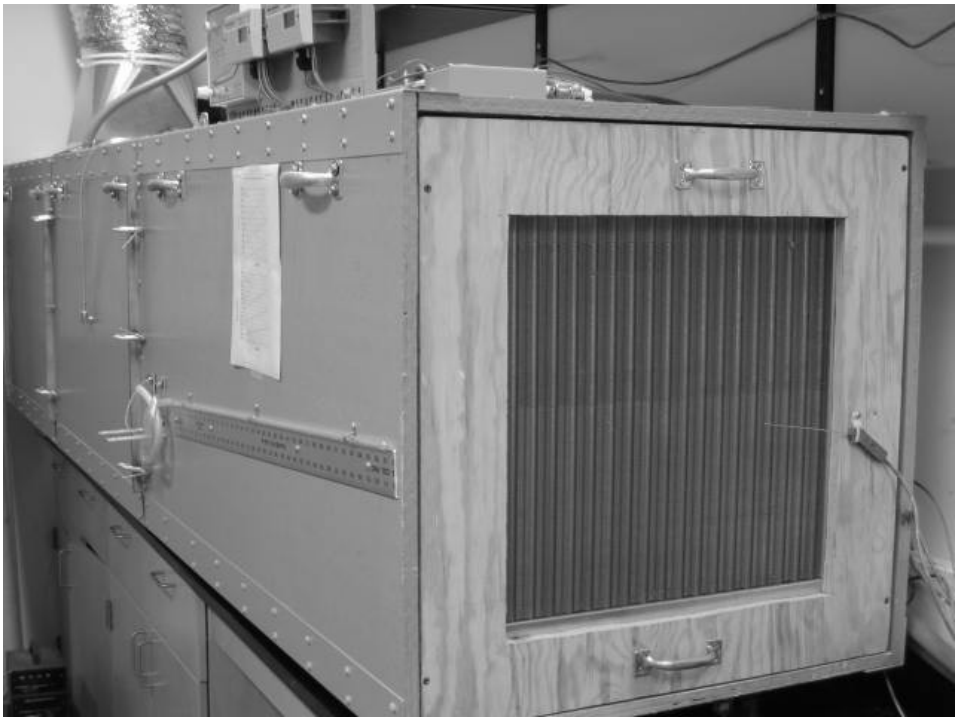

Figure 3.3. Photograph of test apparatus

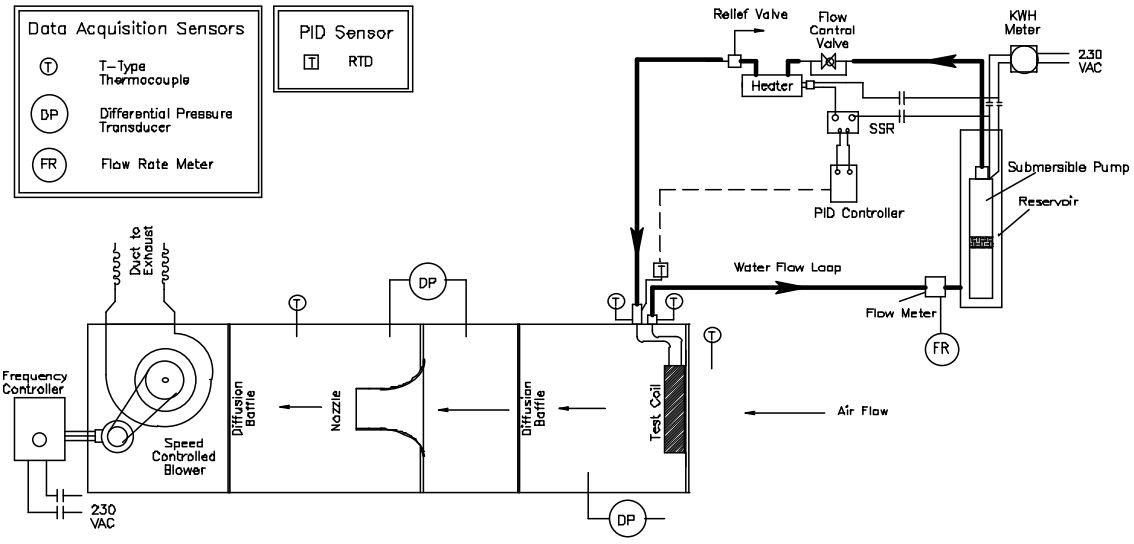

Figure 3.4. Schematic diagram of test apparatus

III.A.2.ii Data Acquisition

The data acquisition system is comprised of instrumentation, a set of hardware computer cards, and software. Instrumentation consists of several transducers namely: four temperature sensors, two differential pressure sensors, and a flow meter. Temperatures were measured using T-type [copper-constantan] thermocouples attached to shielded, grounded, single-strand thermocouple extension wire. The instrumentation accuracy is summarized in Table 3.3. All of the thermocouples were simultaneously calibrated using a NIST traceable thermal calibration block over a range of -10 to 170°F. This was a system calibration including the internal electronics of the data acquisition system. The thermal calibration block is traceable to NIST standards with an accuracy of ±1°F. The block has a thermal stability of ±0.1°F. The resulting accuracy of the thermocouples when measuring temperature relative to each other is ±0.1°F. Differential pressures were measured using calibrated pressure transducers. The pressure transducer used to measure the differential pressure across the test coil has a scale of 0 - 0.5 inH_2O and was factory calibrated to be accurate to ±0.002 inH_2O compared to the NIST standard. The pressure transducer used to measure the differential pressure across the air flow nozzle has a scale of 0 - 2.5 inH_2O and was factory calibrated to be accurate to ±0.01 inH_2O compared to the NIST standard. The rotary water flow meter generates a voltage pulse for a given volume of water, 95 pulses per gallon. The water flow rate was calculated by measuring the number of pulses and the sample time; the resulting resolution is 0.03 gpm. The accuracy of the water flow meter is 0.3 gpm compared to the NIST standard.

Table 3.3. Instrumentation Accuracy

Measure	Transducer	Range	Accuracy	Notes
Temperature	T-Type Thermocouple	-328 – 750°F	±0.1°F	
Pressure	Diaphragm - Strain gage - 4-20 mA output	0 - 2.5 inH_2O	±0.01 inH_2O	Nozzle
Pressure	Diaphragm - Strain gage - 4-20 mA output	0 - 0.5 inH_2O	±0.002 inH_2O	Coil
Flow rate	Rotary - volumetric displacement with pulse output	0 - 20 gpm	±0.33 gpm	

The set of hardware computer cards inputs the thermocouple signals as well as analog signals from the other transducers. The software consists of three programs with three separate and distinct tasks. These are:

1. Visual Basic for Applications – Acts as the task manager controlling when measurements are made, as well as traffic controller for the solver. Visual Basic also calculates several statistical quantities, namely standard deviation, trailing averages and percent change.
2. Excel – Records and displays data.
3. Engineering Equation Solver – Acts as a transcendental equation solver and supplies thermo-physical fluid property data. The equation solver solves the transcendental equations, such as the ε-*NTU* relations iteratively.

Data are recorded once each minute. Also the instantaneous *NTU*, *UA*, and ε are calculated and recorded using the most current temperatures, flow rates and thermo-physical properties.

III.B Methodology

III.B.1 Procedure

Three tests were performed on each coil: a modified Wilson test, a Variable Air test and an Isothermal Friction test. The modified Wilson test will herein be called the Wilson test.

The goal of the Wilson test is to determine the waterside thermal resistance (evaluated as, $R_w = \frac{1}{h_i A_i}$). The heat transfer coefficient for the water inside of a tube has been extensively studied and is known to be a function of the diameter of the tube and the water velocity. Given this, the Wilson test holds the air side thermal resistance constant, by maintaining a constant mean air temperature and air flow rate, while varying the water flow rate. The tube conductive resistance, $R_{t,cond}$, and contact resistance between the fin and tube, $R_{c,cond}$, is assumed to be constant. This isolates the waterside thermal resistance, R_w from the total thermal resistance, $R_o = R_w + R_{t,cond} + R_{c,cond} + R_a$. The Wilson technique is discussed further in Chapter IV.

The goal of the Variable Air test is to determine the airside heat transfer coefficient and the pressure drop due to the fins of each coil over a range of air flow rates. The heat transfer coefficient is expressed as the non-dimensional Coburn *j* factor

and the pressure drop is expressed as the Fanning friction factor. The water flow rate is constant over each coil's test and is set as possible to minimize the water side thermal resistance. The range of the water side to total thermal resistance ratios for the span of air flow rates experienced for five of the coils was 8% – 22% while two coils had a range of 20% - 28%, and one coil (Coil E, the largest air side area coil) had a range of 40%-44%. The water flow rate is limited by the condition that the water temperature drop across the coil is no less than 4°F.

The goal of the Isothermal Friction test is to validate the Variable Air friction factor data, *f*, for each coil. This test ensures that thermal variations on the airside within each heated coil are accounted for and do not skew the friction characteristics. This practice was used by Rich as well as being mentioned by Wang et al. (2000b).

Each day before the experimental tests were started, the accuracy of the thermocouples was checked.

III.B.2 Steady State Criterion

To achieve repeatable data points and sets, a series of criteria for steady state equilibrium was established and satisfied. These criteria were:

1. The ten minute average *UA* changes less than ± 1% over thirty minutes as described in the next paragraph.
2. The heat rate imbalance (between the water and air sides) should be no more than 8%, it was often less than 5%. The uncertainty in the Colburn *j* factor is ±11%.

3. The thermal resistance on the waterside should not constitute more than 30% of the overall thermal resistance.

The procedure for recording a data point is as follows. Thirty minutes of steady state data were averaged and used to determine a *UA* value for each test condition. Temperatures, pressures and flow rates were measured each minute; sampling at this rate is called instantaneous or minute by minute in this present study. Also the instantaneous *UA* was calculated each minute. During the test, the ten minute trailing average of all instantaneous temperatures, pressures, flow rates and *UA* was calculated each minute. The instantaneous *UA* is plotted along with the ten minute trailing average *UA*; an example is shown in Figure 3.5. The thirty minute average of data can be calculated by averaging three independent ten minute averages. The variation of the three independent ten minute average *UA* from the thirty minute average was calculated. The first criterion for steady state equilibrium was considered to be satisfied when these variations were less than ±1%. The heat balance between the airside and waterside was updated each minute. After satisfying the first two criteria for steady state, thirty minute trailing average temperatures, flow rates, and pressures were then recorded. These measurements were reduced and constitute two data points, namely a *j* factor and *f* factor for a given airside Reynolds number. The percentage of overall thermal resistance on the waterside was calculated to ensure that the waterside thermal resistance was no more than 30% of the total thermal resistance. If the waterside resistance dominates the overall resistance then airside thermal resistance will be small, resulting in poor resolution upon calculation of airside heat transfer coefficient. This logically leads to poor resolution on the *j* factor.

As previously mentioned, a low waterside resistance was maintained by setting water velocity high enough.

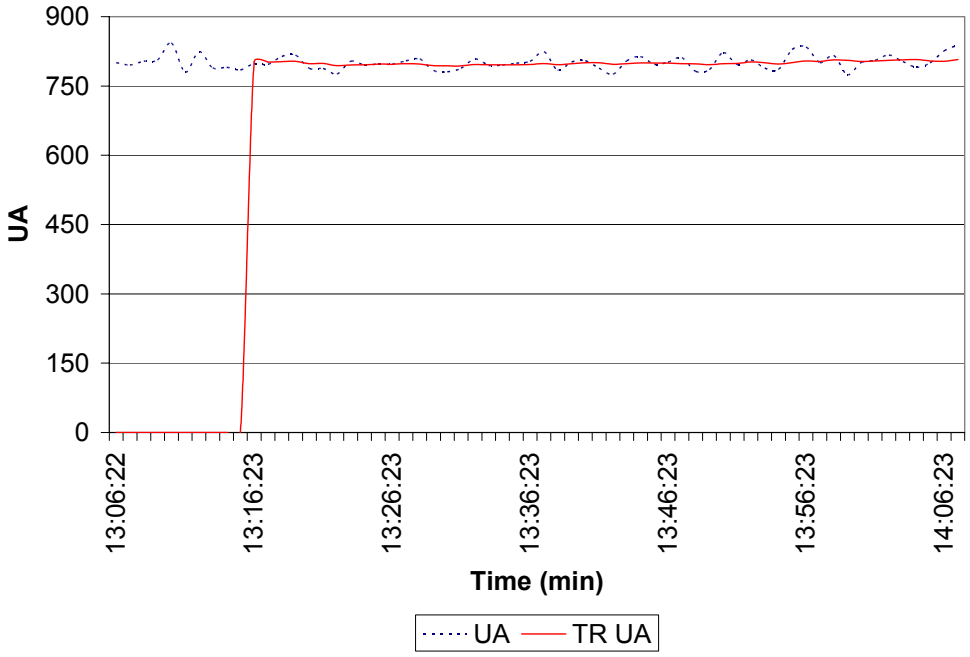

Figure 3.5. Instantaneous UA and Trailing UA vs. time

To satisfy the first criterion for steady state it is useful to investigate the ε-*NTU* relationship to better understand its sensitivity characteristics. Equation 3.1 shows the relationship between ε and *NTU* for pure cross flow with an infinite number of rows. Equation 3.2 shows how C_r, the ratio of heat capacities, is calculated. Figure 3.6 shows the ε-*NTU* relationship graphically for several values of C_r. Notice that for $NTU < 1$ the relationship is fairly linear. However for $NTU > 1$ ε asymptotically approaches a zero slope line.

$$\varepsilon = 1 - \exp\left[\left(\frac{1}{C_r}\right)(NTU)^{0.22}\left(\exp\left[-C_r\,(NTU)^{0.78}\right]-1\right)\right] \tag{3.1}$$

$$C_r = \frac{C_{\min}}{C_{\max}} = \frac{\dot{m}_c c_{p,c}}{\dot{m}_h c_{p,h}} = \frac{T_{h,i} - T_{h,o}}{T_{c,o} - T_{c,i}} \tag{3.2}$$

$$UA = \frac{NTU}{C_{min}} \tag{3.3}$$

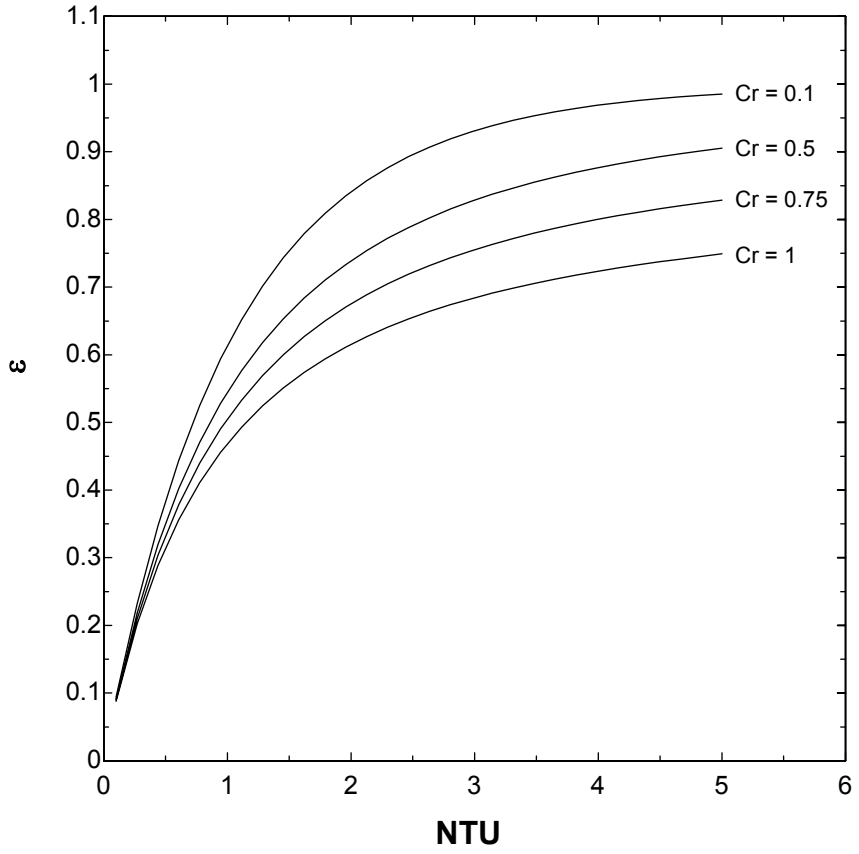

Figure 3.6. ε - *NTU* relationship for varying C_r.

When operating in the *NTU* > 1 region, the asymptotic nature of the ε-*NTU* relationship can result in inaccurate determination of *UA*. Where *UA* is calculated using Equation 3.3. This inaccuracy is a result of high sensitivity of *NTU* to ε as shown in

Figure 3.7. Since ε is the measured parameter and *UA* is determined by using the *ε-NTU* relation and then calculation of *UA* from *NTU*. It is therefore evident that any inaccuracy in determining *NTU* from ε will result in inaccurate determination of *UA*. An error $\delta\varepsilon_1$ in the linear region results in a small error in *NTU* shown as δNTU_1 for both values of C_r. However, an error $\delta\varepsilon_2$ in the asymptotic region (*NTU* > 1) results in a large error in NTU shown as δNTU_2 for both values of C_r. Also in the low ε region the value of C_r has little effect on δNTU_1. However for higher values of ε the value of C_r has a large impact on the sensitivity of δNTU_2 to $\delta\varepsilon_2$.

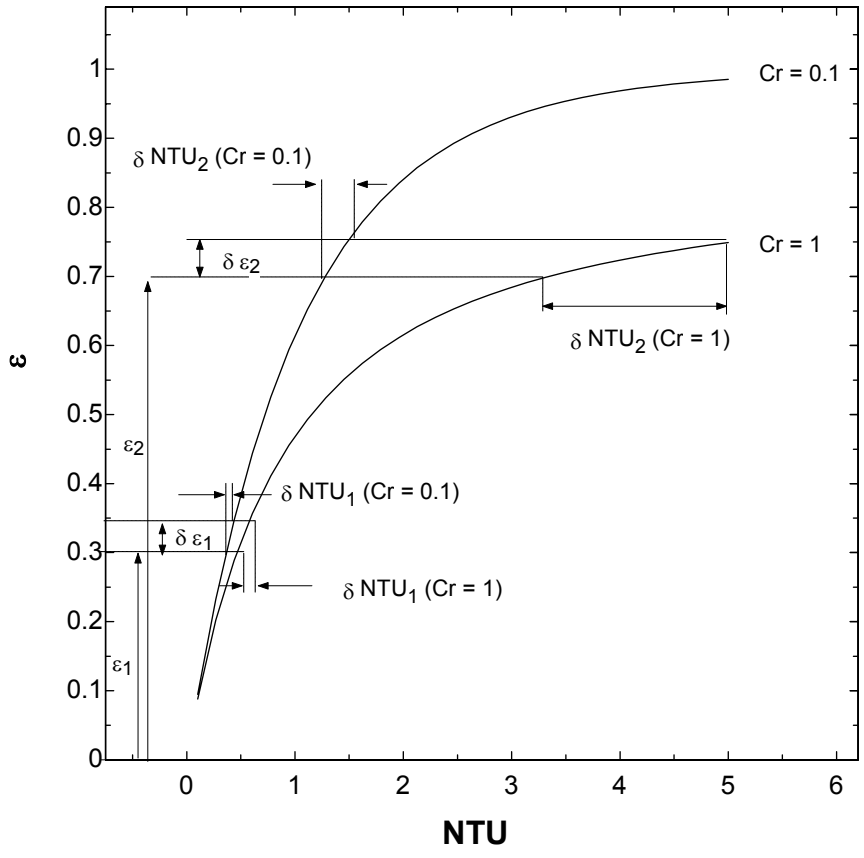

Figure 3.7. *ε-NTU* relationship showing sensitivity at high ε for varying C_r.

The high sensitivity of *NTU* to ε can be seen when testing coil E, which is the largest airside surface area coil with louvers (largest *UA* value). When operating at the highest water flow rate possible (to minimize waterside thermal resistance) and therefore the lowest C_r [approximately 0.12] the sensitivity of *NTU* to ε resulted in large fluctuations in *UA* at these airflow and water set point conditions. This variation is a direct result of the large value of ε (near 1), which places the values in the asymptotic region

Given the previous discussion on the sensitivity of *NTU* to measured values of ε, Coil E was difficult to test because ε being close to 1. Investigating Equation 3.4, it is easy to see that to lower ε, q_{max} should be increased.

$$\varepsilon = \frac{q}{q_{\max}} = \frac{T_{c,o} - T_{c,i}}{T_{h,i} - T_{c,i}} \tag{3.4}$$

To maintain a low waterside thermal resistance, while maintaining good ΔT resolution, the water velocity was increased until the water side temperature difference across the coil was about 4°F. The high water velocity lowered the maximum water inlet temperature because of electrical power limitations to the heater. Conversely, lowering the water velocity allowed for higher water inlet temperatures and reduced the sensitivity of *NTU* to ε, at the cost of higher waterside thermal resistance. So to lower ε and make the *UA* less sensitive to ε, while maintaining a low waterside thermal resistance, a higher electrical heater power is required. In the laboratory where tests were carried out, the electrical power was limited to 8 kW. As a result, heat transfer data from Coil E did not

meet the equilibrium criterion; the water side thermal resistance was approximately 45% of the total thermal resistance.

CHAPTER IV
DATA REDUCTION

IV.A: Overview

The following section gives an overview of the data reduction methods used. The overall thermal resistance of a heat exchanger can be divided up into four major parts: the water side, tube conduction, contact conduction (between the tube and fin), and air side thermal resistance.

$$\frac{1}{UA_o} = R_o = R_w + R_{t,cond} + R_{c,cond} + R_A = \frac{1}{h_i A_i} + \frac{\delta_t}{k_t A_t} + \frac{1}{h_c A_t} + \frac{1}{\eta_o h_o A_o} \qquad (4.1)$$

The conduction resistance through the tube wall, $R_{t,cond}$, was calculated to be less than 0.5% of the total resistance in all cases. The contact conduction resistance, $R_{c,cond}$, between the tube and the collar of the fin is a source of uncertainty. Wang(2000) states that "in practice it is very hard to accurately predict the contact conductance, and most of the published works on the airside performance absorbed contact resistance into the airside performance." The work of Sheffield et al. (1989) gave a range of thermal contact conductance of 10,607 – 30,828 W m^{-2} K^{-1} [1750 – 5400 Btu/ft^2-hr-R] for a similar fin geometry (X_t = 25.4 mm [1 in.], X_l = 22 mm [0.866 in.], D_o = 9.52 mm [0.375 in.], and full fin collar). Based on this range, the contact conductance accounts for 3% - 18% of the total thermal resistance in the coils tested. Both the tube conduction resistance and the contact conduction resistance were absorbed into the airside thermal resistance. Solving Equation 4.1 for the air side heat transfer coefficient produces.

$$h_o = \frac{1}{\eta_o A_o}\left(\frac{1}{UA_o} - \frac{1}{h_i A_i}\right)^{-1} \qquad (4.2)$$

The air side fin efficiency, η_o, is calculated using the Zeller hexagonal fin approximation. This approximation was used for both the plain and louvered fins, although it is known

that the louvers impede radial heat flow from the tube, resulting in an over estimate of the fin efficiency for louvered fins. The UA_o term is calculated using the Variable Air Test; the h_i term is calculated using the Wilson Test.

The heat transfer coefficient is expressed as the Colburn j factor. The Colburn j factor is calculated using:

$$j = St \cdot Pr^{2/3} = \frac{h_o}{\rho V c_p} \cdot Pr^{2/3} \tag{4.3}$$

Where h_o is the convection coefficient, V is the air velocity through the minimum free flow area of the heat exchanger, ρ is the density, c_p is the specific heat, and Pr is the Prandtl number.

The pressure drop over the heat exchanger is broken up into two additive components, as proposed by Rich (1973) and accepted by all studies referenced in this study. The first component is the pressure drop across the staggered tube bank, and the second component is the pressure drop due to the fins. The pressure drop across the staggered tube bank will be calculated using equations from Zukauskas (1998) in section C of this chapter.

The pressure drop due to the fins is expressed as the Fanning friction factor, f. The fanning friction factor, f_{exp}, is calculated using:

$$f_{exp} = \frac{A_{flow}\rho_1}{A_{fin}\rho_{avg}}\left[\frac{2DP_{A,fin}}{G_{max}^2\rho_1} - \left(1+\sigma^2\right)\left(\frac{\rho_1}{\rho_2} - 1\right)\right] \tag{4.4}$$

where $DP_{A,fin}$ is the pressure drop only due to the fins, A_{flow} is the flow area for the air, G_{max} is the mass velocity of the air, σ is the contraction ratio or ratio of minimum flow area to frontal area, ρ is the density, and A_{fin} is the surface area of all of the fins. This formulation is the definition used by Wang (1998a, 1998b, 1998c, 2000a, 2000b). The contraction and expansion coefficients (K_e and K_c) are not included in the formulation because they are represented in the calculation of the pressure drop due to the tubes. The

f_{exp} term is calculated using data from the Variable Air Test and also independently using data from the Isothermal Friction Test.

IV.B: Heat Transfer

IV.B.1: Water-Side UA/Wilson Plot

The objective of the water-side *UA* test is to determine the water side thermal resistance using a graphical method, namely a modified Wilson Plot. To develop the rationale for the water side *UA* test it is noted that the water side convection coefficient can be investigated using the Dittus-Boelter equation:

$$Nu_{Di} = \frac{h_i D_i}{k} = 0.023 \quad Re_{Di}^{0.8} Pr^{0.3} \tag{4.5}$$

Solving for the convection coefficient and substituting in the definitions of the Reynolds number and Prandtl number results in the following equation for the water side convection coefficient that is a function of the water velocity, V_i, the inner diameter, D_i, and the water properties. The properties are a function of the mean water temperature, $\bar{t}_{m,w}$.

$$h_i = \left[(0.023) \left(\frac{k^{0.7} c_p^{0.3} \rho^{0.8}}{\mu^{0.5}} \right) \right] \frac{V_i^{0.8}}{D_i^{0.2}} = C \cdot f\left(\bar{t}_{m,w}\right) \cdot \frac{V_i^{0.8}}{D_i^{0.2}} \tag{4.6}$$

Water side heat transfer tests were preformed to determine the constant *C*. The function of water mean temperature, $f\left(\bar{t}_{m,w}\right)$, was chosen to be consistent with Rich (1973). Water flow rates for these tests ranged from a minimum of 1gpm to a maximum of 12gpm, corresponding to a water velocity range of 0.82 to 3 ft/s. The mean air temperature was kept constant for all of the runs in a Coil's test.

Figure 4.1 shows a modified Wilson Plot for Coil A, where the abscissa, *X*, and the overall thermal resistance, R_o, are defined by:

$$X = \left(\frac{1}{A_i}\right)\left(\frac{D_i^{0.2}}{\left(1+.001\cdot\bar{t}_{m,w}\right)V_i^{0.8}}\right) = \frac{1}{A_i h_i} \tag{4.7}$$

$$UA_o = \frac{1}{R_o} = \frac{\dot{Q}_{avg}}{\Delta T_{lm}} \tag{4.8}$$

where A_i is the water side heat transfer area, D_i is the inside tube diameter, $\bar{t}_w$ is the mean water temperature, V_i is the water velocity through each tube, ΔT_{lm} is the log mean temperature difference, and $\dot{Q}_{avg}$ is the average of the heat transfer rate as calculated from the air side and from the water side. The overall thermal resistance is shown as the solid trend line fitted to the data points. The waterside resistance can be calculated by subtracting the air side resistance from the overall thermal resistance. As X approaches zero the water velocity approaches infinity. From Equations 4.1 and 4.7 the thermal resistance of the water side approaches zero as X approaches zero. Therefore the y intercept corresponds to the point where the overall thermal resistance is equal to the air side resistance. The extrapolation of the y intercept is consistent with the methods used by Rich (1973). The dotted line parallel to the overall thermal resistance line represents the water side thermal resistance as a function of X.

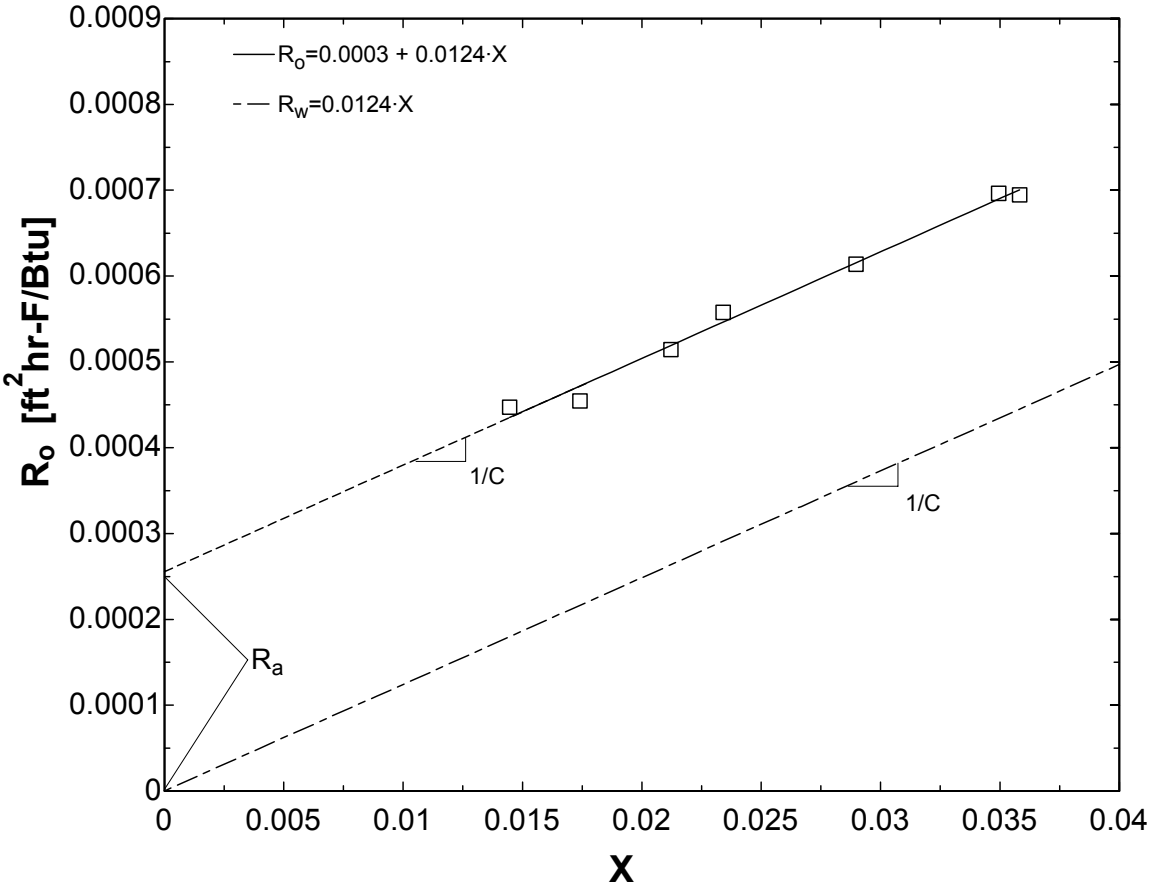

Figure 4.1. Modified Wilson Plot Coil A

A summary of all of the water side heat transfer tests including the inverse of the slope, *C*, is shown in Table 4.1. Figure 4.2 shows this information graphically. Notice that the 4-row coils range of *X* is lower than that of the 2-row coils because of the higher tube area.

Table 4.1. Wilson Plot Summary Data

Coil	N Data Pts	fpi	N Rows	R^2	1/C (slope)	Intercept
A	7	21	4	98.95	0.0124	0.0003
B	7	12	4	99.52	0.0086	0.0007
C	8	21	2	99.31	0.0086	0.0007
D	7	12	2	97.40	0.0092	0.0011
E	6	21	4	96.29	0.0115	0.0001
F	8	12	4	99.56	0.0092	0.0004
G	7	21	2	99.86	0.0086	0.0005
H	7	12	2	98.84	0.0105	0.0007

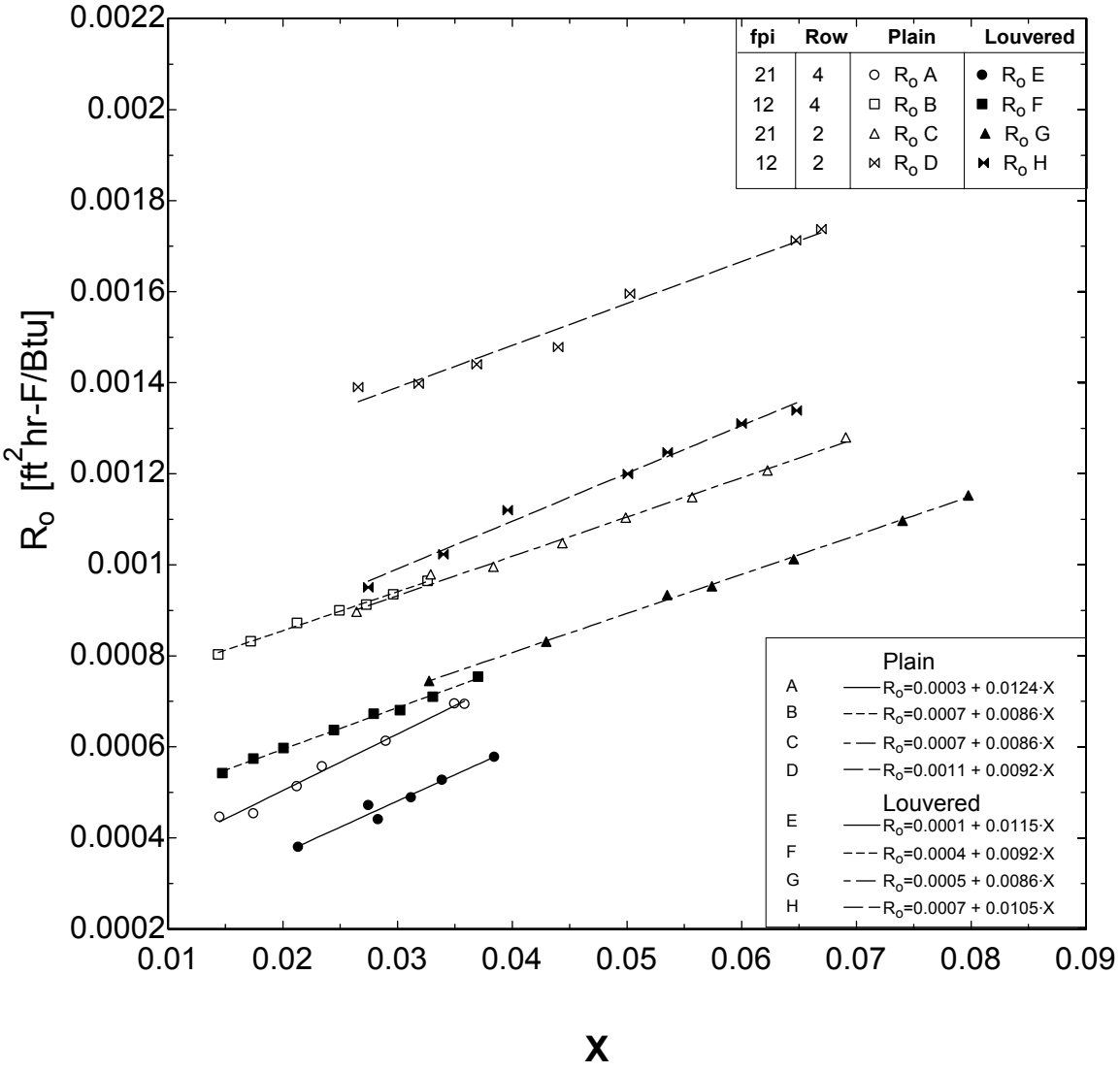

Figure 4.2. Wilson Plot of Coils A-H

IV.B.2: Air-Side UA

To obtain *UA* values the *ε-NTU* method was applied to the test data. The total heat transfer rate used in the calculation is the arithmetic average of the air side and water side heat transfer rates. These are shown in Equations 4.9 - 4.11.

$$\dot{Q}_{air} = \dot{m}_{air} c_{p,air} \Delta T_{air} \tag{4.9}$$

$$\dot{Q}_{water} = \dot{m}_{water} c_{p,water} \Delta T_{water} \tag{4.10}$$

$$\dot{Q}_{avg} = \frac{\left(\dot{Q}_{air} + \dot{Q}_{water}\right)}{2} \tag{4.11}$$

The air side UA tests vary airflow rate while keeping water flow rate constant. The UA_o term in Equation 4.1 is calculated using Equation 4.12.

$$UA_o = \frac{1}{R_o} = \frac{NTU_{tot}}{C_{min}} \tag{4.12}$$

$$C_r = \frac{C_{min}}{C_{max}} = \frac{\dot{m}_{air} c_{p,air}}{\dot{m}_{water} c_{p,water}} \tag{4.13}$$

$$\varepsilon \equiv \frac{\dot{Q}_{ave}}{\dot{Q}_{max}} = \frac{\dot{Q}_{ave}}{\dot{m}_{water} c_{p,water} \left(T_{in,water} - T_{out,air}\right)} \tag{4.14}$$

The minimum heat capacity, $C_{min,}$ is easily calculated directly from measured quantities and physical properties at the fluid temperature. The NTU_{tot} value is calculated from the value of effectiveness, ε, which is calculated from the measured temperatures. But the NTU-ε relationship required for this correlation is not simple because of the water side tube circuiting, which is a mixture of cross flow and counter flow. In each individual row the correct NTU relation is the cross flow relationship. From row to row a counter flow relationship is required. To properly deal with this hybrid cross/counter flow configuration each row was analyzed individually, using the unmixed-unmixed cross flow ε-NTU relation, shown in Equation 4.15. Even though this relation is for an infinite number of tube rows, for low values of ε and therefore NTU this relation is nearly identical to the EDSU 1-row cross flow relation as reported in Wang (2000a) and shown in Equation 4.16.

$$\varepsilon = 1 - \exp\left[\left(\frac{1}{C_r}\right)\left(NTU\right)^{0.22}\left(\exp\left[-C_r\left(NTU\right)^{0.78}\right] - 1\right)\right] \tag{4.15}$$

$$\varepsilon = \left(\frac{1}{C_r}\right)\left[1 - \exp\left(-C_r \cdot \left(1 - \exp\left(-NTU\right)\right)\right)\right] \tag{4.16}$$

Since only the coil water inlet and outlet temperatures were recorded, rather than individual row inlet and outlet temperatures, average intermediate row temperatures had to be calculated. In order to solve for this problem the assumption that all of the rows had the same *UA* and therefore ε was made. It was also assumed that the air temperature entering and leaving rows was uniform, although this is not the case. It should be reiterated that there is not an available ε-*NTU* relation for the water side circuitry used in this study. The total *NTU* for the coil was calculated as the sum of each row's calculated *NTU*.

To calculate the overall air side fin surface efficiency, η_o, for a plate-fin-and-tube heat exchanger with multiple rows of staggered tubes, the continuous fins were symmetrically divided into hexagonal shaped fins. This method was used for both plain and louvered fins, even though it is known that the addition of louvers will interrupt the conduction in the fin, resulting in a decrease in fin efficiency as compared with a plain fin. The behavior of a circular fin was used to model an equivalent hexagonal shaped fin which closely approximates the actual behavior of a continuous fin.

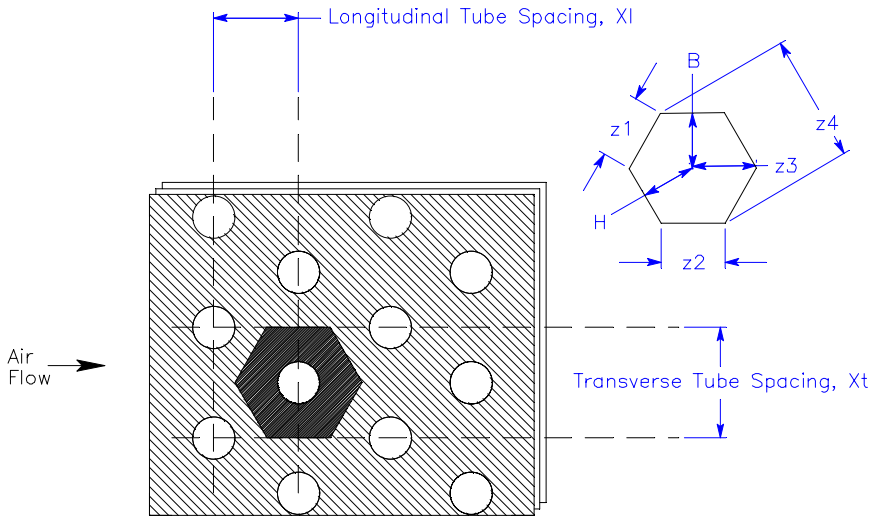

Figure 4.3. Staggered Tube Configuration

The air side surface efficiency is defined as follows:

$$\eta_o = 1 - \frac{A_{fin}}{A_o}\left(1 - \eta_{fin}\right) \tag{4.17}$$

where A_{fin} is the surface area of the fins, and A_o is the total air side heat transfer area (including the fin and the tubes). The fin efficiency of a circular fin , η_{fin} , is defined as:

$$\eta_{fin} = \frac{\tanh\left(mr_t\phi\right)}{mr_t\phi} \tag{4.18}$$

where ϕ is the fin efficiency parameter for a circular fin, r_t is the tube radius with the thickness of the fin collar included and m is the standard extended surface parameter, which is defined as:

$$m = \sqrt{\frac{2h_o}{k_{air}t}} \tag{4.19}$$

where h_o is the airside convection coefficient, k_{air} is the thermal conductivity of the air and t is the fin thickness. This relation assumes that the fin length is much larger than the fin thickness. The fin efficiency parameter for a circular fin, ϕ, is calculated using:

$$\phi = \left(\frac{R_e}{r_t} - 1\right)\left(1 + 0.35\ln\left(\frac{R_e}{r_t}\right)\right) \tag{4.20}$$

where the equivalent circular fin radius, R_e, is defined as:

$$\frac{R_e}{r_t} = \frac{P_{hex}}{2\pi r_t} \tag{4.21}$$

where P_{hex} is the perimeter of the hexagonal fin. The perimeter is defined as:

$$P_{hex} = 4z_1 + 2z_2 \tag{4.22}$$

where the lengths z_1 and z_2, shown in Figure 4.3, can be found from iteratively solving the following four equations.

$$z_2^{\,2} + (2B)^2 = z_4^{\,2} \tag{4.23}$$

$$\left(\frac{z_1}{2}\right)^2 + H^2 = \left(\frac{z_4}{2}\right)^2 \tag{4.24}$$

$$H^2 + \left(\frac{z_1}{2}\right)^2 = \left(z_3 + z_2/2\right)^2 \tag{4.25}$$

$$z_1^{\,2} = z_3^{\,2} + B^2 \tag{4.26}$$

The values of B and H are given for a given tube configuration, by:

$$B = X_l \text{ if } X_l < X_t/2, \text{ otherwise } B = X_t/2 \tag{4.27}$$

$$H = \frac{1}{2}\sqrt{\left(\frac{X_t}{2}\right)^2 + X_l^{\,2}} \tag{4.28}$$

where X_t is the transverse tube spacing and X_l is the longitudinal tube spacing.

Since the air side surface efficiency, η_o, is dependant on airside heat transfer coefficient, h_o, because of Equation 4.19 the surface efficiency and airside heat transfer coefficient must be solved iteratively to obtain the solution combination that satisfies Equation 4.1. Then the Colburn j factor is calculated using Equation 4.3.

For louvered fins, Perrotin & Clodic (2003) concluded that this circular fin approximation analysis overestimates the fin efficiency, by up to 5%. This is because the addition of the enhancement can alter the conduction path through the fin. However,

there is currently no approximation method available in the literature that claims to be valid for enhanced fins, therefore the plain fin assumption was made to calculate the fin effectiveness for the louvered fin cases as well.

IV.C: Air-side Pressure Drop

The air side pressure drop is measured directly. To calculate the friction factor, f_{exp}, from this data, the pressure drop can be split into two components: the pressure drop across a bank of tubes and the pressure drop across the fins as shown in the following equation.

$$DP_{A,tot} = DP_{A,tub} + DP_{A,fin} \tag{4.29}$$

The pressure drop of the fins, $DP_{A,fin}$, is used to calculate the Fanning friction factor, f_{exp}, in Equation 4.4. To arrive at the pressure drop due to the bank of tubes, Zukauskas and Ulinskas relations were used:

$$DP_{A,tub} = \frac{Eu_{cor} \cdot G_{max}^2 \cdot N_{row}}{2 \cdot \rho} \tag{4.30}$$

where Eu_{cor} is the corrected Euler number, N_{row} is the number of rows, ρ is the average density of the entrance and exit air and G_{max} is the mass velocity of air through the minimum flow area which is expressed as:

$$G_{max} = \frac{\dot{m}_{air}}{A_{min}}, \tag{4.31}$$

The minimum free flow area, A_{min}, is the passage height (fin spacing – fin thickness) multiplied by the minimum of the distances X_t or $2 \cdot X_{diag}$, as shown in Figure 4.4.

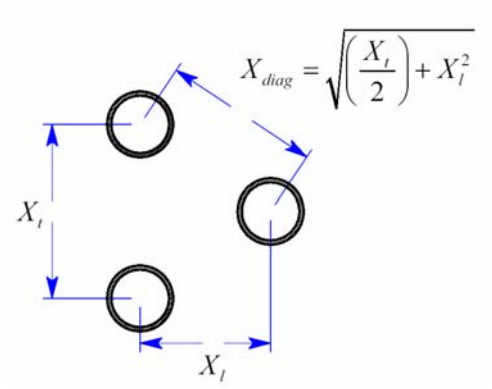

Figure 4.4. Diagram of Minimum Free Flow Area

For staggered, equilateral triangle tube banks with several rows, Zukauskas expresses the Euler number by a fourth order inverse power series by the following:

$$Eu = q_{cst} + \frac{r_{cst}}{Re_{D_o}} + \frac{s_{cst}}{Re_{D_o}^2} + \frac{t_{cst}}{Re_{D_o}^3} + \frac{u_{cst}}{Re_{D_o}^4} \tag{4.32}$$

$$Re_{D_o} = \frac{G_{\max} D_o}{\mu} \tag{4.33}$$

where Re_{Do} is the Reynolds number based on the outer tube diameter. The coefficients q_{cst}, r_{cst}, s_{cst}, t_{cst}, and u_{cst} are dependent on the Reynolds number and the parameter "a", which is defined as the ratio of the transverse tube spacing to the tube diameter (X_t/D_o). The coefficients for a range of Reynolds numbers and spacing to diameter ratios have been determined from experimental data by Zukauskas and Ulinskas (1998) and are expressed in Table 4.2.

Table 4.2. Coefficients for the Euler Number Inverse Power Series

a	Reynolds Number	q_{cst}	r_{cst}	s_{cst}	t_{cst}	u_{cst}
1.25	$3 < Re_{Do} < 10^3$	0.795	0.247×10^3	0.335×10^3	-0.155×10^4	0.241×10^4
	$10^3 < Re_{Do} < 2 \times 10^6$	0.245	0.339×10^4	-0.984×10^7	0.132×10^{11}	-0.599×10^{13}
1.5	$3 < Re_{Do} < 10^3$	0.683	0.111×10^3	-0.973×10^2	0.426×10^3	-0.574×10^3
	$10^3 < Re_{Do} < 2 \times 10^6$	0.203	0.248×10^4	-0.758×10^7	0.104×10^{11}	-0.482×10^{13}
2.0	$7 < Re_{Do} < 10^2$	0.713	0.448×10^2	-0.126×10^3	-0.582×10^3	0.000
	$10^2 < Re_{Do} < 10^4$	0.343	0.303×10^3	-0.717×10^5	0.880×10^7	-0.380×10^9
	$10^4 < Re_{Do} < 2 \times 10^6$	0.162	0.181×10^4	-0.792×10^8	-0.165×10^{13}	0.872×10^{16}
2.5	$10^2 < Re_{Do} < 5 \times 10^3$	0.330	0.989×10^2	-0.148×10^5	0.192×10^7	0.862×10^8
	$5 \times 10^3 < Re_{Do} < 2 \times 10^6$	0.119	0.848×10^4	-0.507×10^8	0.251×10^{12}	-0.463×10^{15}

For non-equilateral triangle tube bank arrays, the staggered array geometry factor, k_1, must be used as a correction factor to the coefficients in Table 4.2. The staggered array geometry factor is dependent on the Reynolds number based on: 1) the outer tube diameter; 2) the parameter "a", which again is defined as the ratio of the transverse tube spacing to the tube diameter; and 3) the parameter "b", which is defined as the ratio of the tube spacing in the direction normal to the air flow and the tube diameter (X_l/D_o). The equations for k_1 are found in Table 4.3.

Table 4.3. Staggered Array Geometry Factor

Re_D	a/b	k_1
10^2	1.25 < a/b < 3.5	$k_1 = 0.93\left(\frac{a}{b}\right)^{0.48}$
10^3	0.5 < a/b < 3.5	$k_1 = \left(\frac{a}{b}\right)^{-0.048}$
	1.25 < a/b < 3.5	$k_1 = 0.951\left(\frac{a}{b}\right)^{0.284}$
10^4	0.45 < a/b < 3.5	$k_1 = 1.28 - \frac{0.708}{(a/b)} + \frac{0.55}{(a/b)^2} - \frac{0.113}{(a/b)^3}$
10^5	0.45 < a/b < 3.5	$k_1 = 2.016 - 1.675\left(\frac{a}{b}\right) + 0.948\left(\frac{a}{b}\right)^2$ $-0.234\left(\frac{a}{b}\right)^3 + 0.021\left(\frac{a}{b}\right)^4$
10^6	0.45 < a/b < 1.6	

If the tube bank has a small number of transverse rows, an average row correction factor, C_z, must be applied because the pressure drop over the first few rows will be different from the pressure drop over the subsequent rows. C_z is the average of the individual row correction factors, c_z.

$$C_z = \frac{1}{z}\sum_{z=1}^{z} c_z \tag{4.34}$$

The equations for the individual row correction factors are given in Table 4.4. Once the average row correction factor is found, the corrected Euler number can be determined as:

$$Eu_{cor} = k_1 C_z Eu. \tag{4.35}$$

where Eu is the Euler number, k_1 is the staggered array geometry factor, and C_z is the average row correction factor.

Table 4.4. Correction Factors for Individual Rows of Tubes

Re_D	N_{row}	c_z
10	< 3	$c_z = 1.065 - \frac{0.18}{z - 0.297}$
10^2	< 4	$c_z = 1.798 - \frac{3.497}{z + 1.273}$
10^3	< 3	$c_z = 1.149 - \frac{0.411}{z - 0.412}$
10^4	< 3	$c_z = 0.924 - \frac{0.269}{z + 0.143}$
$> 10^5$	< 4	$c_z = 0.62 - \frac{1.467}{z + 0.667}$
For values of z greater than 4, $c_z = 1$		

The corrected Euler factor, Eu_{cor} can then be used in Equation 4.30 to determine the pressure drop over the tubes.

It should be noted that since the relations in Table 4.2 - Table 4.3, are given for discrete values of the "a" parameter, the "a/b" parameter, and the Reynolds number, a linear interpolation is used for non-integer values to estimate the values of Eu, k_1, and c_z.

CHAPTER V

EXPERIMENTAL RESULTS

V.A: Air Side UA

The air side *UA* can be expressed by a plot of the Colburn *j* factor vs. Reynolds number based on the tube diameter (including the fin collar) as shown in Figure 5.1. There are two distinct groups of data, the upper group is the louvered fin-tube heat exchangers, and the lower group is the plain fin-tube heat exchangers. As expected, the data shows that the addition of louvers increases the Colburn *j* factor. The ratio of the louvered *j* factor to the plain *j* factor is 1.75. This is due to the louvers breaking and renewing boundary layers on the airside. It should be noted that although data are plotted for Coil E, the largest *UA* value coil with effectiveness values close to one, it does not meet the equilibrium criterion due to experimental system limitations, as previously mentioned in Chapter III. Another trend that should be noted is the curvature of the *j* factor for 4-row coils when plotted on a log-log scale versus Reynolds number. This trend is discussed in the review of the publication by Rich (1975) in Chapter II and will be further discussed in Chapter VI.

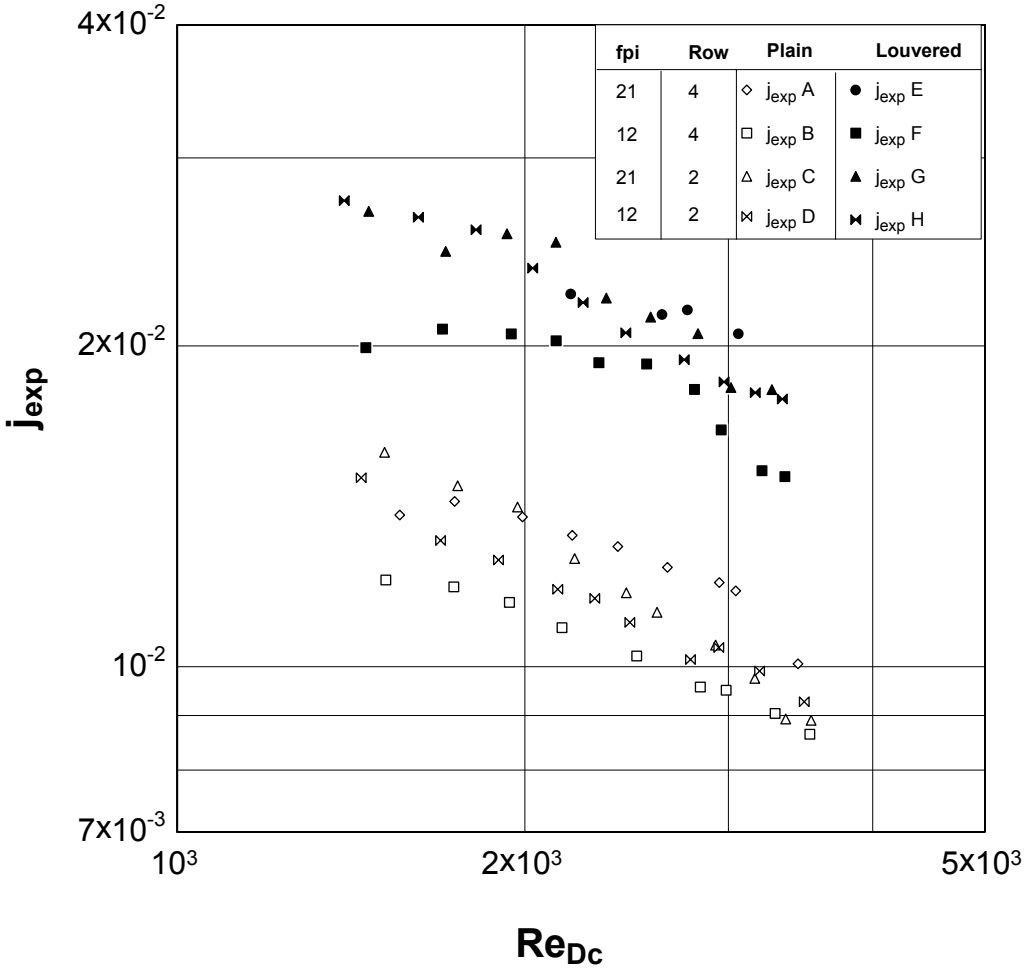

Figure 5.1. Colburn *j* factor for all coils

V.B: Air Side Pressure Drop

The air side pressure drop can be expressed using a plot of the Fanning friction factor, *f*, vs. Reynolds number based on the tube diameter (including the fin collar) as shown in Figure 5.2. There are two distinct groups of data, the upper group is the louvered fin-tube heat exchangers, and the lower group is the plain fin-tube heat exchangers. The addition of louvers increases the fanning fin friction factor. The ratio of the louvered friction factor to the plain friction factor ranges from 1.7 to 2.2.

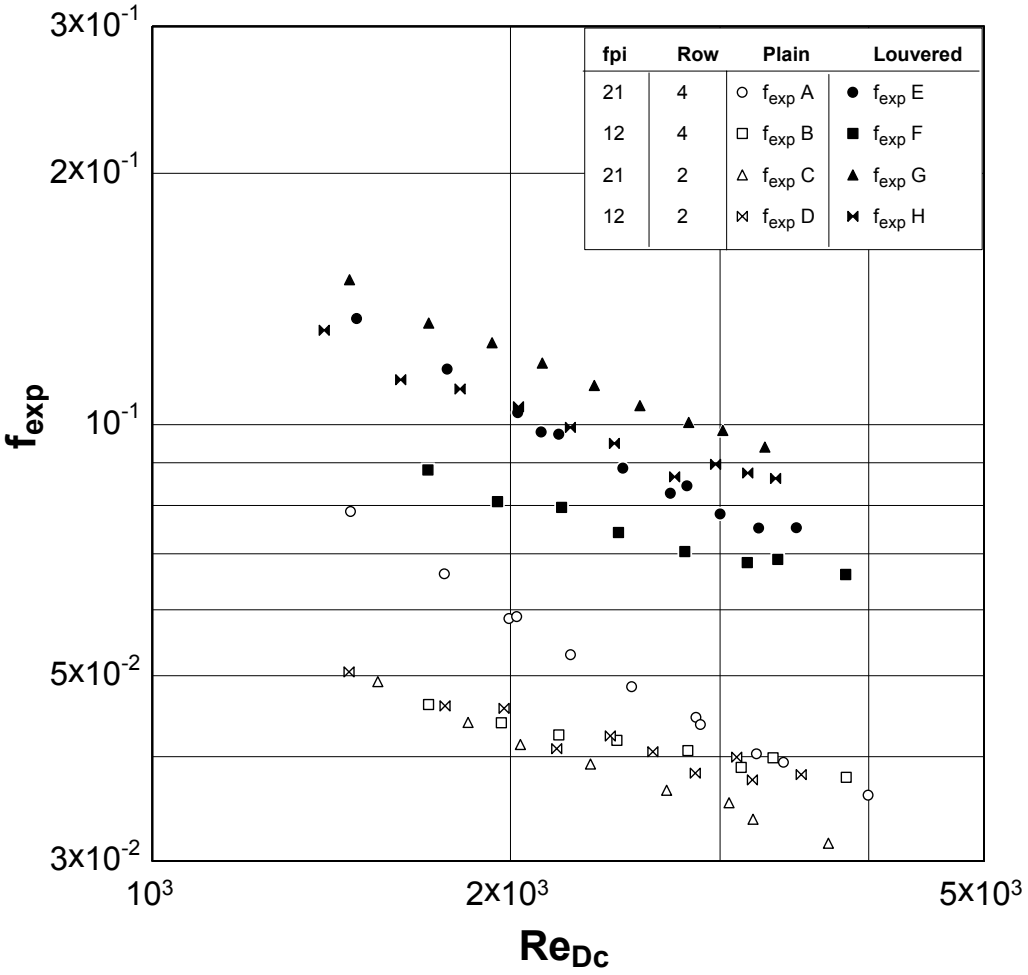

Figure 5.2. Fanning friction factor, *f*, for all coils

V.C: Uncertainty Analysis

The Engineering Equation Software was used to calculate the combined uncertainty of the indirectly measured Colburn *j* and the Fanning friction *f* factors. This is especially advantageous because of the transcendental nature of the *ε-NTU* relation. Uncertainty for both *j* factor and *f* factor data were calculated using values from Table 5.1. The uncertainty of each measure was calculated based on the accuracy of the instrumentation as discussed in Chapter III. As mentioned in Chapter III and Chapter IV the average heat transfer rate was used for calculation of the Colburn *j* factor, any

uncertainty in the calculated heat transfer rate from either the water side or air side is represented by the uncertainty in the measures. Error bars are plotted along with experimental data for each coil vs. Reynolds number based on tube diameter (including fin collar) in Figures 5.3 – 5.10. The uncertainty bars for the Colburn *j* factor are less than ±11% of the calculated Colburn *j* factor, with the exception of coil E which is ±14%. The uncertainty bars for the Fanning friction factor are less than ±5% of the calculated friction factor in all cases.

Table 5.1. Uncertainty of measurements

Measure	**Uncertainty**
Temperature [°F]	0.1
Water Flow Rate [lbm/hr]	165
Air Flow Rate [lbm/hr]	18
Differential Air Pressure [inH_2O]	0.002

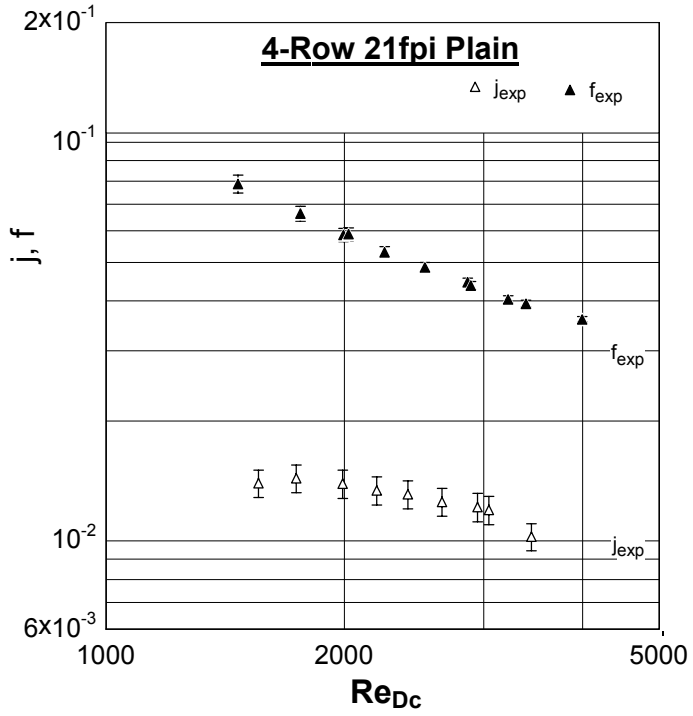

Figure 5.3. Coil A Data uncertainty

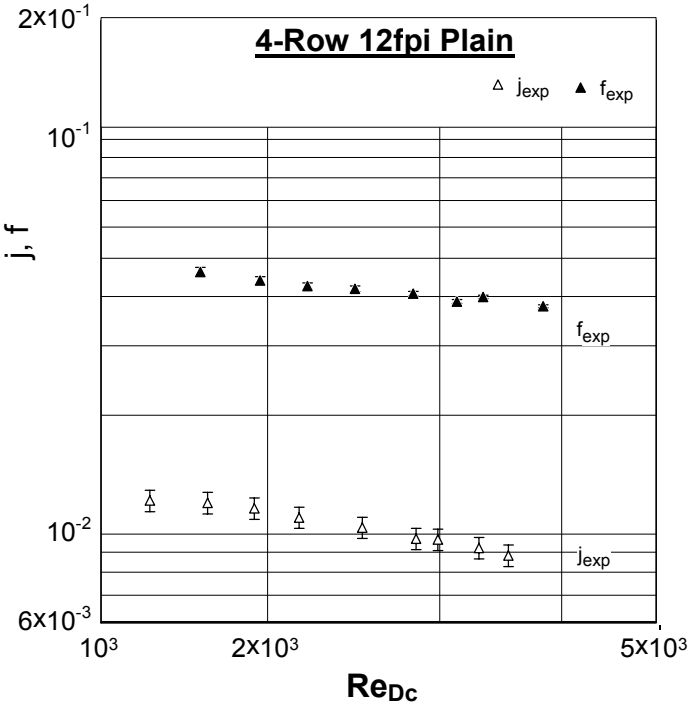

Figure 5.4. Coil B Data uncertainty

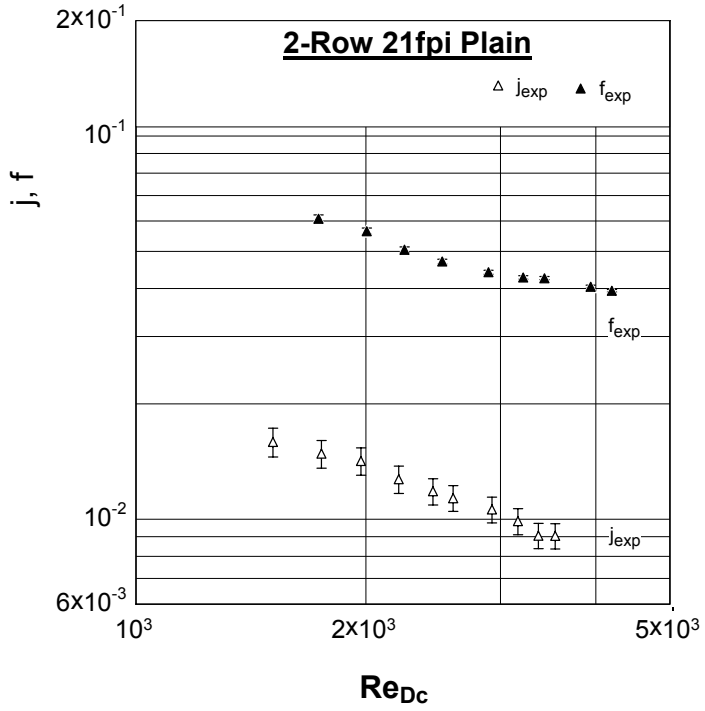

Figure 5.5. Coil C Data uncertainty

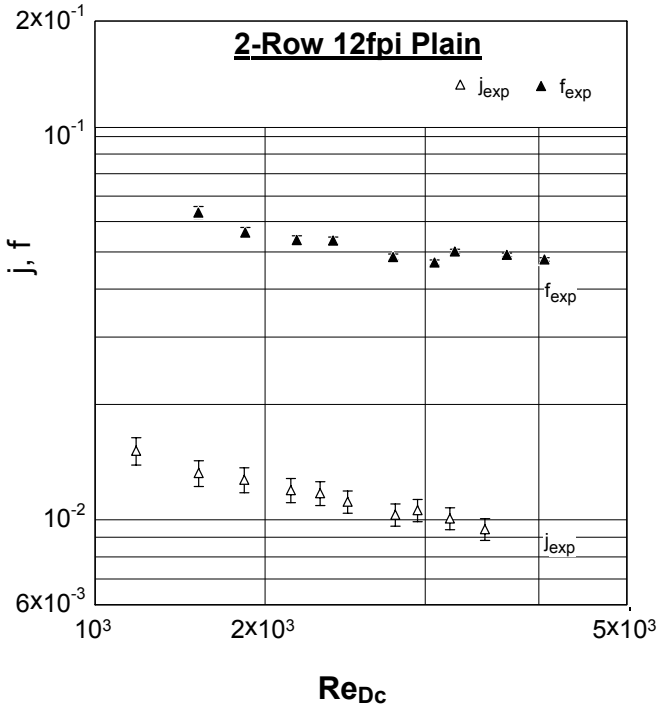

Figure 5.6. Coil D Data uncertainty

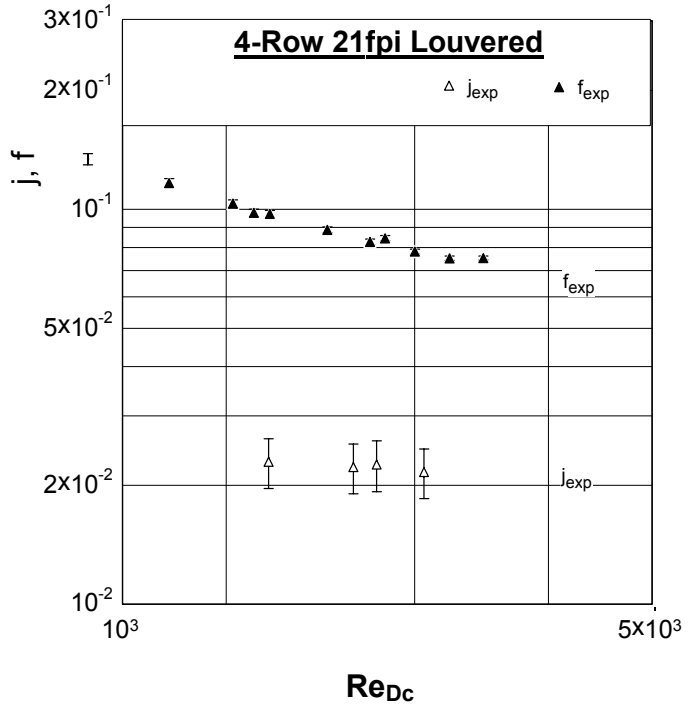

Figure 5.7. Coil E Data uncertainty

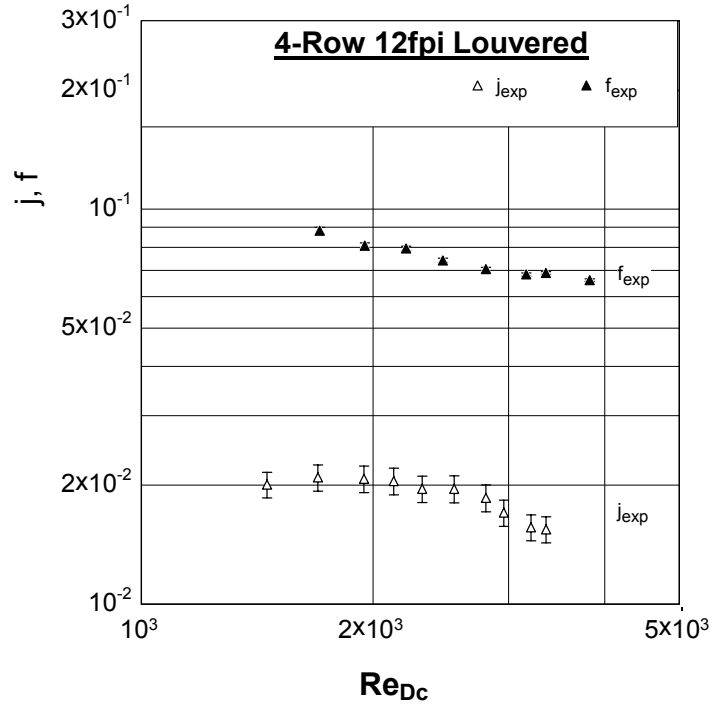

Figure 5.8. Coil F Data uncertainty

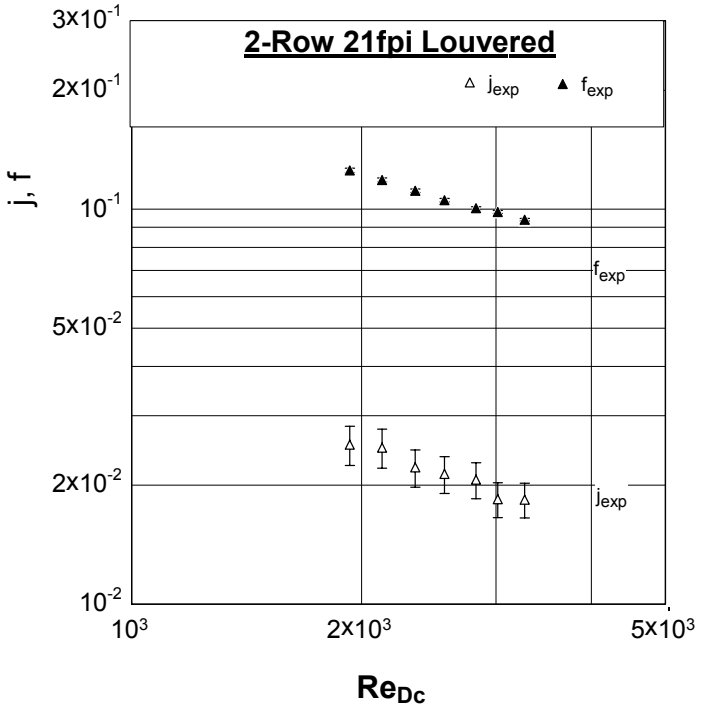

Figure 5.9. Coil G Data uncertainty

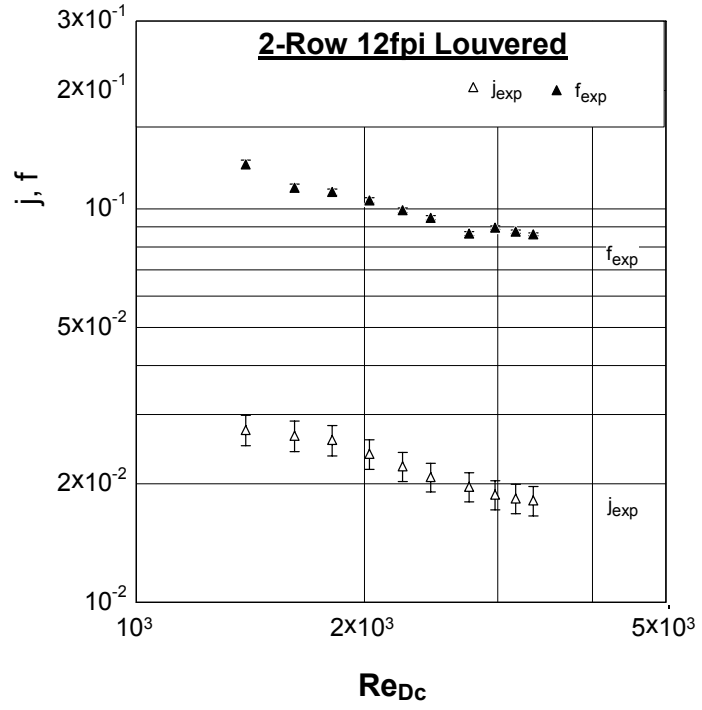

Figure 5.10. Coil H Data uncertainty

CHAPTER VI

ANALYSIS AND DISCUSSION

VI.A: Comparison of Heat Exchangers

The following section presents the graphical comparison of data sets in this present study. General trends in data are discussed qualitatively and compared with published trends from previous researchers. Graphical and quantitative comparisons of data with published correlations will be presented and discussed in section B.

It is informative to look at the performance of all of the 4-row coils in one plot. The Colburn *j* factor and the Fanning friction factor, *f*, are plotted for all 4-row heat exchangers vs. Reynolds number based on outside tube diameter (including the fin collar), Re_{Dc}, in Figure 6.1.

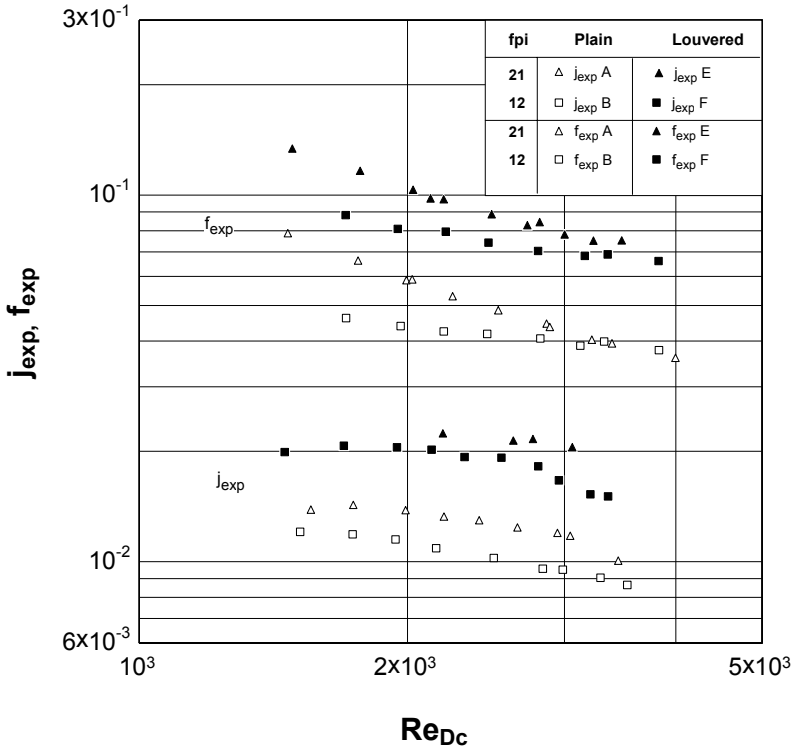

Figure 6.1. Colburn *j* factor and Fanning friction factor, *f*, for all 4-row coils

Similarly, it is informative to look at the performance of all of the 2-row coils in one plot. The Colburn *j* factor and the Fanning friction factor, *f*, are plotted for all 2-row heat exchangers vs. Re_{Dc} in Figure 6.2.

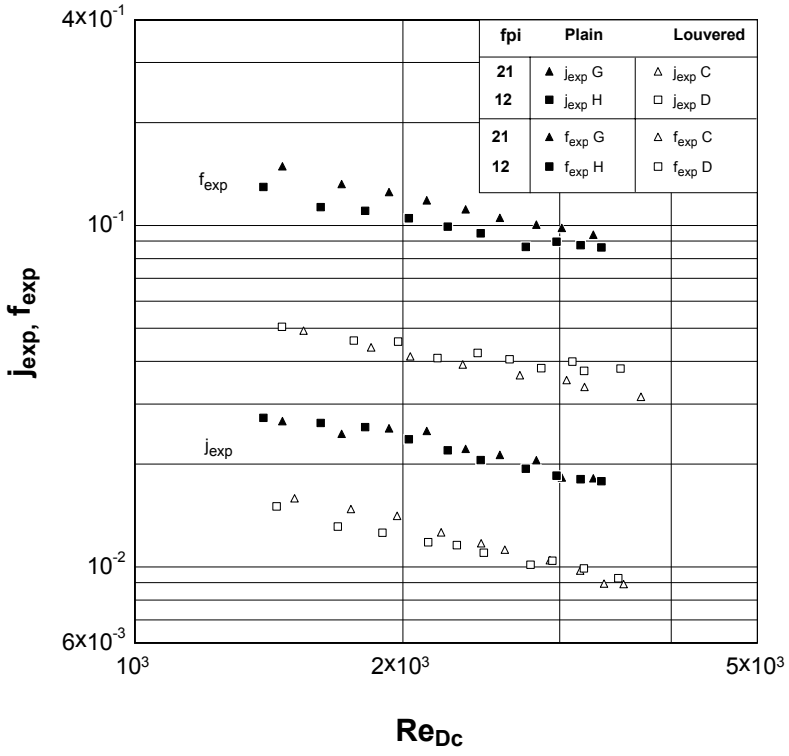

Figure 6.2. Colburn *j* factor and Fanning friction factor, *f*, for all 2-row coils

These plots are useful for comparison of over arching trends. In the following sections, data will be plotted in a number of graphical comparisons. However, the overall picture should not be overlooked.

VI.A.1 Row Dependence

The *j* and *f* characteristics of a 4-row coil and its 2-row counterpart are shown in Figures 6.3 - 6.6. At low Reynolds number the heat transfer coefficient for 4-row coils is generally lower than for 2-row coils, with all other parameters being equal. For 2-row coils, the *j* factor data is nearly linear with respect to Reynolds number when plotted on a log-log scale, while the 4-row coil is generally curved. These general characteristics agree with D.G. Rich's 1975 experimental study's trends specifically trends 1 and 4, as discussed in Chapter II. A graphical representation of Rich's data trends is shown in Figure 2.1. These general characteristics also agree with data used to develop correlations by Wang (1998b, 1998c, and 1999), as discussed in Chapter II. A possible explanation of this characteristic as proposed by Rich is that there are standing vortices behind the tubes in a heat exchanger especially with a high number of fins per inch at low Reynolds number and that at some critical value of Reynolds number these vortices break away. These vortices would reduce the effectiveness of the fins behind the tubes, because the flow into and out of the wake region is small compared with the mainstream flow. Also, because the bank of tubes is staggered the effect of the vortices would be to reduce the effectiveness of every second tube row. The characteristics of the friction factor are less apparent. Generally the friction factor for 2-row coils is higher than for 4-row coils, although this is not the case over the entire range of Reynolds number for coils A and C.

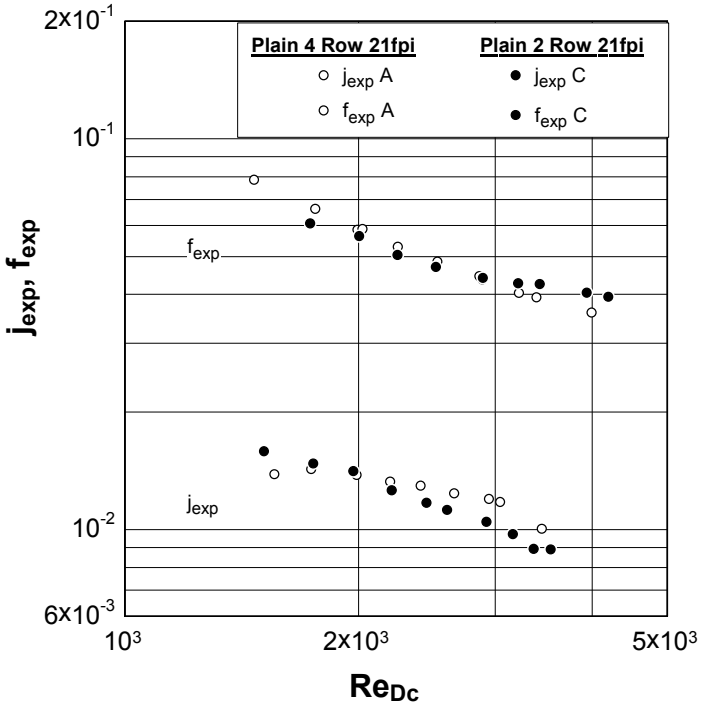

Figure 6.3. A-C *j* and *f* factors vs. Re_{Dc}

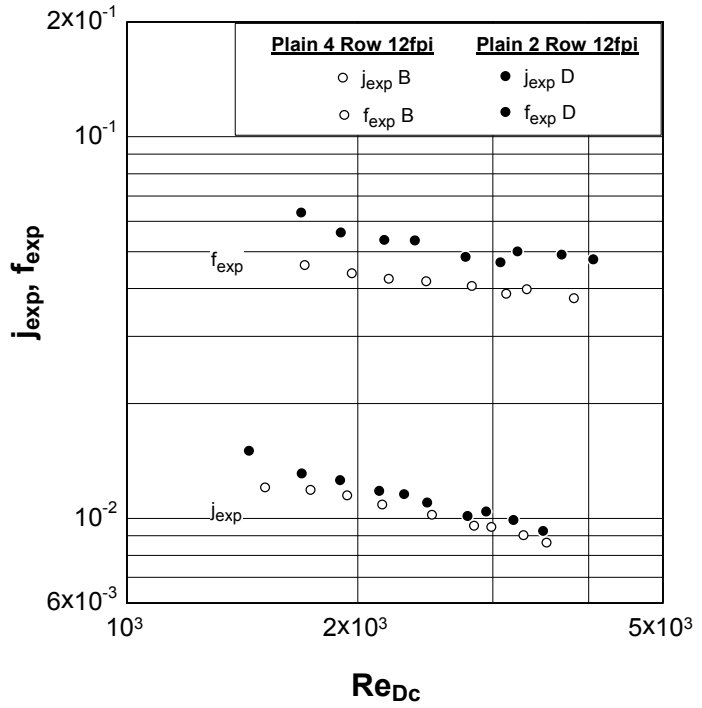

Figure 6.4. B-D *j* and *f* factors vs. Re_{Dc}

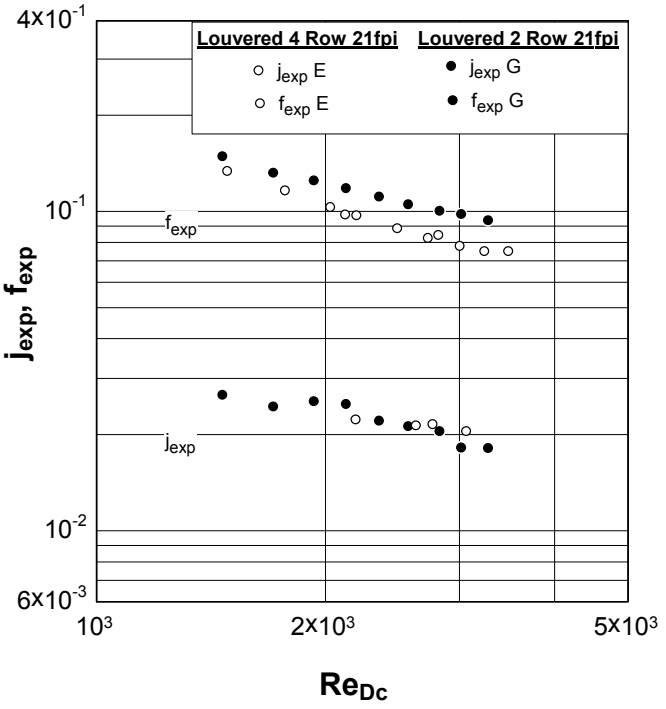

Figure 6.5. E-G *j* and *f* factors vs. Re_{Dc}

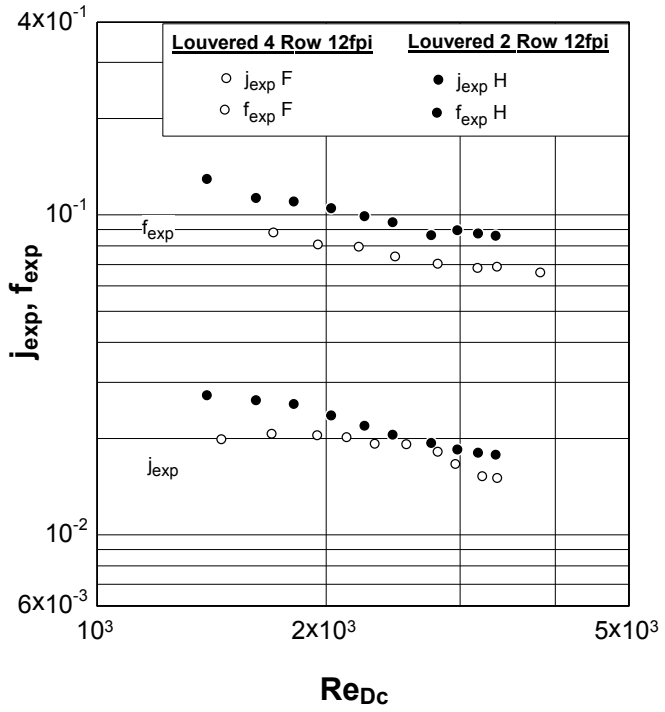

Figure 6.6. F-H *j* and *f* factors vs. Re_{Dc}

VI.A.2 Fin Dependence

The *j* and *f* characteristics of a 21 fpi coil and its 12 fpi counterpart are shown in Figures 6.7 - 6.10. The 2-row coils heat transfer data show little to no dependence on fin spacing, over the range of Reynolds numbers tested. The 4-row coils heat transfer data does show an increase in the heat transfer coefficient with the increase in fin spacing. Rich's 1973 experimental study's trends, as discussed in Chapter II, indicate that for 4-row coils the heat transfer coefficient is independent of fin spacing. Wang (1998c) states that for Reynolds number above 1,000 the heat transfer performance is independent of fin pitch for four-row configuration. He further states that for Reynolds number less than 1,000 the heat transfer performance is strongly related to fin pitch. At low Reynolds numbers, the friction factor for the 4-row 21 fpi coils is significantly higher than for the 4-row 12 fpi coils.

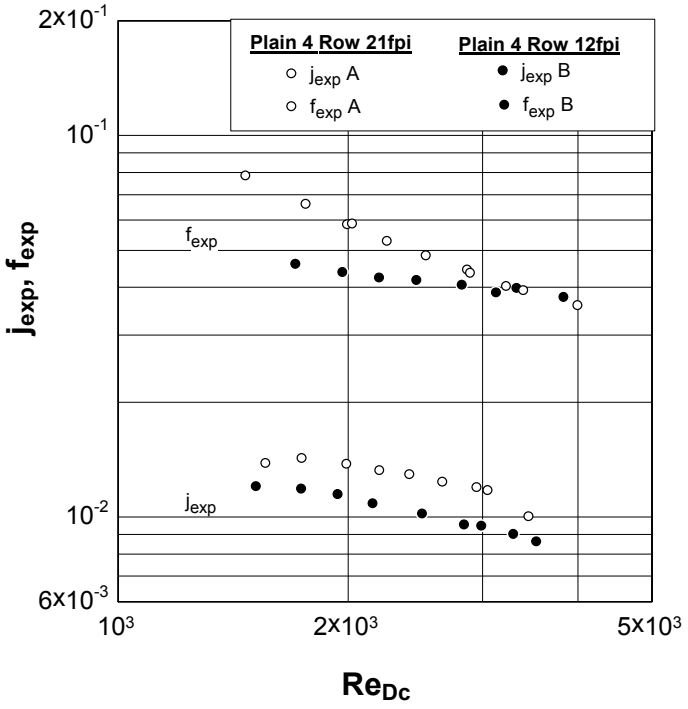

Figure 6.7. A-B *j* and *f* factors vs. Re_{Dc}

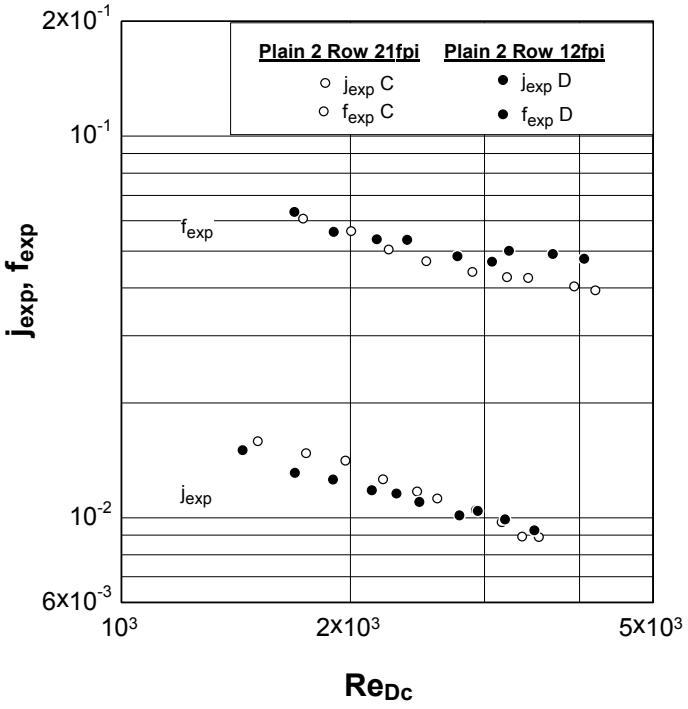

Figure 6.8. C-D *j* and *f* factors vs. Re_{Dc}

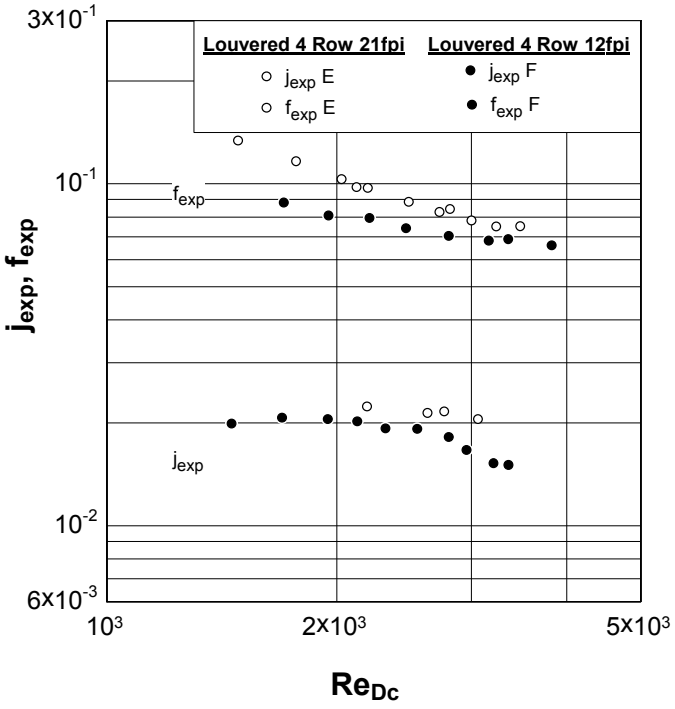

Figure 6.9. E-F *j* and *f* factors vs. Re_{Dc}

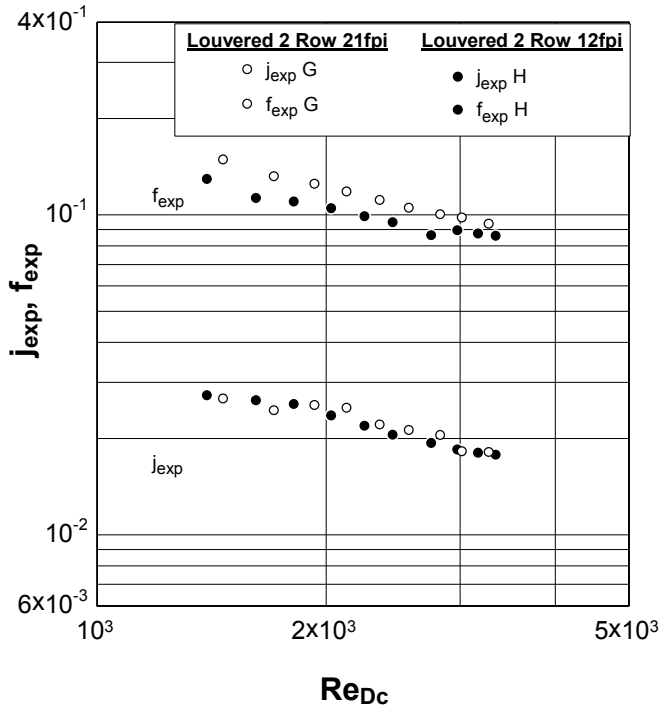

Figure 6.10. G-H *j* and *f* factors vs. Re_{Dc}

VI.A.3 Plain vs. Louvered

The *j* and *f* characteristics of a plain fin coil and its louvered fin counterpart are shown in Figures 6.11 - 6.14. As expected the louvered coils have higher *j* factors as well as higher fanning fin friction factors compared with plain coils because the louvers break and renew the boundary layer of the air flow. The *j* factors for louvered fin coils are 1.75 times higher than for plain fin coils, and the fanning friction factors for louvered coils are 1.7 – 2.2 times higher than for plain fin coils. The slope of the fanning friction factor for plain coils is close to the corresponding slope for louvered coils. Also, the slope of the *j* factor for plain coils is close to the corresponding slope for louvered coils.

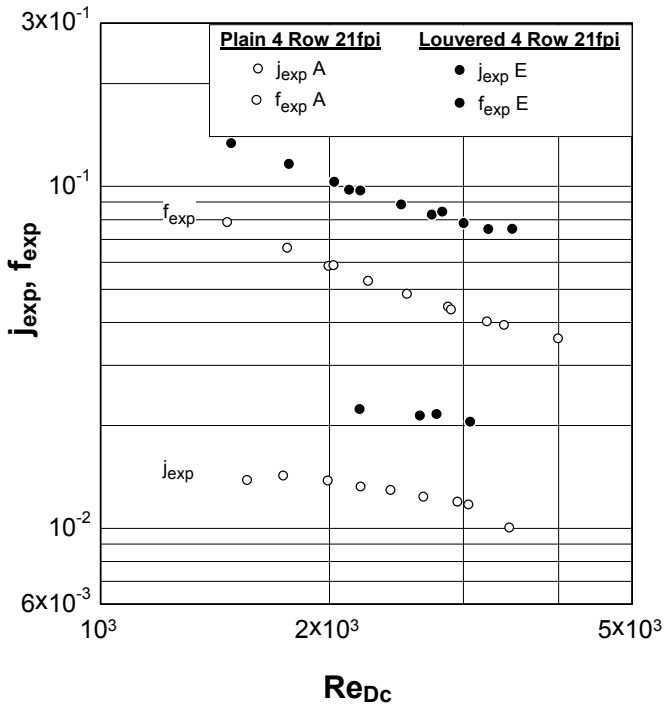

Figure 6.11. A-E *j* and *f* factors vs. Re_{Dc}

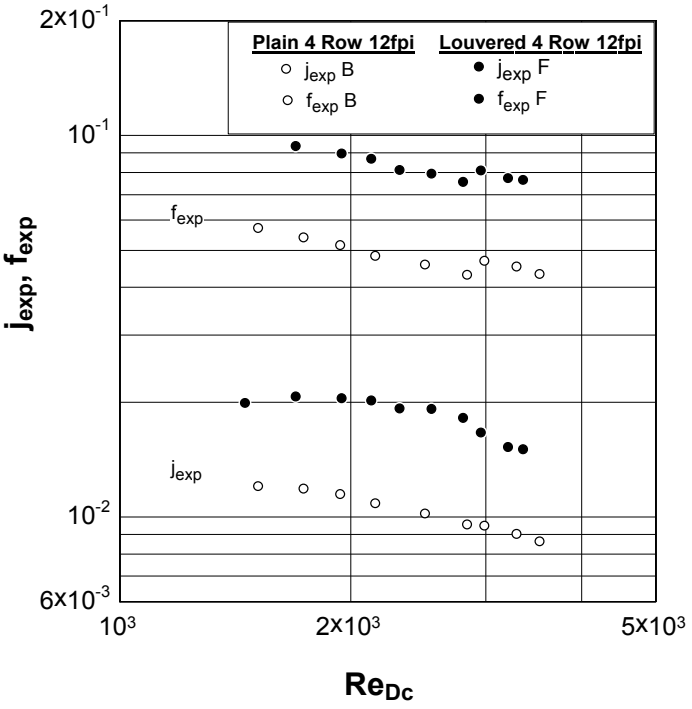

Figure 6.12. B-F *j* and *f* factors vs. Re_{Dc}

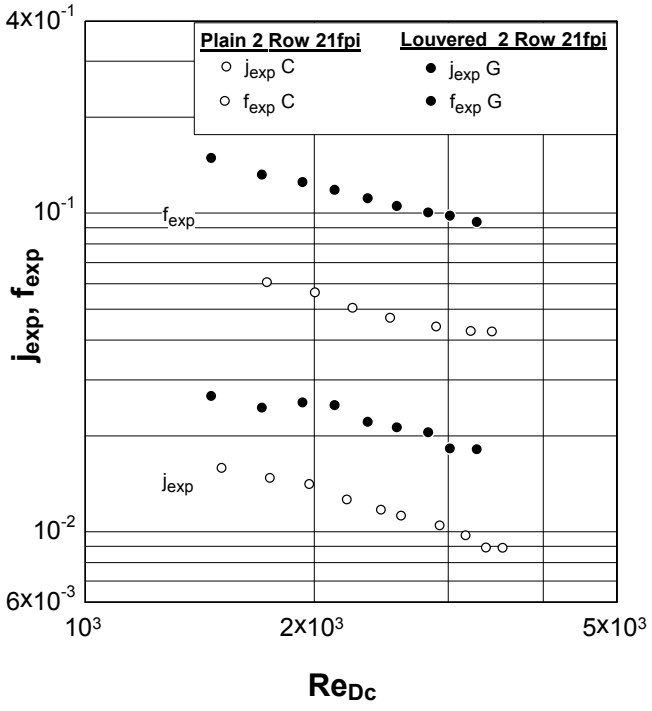

Figure 6.13. C-G *j* and *f* factors vs. Re_{Dc}

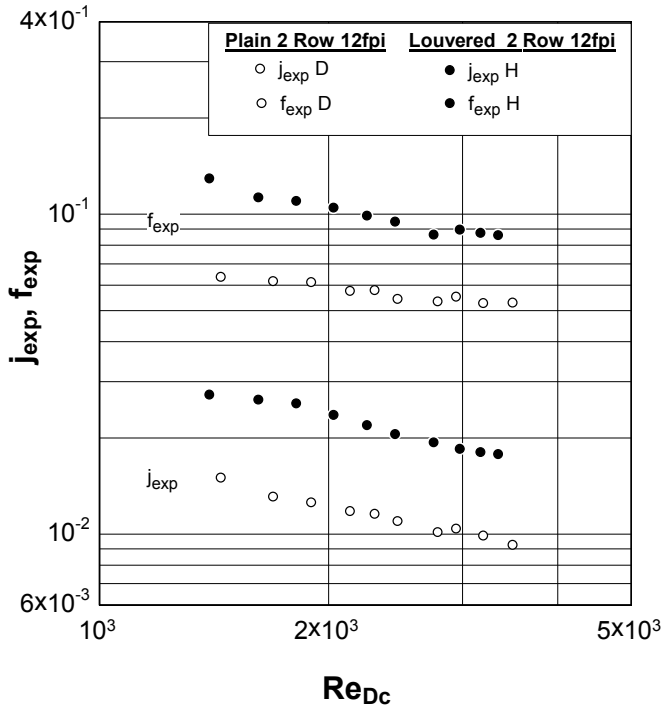

Figure 6.14. D-H *j* and *f* factors vs. Re_{Dc}

VI.B: Comparison with Available Correlations

This section describes in detail available plain and louvered fin coil correlations, and shows the accuracy of the correlations in predicting the experimental data. Again it should be reiterated that the correlation equations are given in the original nomenclature to maintain dimensional and historical consistency. Some of the most important nomenclature is shown in Table 2.1. Following the correlation equations, experimental data are plotted along with available correlations. Table 6.1 gives the correlation legend for identification of symbols within Figures 6.15 – 6.22.

It should be noted that all of the available correlations are for flat edge profile fins. Furthermore in the present study the fins had a rippled edge profile for the first and

last 0.1" in the flow direction, as shown in Figure I.3. The effect of this difference in fin geometry is not known.

Table 6.1. Correlation Legend

Correlation	Number of Rows	Fin Type	Subscript	Equation(s)
Rich (1973)	4	Plain	r	6.1 - 6.2.
McQuiston (1978)	2,4	Plain	m	6.3 - 6.8
Webb (1986)	2,4	Plain	wg	6.9 - 6.10
Wang (1999)	2,4	Plain	wp	6.11 - 6.19
Modified Wang (1999)	2,4	Plain	wp,m	6.16 - 6.19
Webb (1998)	2	Louvered	wk	6.20
Wang (1998b)	2,4	Louvered	wl	6.21 - 6.31
Modified Wang (1998b)	2,4	Louvered	wl,m	6.21 - 6.31

VI.B.1: Plain Fin Coil Correlations

Rich (1973) developed plain fin coil correlations for Colburn *j* factor and Fanning friction factor based on data from eight coil configurations. These configurations were all 4-row plain fin coils with a tube diameter of 0.525 in. and fin spacing between 3 and 20 fins/in, as seen in Figure 2.3. Rich's correlations for *j* and *f* factors are:

$$j_r = 0.195 \cdot Re_L^{-0.35} \quad 3 < N_f < 20 \text{ fins/in} \tag{6.1}$$

$$f_r = 1.70 \cdot Re_L^{-0.5} \quad 3 < N_f < 14 \text{ fins/in} \tag{6.2}$$

The correlation parameter is the Reynolds number based on longitudinal tube spacing. Differences between Rich's test coils and this current study's test coils include the following: tube diameter, longitudinal tube spacing, transverse tube spacing, fin thickness and fin edge profile.

F.C. McQuiston (1978) developed plain fin coil correlations for Colburn *j* factor and Fanning friction factor based on data from eight plain fin coils configurations. McQuiston's correlations for *j* and *f* factors are:

$$j_{m,4} = 0.0014 + 0.2618 \cdot (JP) \tag{6.3}$$

$$JP = Re_D^{-0.4} \left[\left(\frac{4}{\pi} \right) \left(\frac{X_b}{D_h} \right) \left(\frac{X_a}{D} \right) \sigma \right]^{-0.15} \tag{6.4}$$

$$j_{m,n} = \left[\frac{1 - 1280 \cdot N_r \cdot Re_b^{-1.2}}{1 - 5120 \cdot Re_b^{-1.2}} \right] \left[0.0014 + 0.2618 \cdot (JP) \right] \tag{6.5}$$

$$f_{m,4} = f_{m,n} = 0.004904 + 1.382 \cdot (FP)^2 \tag{6.6}$$

$$FP = Re_D^{-0.25} \left(\frac{R}{R^*} \right)^{0.25} \left[\frac{\left(X_a - 2R \right) P_s}{4\left(1 - P_s y \right)} \right]^{-0.4} \left[\frac{X_a}{2R^*} - 1 \right]^{-0.5} \tag{6.7}$$

$$\frac{R}{R^*} = \frac{\left(X_a - 2R \right) P_s + 1}{\left(A_o / A_t \right)} \tag{6.8}$$

McQuiston defines two correlation parameters: one to correlate *j* factor, *JP*, and one to correlate *f* factor, *FP*. Both have a dependence on Reynolds number as well as longitudinal and transverse tube spacing. The Reynolds number used in the correlations parameters is Reynolds number based on the outer tube diameter. The square bracketed

term in Equation 6.4 is equal to the total air side surface area divided by the tube area. Table 2.3 and Figure 2.3 show the range of parameters used to develop these correlations. Differences between McQuiston's test coils and this current study's test coils include the following: longitudinal tube spacing, fin spacing and fin edge profile.

Webb and Gray (1986) developed plain fin coil correlations for Colburn *j* factor and Fanning friction factor based on data from sixteen plain fin coil configurations. Webb's correlations for the *j* and *f* factors are:

$$j_{wg} = 0.14 Re_D^{-0.328} \left(\frac{S_t}{S_l} \right)^{-0.502} \left(\frac{s}{D} \right)^{0.0312} \tag{6.9}$$

$$f_{wg} = 0.508 Re_D^{-0.521} \left(\frac{S_t}{D} \right)^{1.318} \tag{6.10}$$

The correlation parameter is the Reynolds number, based on the outer tube diameter. Table 2.4 and Figure 2.3 show the range of parameters used to develop these correlations. Differences between Webb's test coils and this current study's test coils include the following: tube diameter and fin edge profile.

Wang (1999) developed plain fin coil correlations for Colburn *j* factor and Fanning friction factor based on data from 74 coil configurations. Wang's correlations for the *j* and *f* factors are:

$$j_{wp} = 0.086 Re_D^{P3} N^{P4} \left(\frac{F_p}{D_c} \right)^{P5} \left(\frac{F_p}{D_h} \right)^{P6} \left(\frac{F_p}{P_t} \right)^{-0.93} \tag{6.11}$$

$$P3 = -0.361 - \frac{0.042N}{\ln\left(Re_D\right)} + 0.158\ln\left(N\left(\frac{F_p}{D_c}\right)^{0.41}\right) \tag{6.12}$$

$$P4 = -1.224 - \frac{0.076\left(\frac{P_l}{D_h}\right)^{1.42}}{\ln\left(Re_D\right)} \tag{6.13}$$

$$P5 = -0.083 + \frac{0.058N}{\ln\left(Re_D\right)} \tag{6.14}$$

$$P6 = -5.735 + 1.21 \cdot \ln\left(\frac{Re_D}{N}\right) \tag{6.15}$$

$$f_{wp} = 0.0267 Re_D^{F1}\left(\frac{P_t}{P_l}\right)^{F2}\left(\frac{F_p}{D_c}\right)^{F3} \tag{6.16}$$

$$F1 = -0.764 + 0.739\frac{P_t}{P_l} + 0.177\frac{F_p}{D_c} - \frac{0.00758}{N} \tag{6.17}$$

$$F2 = -15.689 + \frac{64.021}{\ln\left(Re_D\right)} \tag{6.18}$$

$$F3 = 1.696 - \frac{15.695}{\ln\left(Re_D\right)} \tag{6.19}$$

Wang defines multiple correlation parameters: one set for *j* factor, *P3 – P6*, and one set for *f* factor, *F1 – F3*. These parameters include the dependence on number of rows, fin pitch, hydraulic diameter, transverse tube spacing, and longitudinal tube spacing. Table 2.5 and Figure 2.3 show the range of parameters used to develop these correlations. The only difference between Wang's test coils and this current study's test coils is the fin edge profile.

All investigated plain fin correlations under predict the friction factor data. Therefore, a modified version of the Fanning friction correlation developed by Wang (1999) was fit to this current study's data. The only modification necessary was to increase the leading coefficient in Equation 6.16 from 0.0267 to 0.0335.

The plain fin coil experimental data from this current study is plotted along with correlations in Figures 6.15 - 6.18.

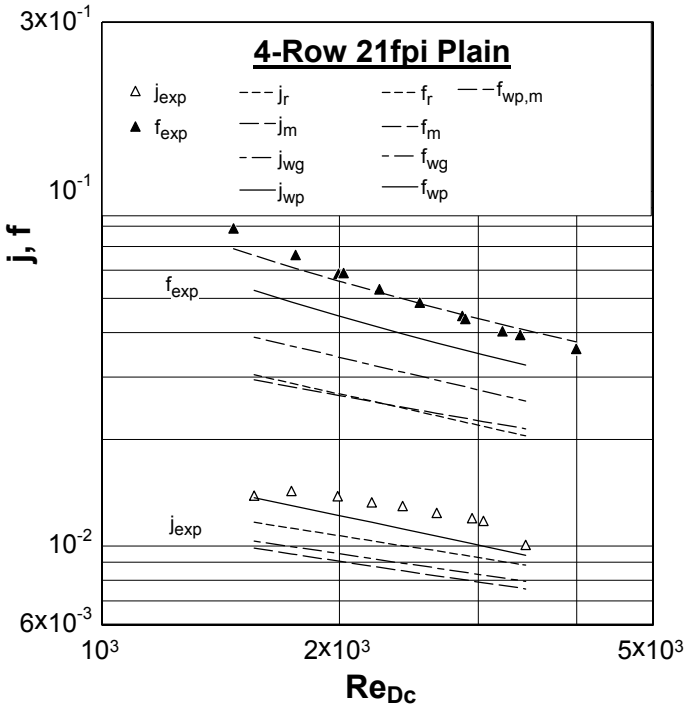

Figure 6.15. Data & Correlations :Coil A

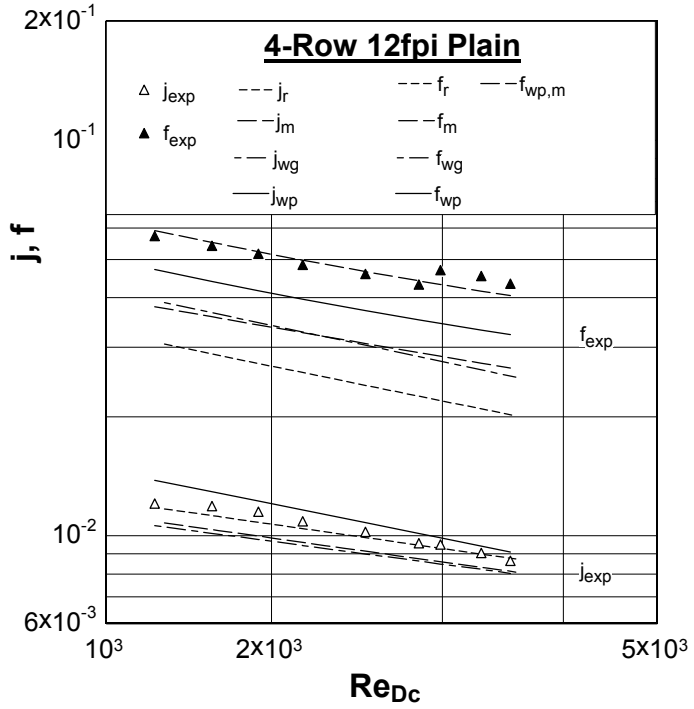

Figure 6.16. Data & Correlations :Coil B

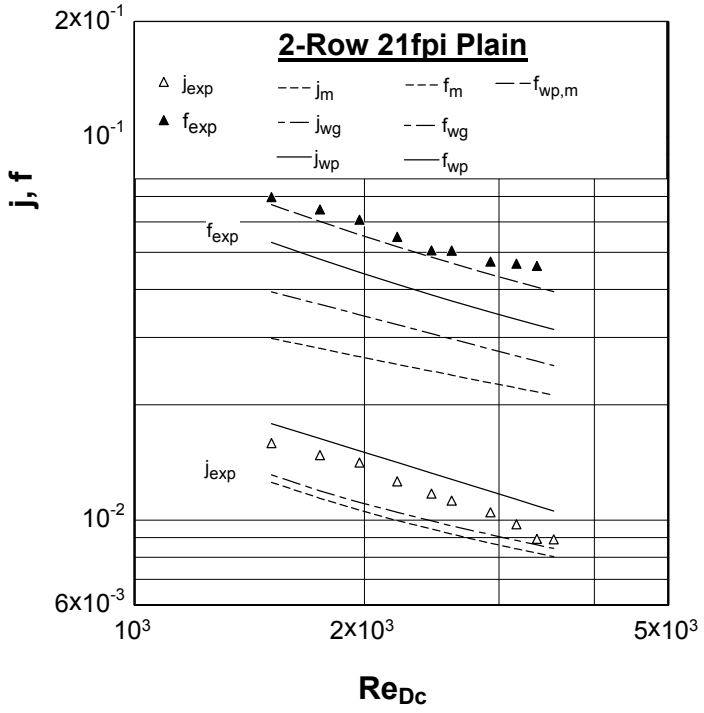

Figure 6.17. Data & Correlations :Coil C

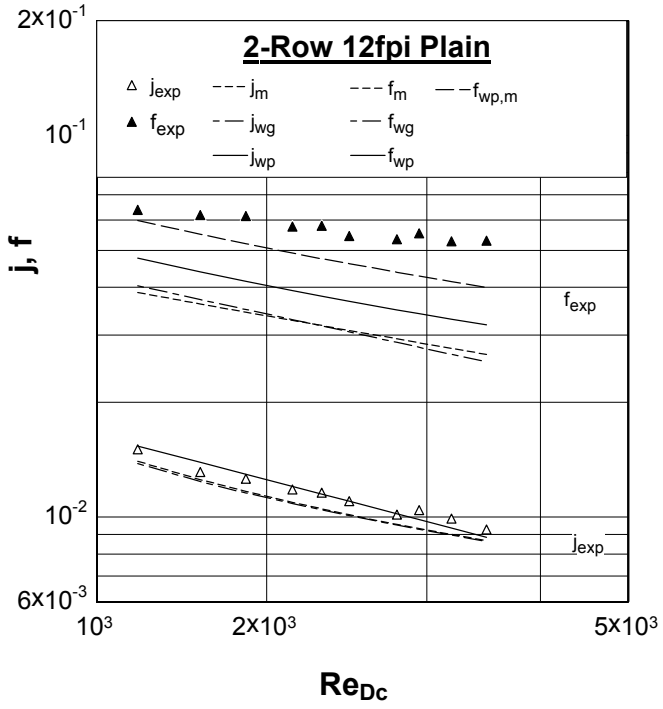

Figure 6.18. Data & Correlations :Coil D

VI.B.2: Louvered Correlations

Webb and Kang (1998) developed a Colburn *j* factor correlation for louvered fin coils based on data from nine different coil configurations (1 and 2 row coils only). Webb and Kang's correlation for the *j* factor is:

$$j_{wk} = 0.660 Re_{Ls}^{-0.544} \left(\frac{A_{lou}}{A_{fin}} \right)^{0.637} \tag{6.20}$$

A friction factor correlation was not included in the publication. The correlation parameter is the Reynolds number, based on the "strip length" of the louvers in the flow direction. Notice that common correlation parameters are not included in this correlation, such as tube diameter, transverse tube spacing, longitudinal spacing, fin thickness and fin

pitch. Table 2.6 and Figure 2.3 show the range of parameters used to develop this correlation. The only difference between Webb's test coils and this current study's test coils is the fin edge profile.

Wang (1998b) developed louvered fin coil correlations for Colburn j factor and Fanning friction factor based on data from 49 coil configurations. Wang's correlations for the *j* and *f* factors are:

$$j_{wl} = 1.1373 Re_D^{J5} \left(\frac{F_p}{P_l}\right)^{J6} \left(\frac{L_h}{L_p}\right)^{J7} \left(\frac{P_l}{P_t}\right)^{J8} (N)^{0.3545} \tag{6.21}$$

$$J5 = -0.6027 + 0.02593 \left(\frac{P_l}{D_h}\right)^{0.52} (N)^{-0.5} \ln\left(\frac{L_h}{L_p}\right) \tag{6.22}$$

$$J6 = -0.4776 + 0.40774 \left(\frac{N^{0.7}}{\ln(Re_D) - 4.4}\right) \tag{6.23}$$

$$J7 = -0.58655 \left(\frac{F_p}{D_h}\right)^{2.3} \left(\frac{P_l}{P_t}\right)^{-1.6} N^{-0.65} \tag{6.24}$$

$$J8 = 0.0814 \left(\ln(Re_D) - 3\right) \tag{6.25}$$

$$f_{wl} = 0.06393 Re_D^{F5} \left(\frac{F_p}{D_c}\right)^{F6} \left(\frac{D_h}{D_c}\right)^{F7} \left(\frac{L_h}{L_p}\right)^{F8} N^{F9} \left(\ln(Re_D) - 4.0\right)^{-1.093} \tag{6.26}$$

$$F5 = 0.1395 - 0.0101 \left(\frac{F_p}{P_l}\right)^{0.58} \left(\frac{L_h}{L_p}\right)^{-2} \left[\ln\left(\frac{A_o}{A_t}\right)\right] \left(\frac{P_l}{P_t}\right)^{1.9} \tag{6.27}$$

$$F6 = -6.4367 \left(\frac{1}{\ln(Re_D)}\right) \tag{6.28}$$

$$F7 = 0.07191 \cdot \ln\left(Re_D\right) \tag{6.29}$$

$$F8 = -2.0585\left(\frac{F_p}{P_t}\right)^{1.67} \ln\left(Re_D\right) \tag{6.30}$$

$$F9 = 0.1036 \cdot \ln\left(\frac{P_l}{P_t}\right) \tag{6.31}$$

Similar to his earlier correlation, Wang defines multiple correlation parameters: one set for *j* factor, *J5 – J8*, and one set for *f* factor, *F5 – F9*. These parameters include the dependence on number of rows, fin pitch, hydraulic diameter, transverse tube spacing, longitudinal tube spacing, louver height and major louver pitch. Table 2.7 and Figure 2.3 show the range of parameters used to develop this correlation. Differences between Wang's test coils and this current study's test coils include the following: the longitudinal tube spacing, major louver pitch, and the fin edge profile.

The louvered correlations developed by Wang (1998b) over predict the Colburn *j* factor data and under predict the Fanning friction factor data. Therefore a modified version of the Colburn *j* and Fanning friction correlations developed by Wang (1998b) were fit to this current study's data. Three modifications were necessary to fit the data: the leading coefficient in Equation 6.21 was changed from 1.1373 to 0.978078, the leading coefficient in Equation 6.26 was changed from 0.06393 to 0.09081, and the leading coefficient in Equation 6.31 was changed from 0.1036 to 0.8088.

The louvered fin coil experimental data from this study is plotted along with correlations in Figures 6.19 - 6.22.

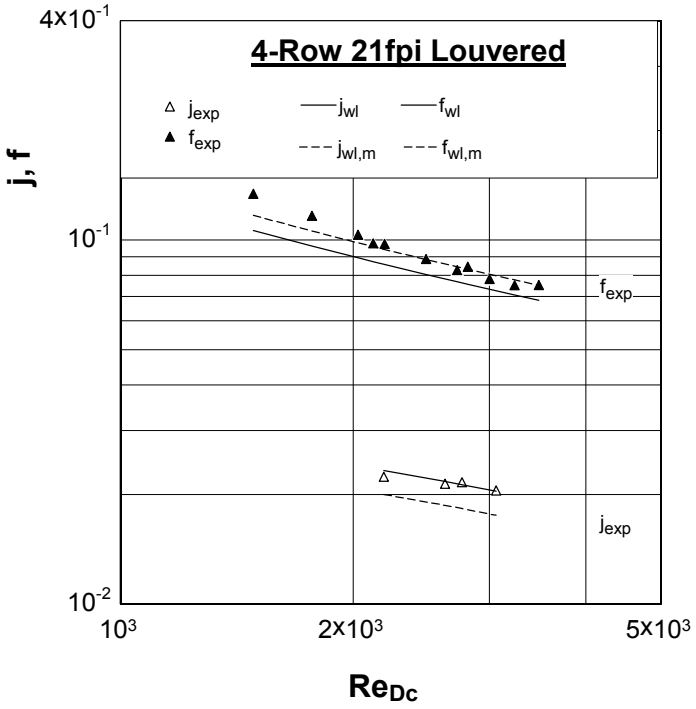

Figure 6.19. Data & Correlations :Coil E

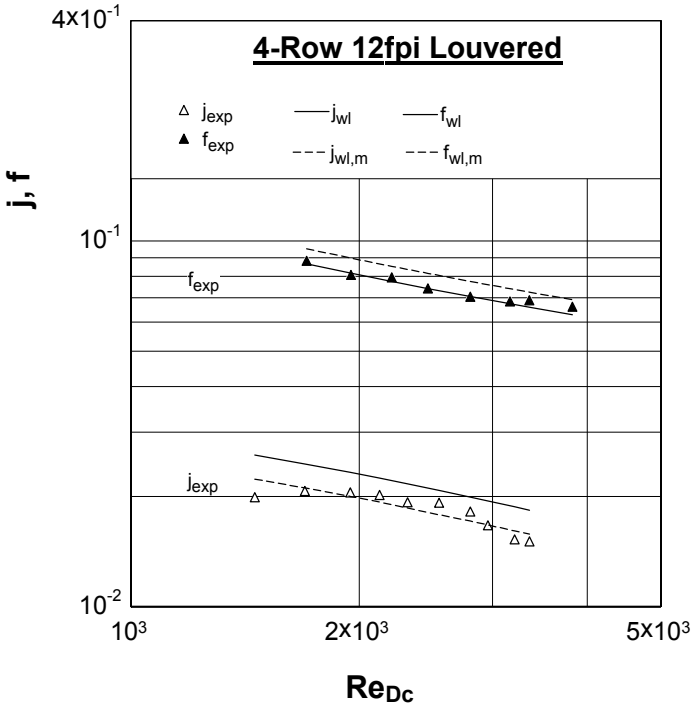

Figure 6.20. Data & Correlations :Coil F

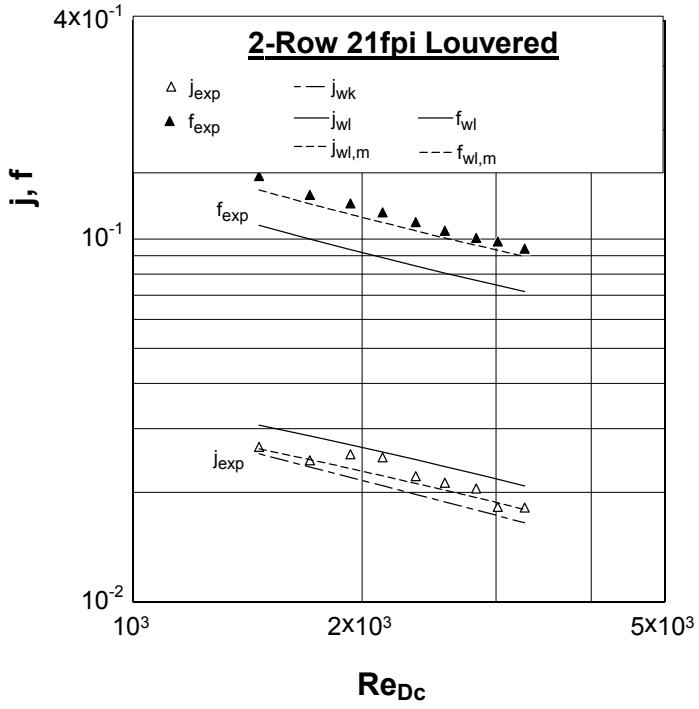

Figure 6.21. Data & Correlations :Coil G

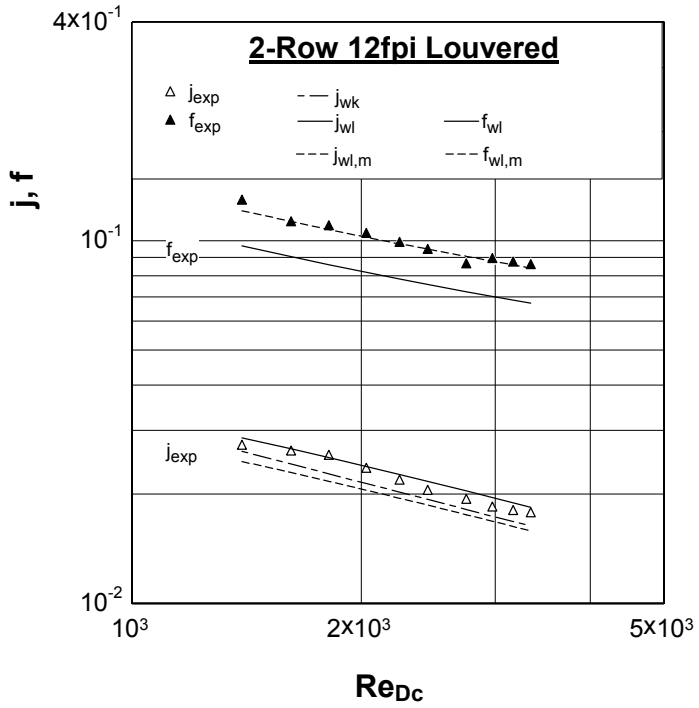

Figure 6.22. Data & Correlations :Coil H

VI.B.3: Overall Agreement of Correlations and Experimental Data

The overall agreement of Rich's (1973) *j* and *f* factor plain fin coil correlations to experimental data can be seen in Figures 6.23 and 6.24. The *j* factor figure shows the correlation, a 23% error band (the maximum deviation) and the appropriate experimental data from this research. The *f* factor figure shows the correlation, a 60% error band (the maximum deviation) and the appropriate experimental data from this research.

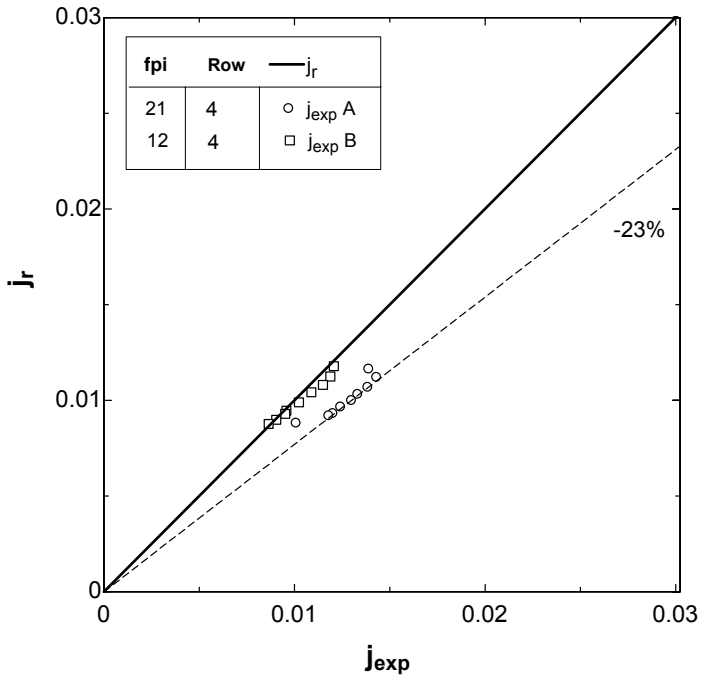

Figure 6.23. Rich's plain *j* factor

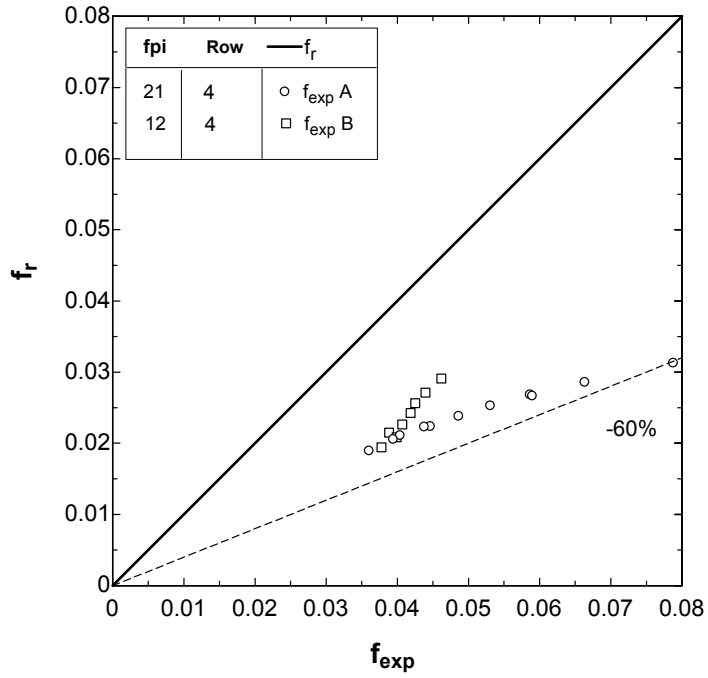

Figure 6.24. Rich's plain *f* factor

The overall agreement of McQuiston's (1978) *j* and *f* factor plain fin coil correlations to experimental data can be seen in Figures 6.25 and 6.26. The *j* factor figure shows the correlation, a 34% error band (the maximum deviation) and the appropriate experimental data from this research. The *f* factor figure shows the correlation, a 62% error band (the maximum deviation) and the appropriate experimental data from this research.

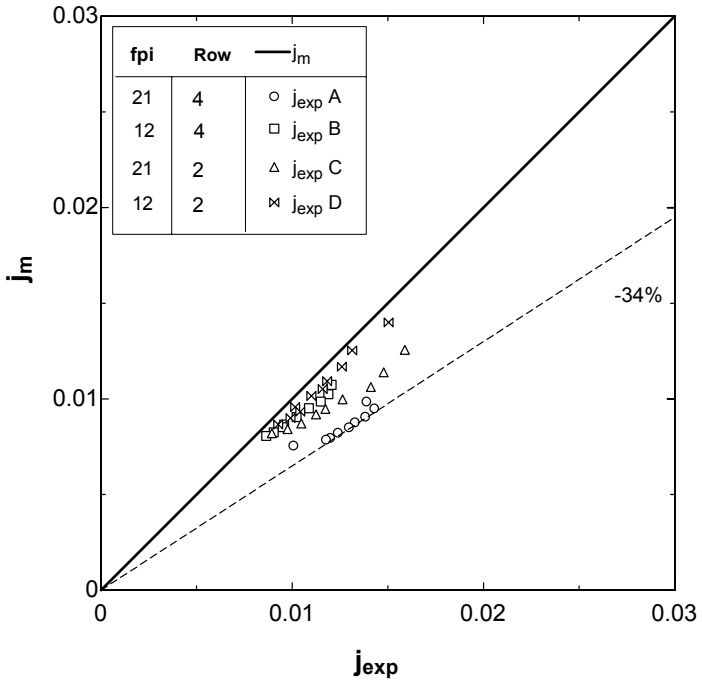

Figure 6.25. McQuiston's plain *j* factor

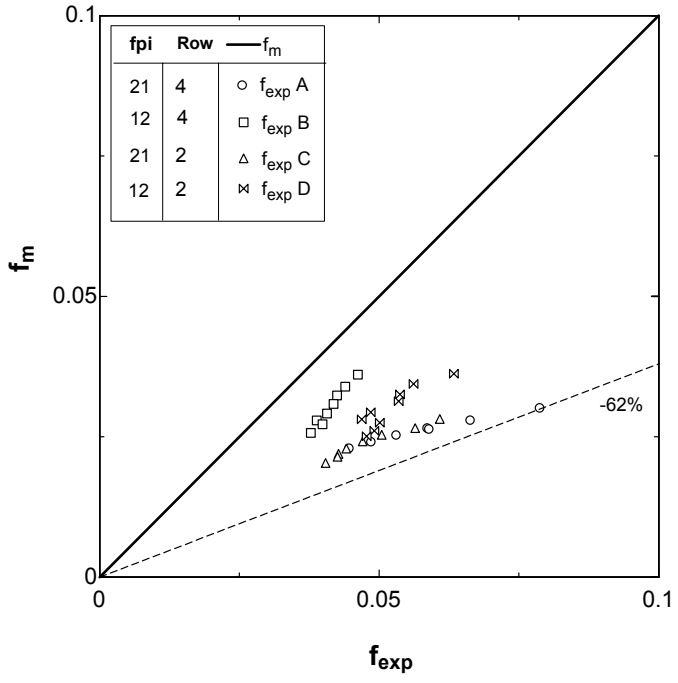

Figure 6.26. McQuiston's plain *f* factor

The overall agreement of Webb's (1986) *j* and *f* factor plain fin coil correlations to experimental data can be seen in Figures 6.27 and 6.28. The *j* factor figure shows the correlation, a 31% error band (the maximum deviation) and the appropriate experimental data from this research. The *f* factor figure shows the correlation, a 51% error band (the maximum deviation) and the appropriate experimental data from this research.

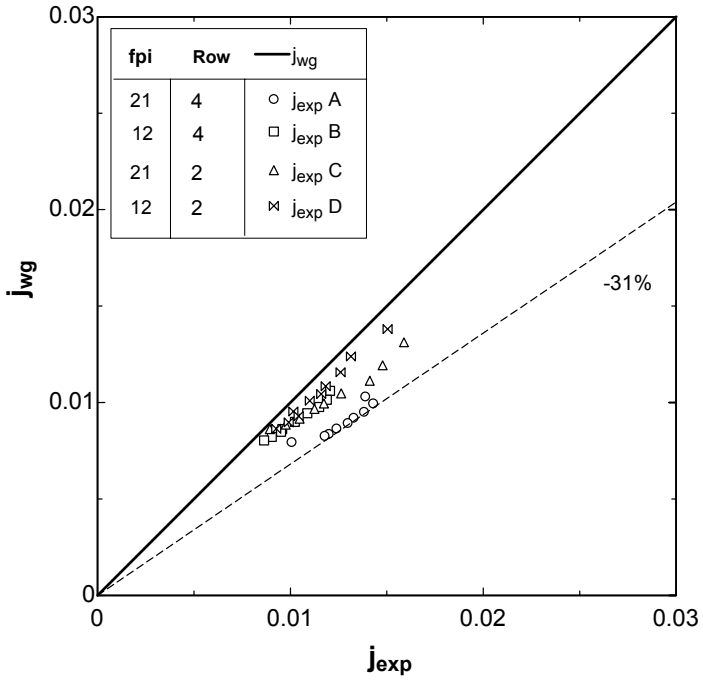

Figure 6.27. Webb's plain *j* factor

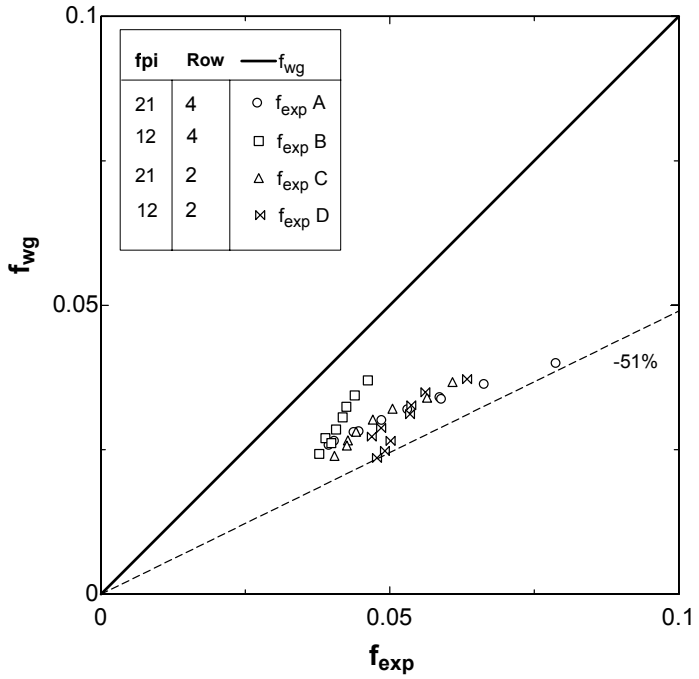

Figure 6.28. Webb's plain *f* factor

The overall agreement of Wang's (1999) *j* and *f* factor plain fin coil correlations to experimental data can be seen in Figures 6.29 and 6.30. The *j* factor figure shows the correlation, a 22% error band (the maximum deviation), a 15% error band and the appropriate experimental data from this research. The *f* factor figure shows the correlation, a 37% error band (the maximum deviation) and the appropriate experimental data from this research.

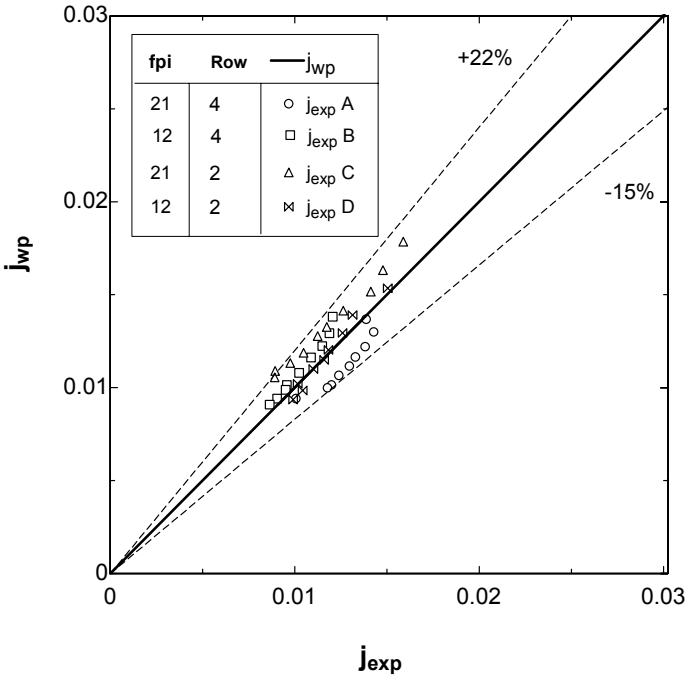

Figure 6.29. Wang's plain *j* factor

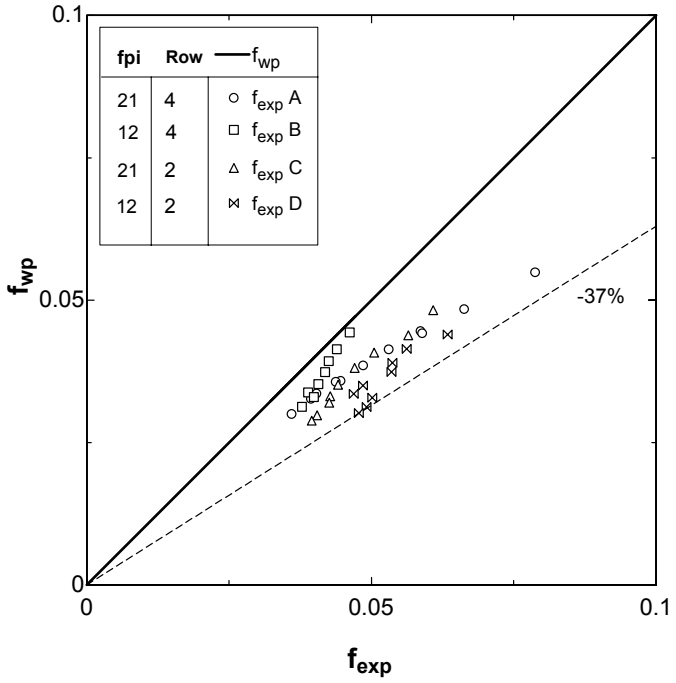

Figure 6.30. Wang's plain *f* factor

The overall agreement of the modified Wang (1999) *f* factor plain fin coil correlations to experimental data can be seen in Figure 6.31. This figure shows the correlation, a 21% error band (the maximum deviation), a 20% error band and the appropriate experimental data from this research.

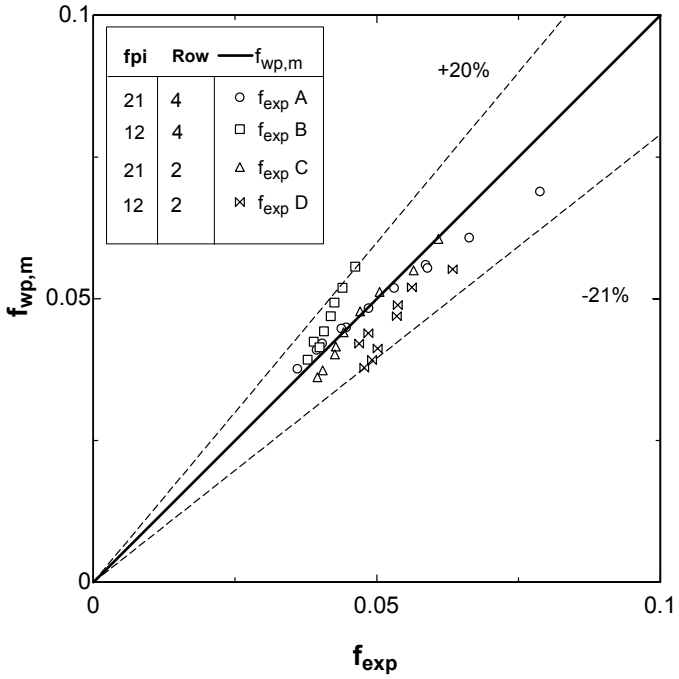

Figure 6.31. Modified Wang plain *f* factor

The overall agreement of Webb and Kang's *j* factor louvered fin coil correlation to experimental data can be seen in Figure 6.31. This figure shows the correlation, a 16% error band (the maximum deviation) and the appropriate experimental data from this research.

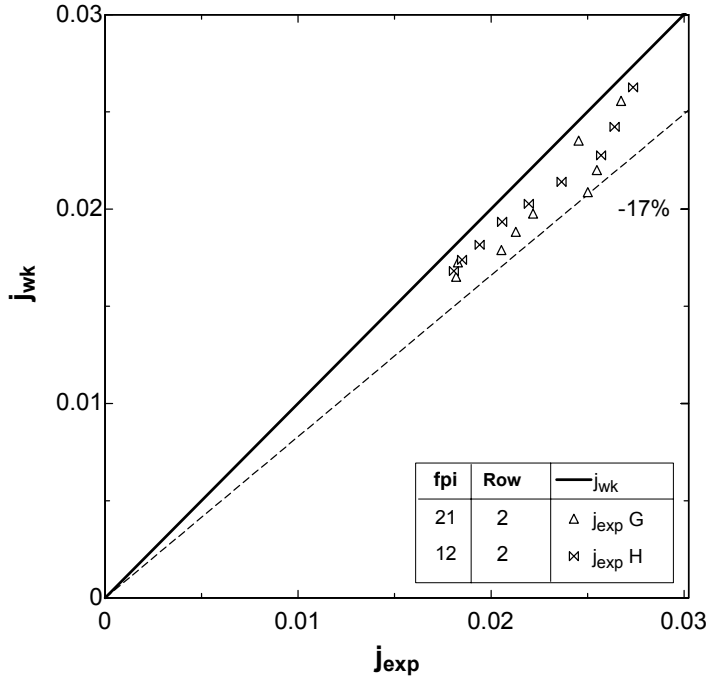

Figure 6.32. Webb's louvered *j* factor

The overall agreement of Wang's *j* and *f* factor louvered fin coil correlations to experimental data can be seen in Figures 6.32 and 6.33. The *j* factor figure shows the correlation, a 29% error band (the maximum deviation) and the appropriate experimental data from this research. The *f* factor figure shows the correlation, a 27% error band (the maximum deviation) and the appropriate experimental data from this research.

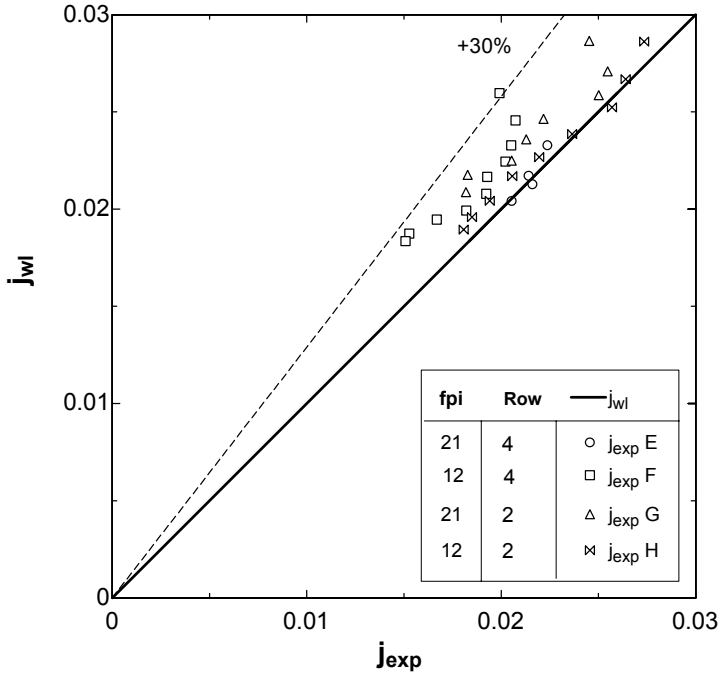

Figure 6.33. Wang's louvered *j* factor

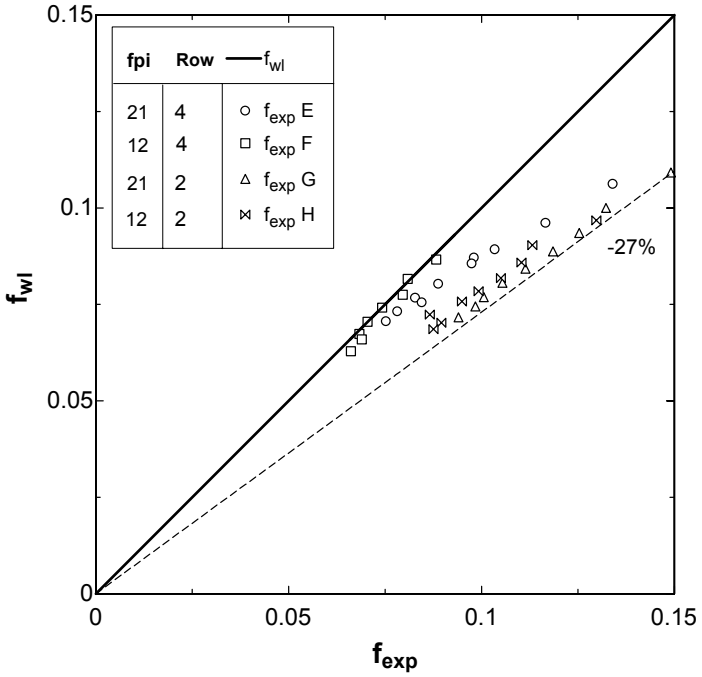

Figure 6.34. Wang's louvered *f* factor

The overall agreement of the modified Wang (1998b) *j* and *f* factor louvered fin coil correlations to experimental data can be seen in Figures 6.35 and 6.36. The *j* factor figure shows the correlation, a 16% error band (the maximum deviation), a 15% error band and the appropriate experimental data from this research. The *f* factor figure shows the correlation, a 13% error band (the maximum deviation), an 11% error band and the appropriate experimental data from this research.

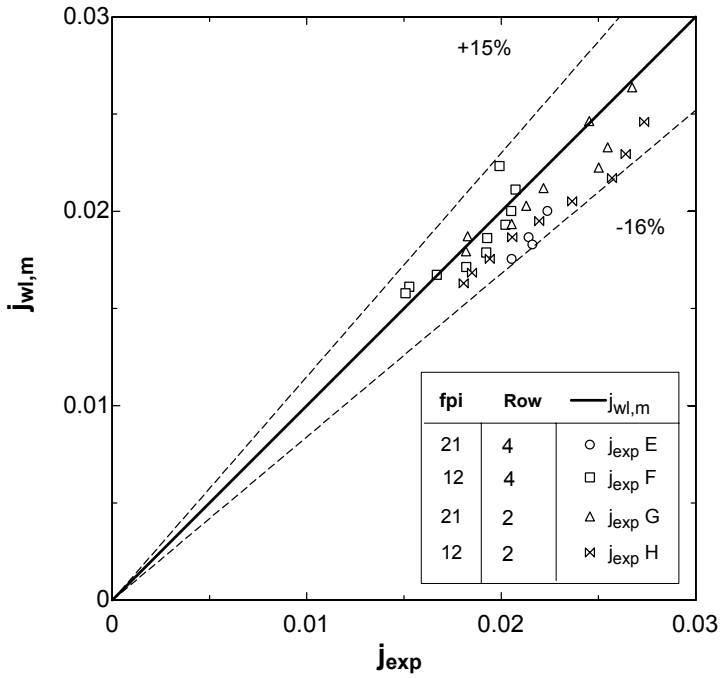

Figure 6.35. Modified Wang louvered *j* factor

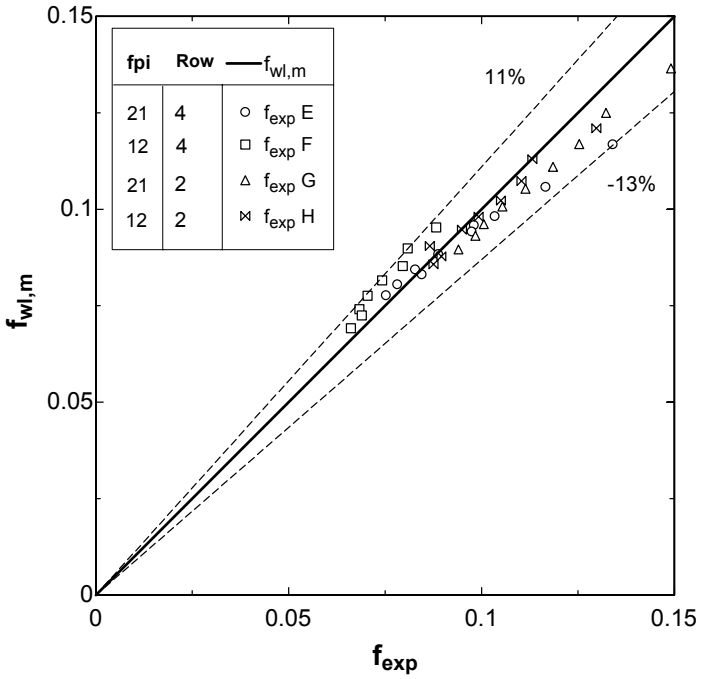

Figure 6.36. Modified Wang louvered *f* factor

The maximum deviation of each coil's experimental data as shown in Figures 6.23 - 6.36, is shown in Table 6.2. The maximum deviation is calculated for each coil and correlation combination using Equation 6.32.

$$Maximum\ deviation = \max\left(\frac{\left|j_{\text{pred}} - j_{\text{exp}}\right|}{j_{\text{exp}}}\right) \times 100\% \tag{6.32}$$

Table 6.2. Correlation and data comparison – max deviation

		Heat Transfer							Friction						
		j_r	j_m	j_{wg}	j_{wp}	j_{wk}	j_{wl}	j_{wlm}	f_r	f_m	f_{wg}	f_{wp}	$f_{wp,m}$	f_{wl}	$f_{wl,m}$
Plain Fin	A	23%	34%	31%	15%	-	-		60%	62%	49%	30%	12%	-	-
	B	6%	14%	15%	15%	-	-		49%	32%	36%	17%	20%	-	-
	C	-	25%	21%	22%	-	-		-	54%	41%	27%	8%	-	-
	D	-	10%	11%	6%	-	-		-	47%	51%	37%	21%	-	-
Louvered Fin	E	-	-	-	-	-	4%	15%	-	-	-	-		21%	13%
	F	-	-	-	-	-	30%	12%	-	-	-	-		5%	11%
	G	-	-	-	-	17%	19%	11%	-	-	-	-		27%	8%
	H	-	-	-	-	11%	6%	16%	-	-	-	-		25%	7%

The mean deviation of each coil's experimental data was calculated for each coil and correlation combination. The mean deviation is calculated using Equation 6.33, where M is the number of data points and is shown in Table 6.3.

$$Mean\ deviation = \frac{1}{M}\left(\sum_{1}^{M}\frac{\left|j_{\text{pred}} - j_{\text{exp}}\right|}{j_{\text{exp}}}\right)\times 100\% \tag{6.33}$$

Table 6.3. Correlation and data comparison – mean deviation

		Heat Transfer							Friction						
		j_r	j_m	j_{wg}	j_{wp}	j_{wk}	j_{wl}	j_{wlm}	f_r	f_m	f_{wg}	f_{wp}	$f_{wp,m}$	f_{wl}	$f_{wl,m}$
Plain Fin	A	20%	32%	29%	11%	-	-		52%	51%	39%	22%	5%	-	-
	B	3%	11%	12%	7%	-	-		43%	27%	28%	11%	12%	-	-
	C	-	18%	14%	13%	-	-		-	50%	39%	22%	3%	-	-
	D	-	8%	8%	3%	-	-		-	42%	43%	31%	13%	-	-
Louvered Fin	E	-	-	-	-	-	2%	13%	-	-	-	-		12%	4%
	F	-	-	-	-	-	16%	5%	-	-	-	-		2%	8%
	G	-	-	-	-	10%	12%	4%	-	-	-	-		25%	6%
	H	-	-	-	-	7%	4%	11%	-	-	-	-		21%	2%

CHAPTER VII

CONCLUSIONS AND RECOMMENDATIONS

VII.A: Conclusions

This study built an experimental system and developed methodology for measuring the air side heat transfer and pressure drop characteristics of finned tube heat exchangers. The *j* factor data is measured within ±11% confidence, and the *f* factor data is measured within ±5% confidence. This capability was used to test eight commercially available finned-tube heat exchangers over a range of air flow face velocity (5-12 ft/s). Data from these heat exchangers were compared with each other and the following trends were noted:

1. The 4-row coils' *j* factors were generally lower than the corresponding 2-row coils' *j* factor at low Reynolds number. The 2-row coils' *j* factor data is linear when plotted on a log-log scale versus Reynolds number while the 4-row coils' *j* factor data is curved. It was suggested by Rich (1975) that this could be due to standing vortices behind tubes reducing the effectiveness of the fins in that region.
2. The 2-row coils' *j* factor data show no dependence on fin spacing, while the *j* factor data for 4-row coils show an increase in heat transfer coefficient for an increase in the number of fins per inch.
3. The *f* factor for 4-row 21 fpi coils is significantly higher than the *f* factor for 4-row 12 fpi coils at low Reynolds number.

4. As expected, the *j* factor for louvered fin coils is significantly higher than the *j* factor for plain fin coils. The ratio of louvered *j* factor to plain *j* factor is 1.75. Also, the *f* factor for louvered fin coils is significantly higher than the *f* factor for plain fin coil. The ratio of louvered *f* factor to plain *f* factor ranged from 1.7 to 2.2.

Experimental data from heat exchangers were also compared with several correlations and the following trends were noted:

1. Rich's (1973) correlations are limited to plain fin 4-row coils. Rich's *j* factor correlation under predicts the data, with a maximum deviation of -23% from experimental data. Rich's *f* factor correlation also under predicts the data, with a maximum deviation of -60% from experimental data.
2. McQuiston's (1978) correlations are limited to plain fin coils. McQuiston's *j* factor correlation has a maximum deviation of -35% from experimental data. McQuiston's *f* factor correlation under predicts the data, with a maximum deviation of -62% from experimental data.
3. Webb's (1986) correlations are limited to plain fin coils. Webb's *j* factor correlation has a maximum deviation of -32% from experimental data. Webb's *f* factor correlation under predicts the data, with a maximum deviation of -51% from experimental data.
4. Wang's (1999) plain fin correlations have the widest parametric range of all of the plain fin coil correlations investigated. Wang's *j* factor correlation has a maximum deviation of 20% from experimental data. Wang's *f* factor correlation

under predicts the data, with a maximum deviation of -37% from experimental data.

5. A modified version of Wang's (1999) plain fin correlation for *f* factor was introduced to fit this study's data. The modified Wang *f* factor correlation has a maximum deviation of -21% from experimental data.
6. Webb's (1998) louvered correlations are limited to louvered fin one and two row coils. Webb's *j* factor correlation has a maximum deviation of 16% from experimental data. Webb did not correlate louvered *f* factor data.
7. Wang's (1998b) louvered correlations have the widest parametric range of all of the louvered fin coil correlations. Wang's *j* factor correlation has a maximum deviation of 29% from experimental data. Wang's *f* factor correlation has a maximum deviation of -27% from experimental data.
8. A modified version of Wang's (1998b) louvered fin correlation for *j* and *f* factors were introduced to fit this study's data. The modified Wang *j* factor correlation has a maximum deviation of -16% from experimental data. The modified Wang *f* factor correlation has a maximum deviation of -13% from experimental data.

VII.B: Recommendations

The experimental system was the limiting factor on the accuracy and range of the data in several ways. These are: the maximum water flow rate, the maximum power to the heater and the airflow rate range. The system should be improved to eliminate these limiting factors by employing the following recommendations:

1. The pump should be replaced with a pump capable of 20 gal/min maximum flow rate instead of the current 12 gal/min maximum. This would improve the accuracy of the air side heat transfer coefficient by reducing the waterside thermal resistance. For coil E the waterside thermal resistance was larger than the desired maximum percent of the overall thermal resistance, 30%. Also, different circuiting could be employed, since water side heat transfer coefficients are dependent on water velocity.
2. The heating power should be increased by at least 5kW, bringing the total heating capacity up to 14kW. Increasing the heating capacity would lower the effectiveness, ε, for all coils. Lowering ε would result in lowering the sensitivity of NTU to ε.
3. Although the air flow range is typical for application to residential air conditioning, the airside flow rate range should be increased especially on the lower bound. This could be accomplished by 3", 4", and 8" elliptical nozzles. The lower Reynolds number range is one of high interest and debate. Testing at lower Reynolds number would allow for clearer identification of trends like row dependence on heat transfer, where the 4-row coils j factor is generally lower than 2-row coils at lower Reynolds number.

Although the water was flushed several times a month, and sometimes more often, a more rigorous water changing regiment should be implemented, to prevent corrosion and/or fouling inside the coil's tubes. Another possibility is to use a well documented glycol solution.

Now that the experimental system and data reduction methods are in place, the system has the capacity to increase the knowledge base of present heat exchanger data and theory. Heat exchangers with defining parameters outside the parametric range of common correlations should be tested and correlated. The effect of non circular tubes could be investigated as well as the effect of various innovative fin enhancements. Independent experimental studies of this type would assist the heat exchanger designer in improving performance of finned-tube heat exchangers.

APPENDIX I
Sample Test Data

Date	5/10/2004	Pbar	29.17	RH	0.59	Coil	C	Nozzle Dia (in)	7			Max Run	90	offset	0									
Time	Water In (°F)	Water Out (°F)	Air In (°F)	Air Out (°F)	RUN	Coil DP (in H2O)	Nozzle DP (in H2O)	Water DP (psi)	Water Flowrate (gal/min)	SDEV Win	SDEV Wout	SDEV Ain	SDEV Aout	SDEV Coil	SDEV Nozz	SDEV Water	m H2O (lb/hr)	m Air (lb/hr)	Q H2O (kW)	Q Air (kW)	Error (%)	UA
12:50:05	112.2	108.1	78.9	96.2	1	0.45	2.01	5.52	12.58	0.03	0.02	0.10	0.03	0.006	0.05	0.21	6242	6256	7.49	7.86	-4.93	1169
12:51:06	112.0	108.0	78.9	96.3	2	0.45	2.01	5.51	12.58	0.01	0.01	0.13	0.02	0.006	0.04	0.22	6242	6255	7.31	7.90	-8.15	1136
12:52:06	111.9	107.9	79.6	96.1	3	0.44	2.00	5.53	12.58	0.02	0.02	0.06	0.02	0.005	0.04	0.21	6242	6242	7.31	7.48	-2.37	1180
12:53:06	111.8	107.8	79.6	96.0	4	0.44	2.00	5.52	12.58	0.03	0.03	0.40	0.04	0.005	0.04	0.21	6243	6244	7.31	7.44	-1.77	1186
12:54:06	111.8	107.8	79.6	96.0	5	0.44	2.00	5.53	12.58	0.03	0.03	0.26	0.04	0.006	0.04	0.22	6243	6244	7.31	7.44	-1.77	1186
12:55:06	111.8	107.8	79.5	96.1	6	0.44	1.99	5.53	12.58	0.04	0.04	0.24	0.04	0.007	0.05	0.26	6243	6226	7.31	7.51	-2.73	1182
12:56:06	111.8	107.8	80.0	96.1	7	0.44	2.01	5.52	12.58	0.03	0.03	0.22	0.02	0.007	0.05	0.21	6243	6258	7.31	7.32	-0.16	1208
12:57:06	111.7	107.8	79.9	96.1	8	0.44	1.99	5.51	12.58	0.02	0.02	0.16	0.03	0.006	0.04	0.23	6243	6226	7.13	7.33	-2.84	1164
12:58:06	111.8	107.8	79.8	96.1	9	0.44	2.00	5.52	12.58	0.03	0.03	0.37	0.03	0.007	0.05	0.25	6243	6242	7.31	7.39	-1.14	1198
12:59:06	111.8	107.9	79.5	96.2	10	0.44	2.00	5.53	12.58	0.03	0.03	0.12	0.03	0.006	0.04	0.21	6243	6241	7.13	7.57	-6.25	1135
13:00:06	111.8	107.9	80.1	96.3	11	0.44	1.99	5.51	12.58	0.03	0.03	0.09	0.03	0.006	0.05	0.22	6243	6224	7.13	7.33	-2.82	1170
13:01:06	111.8	107.9	80.5	96.3	12	0.44	1.99	5.52	12.56	0.01	0.01	0.51	0.02	0.006	0.04	0.22	6233	6224	7.12	7.15	-0.46	1190
13:02:06	111.9	108.0	80.0	96.3	13	0.44	1.99	5.53	12.58	0.01	0.02	0.26	0.02	0.006	0.04	0.21	6242	6224	7.13	7.37	-3.45	1158
13:03:06	112.0	108.0	80.0	96.4	14	0.44	2.00	5.53	12.58	0.01	0.02	0.34	0.02	0.006	0.04	0.22	6242	6238	7.31	7.43	-1.72	1198
13:04:06	112.0	108.1	80.4	96.4	15	0.44	1.99	5.52	12.58	0.01	0.02	0.26	0.05	0.007	0.05	0.21	6242	6222	7.13	7.24	-1.55	1176
13:05:06	112.1	108.1	80.1	96.5	16	0.44	1.99	5.53	12.58	0.01	0.02	0.41	0.01	0.006	0.04	0.24	6242	6221	7.31	7.41	-1.45	1200
13:06:06	112.0	108.1	79.8	96.5	17	0.44	1.99	5.53	12.58	0.02	0.01	0.28	0.02	0.007	0.05	0.20	6242	6221	7.13	7.55	-5.94	1142
13:07:06	112.1	108.1	80.8	96.5	18	0.44	1.99	5.52	12.58	0.03	0.04	0.18	0.04	0.006	0.05	0.23	6242	6221	7.31	7.10	2.84	1243
13:08:06	112.2	108.2	80.3	96.6	19	0.44	1.99	5.52	12.58	0.02	0.03	0.23	0.02	0.007	0.05	0.21	6242	6219	7.31	7.37	-0.83	1206
13:09:06	112.3	108.3	80.6	96.7	20	0.44	1.98	5.53	12.56	0.03	0.02	0.11	0.03	0.007	0.05	0.26	6232	6202	7.30	7.26	0.50	1216
13:10:06	112.3	108.3	79.9	96.8	21	0.44	1.98	5.53	12.58	0.01	0.02	0.21	0.03	0.006	0.04	0.23	6242	6201	7.31	7.62	-4.22	1178
13:11:06	112.3	108.4	80.9	96.8	22	0.44	1.99	5.54	12.58	0.02	0.02	0.24	0.02	0.006	0.05	0.21	6242	6216	7.13	7.19	-0.87	1187
13:12:06	112.4	108.4	80.2	96.9	23	0.44	2.00	5.53	12.58	0.03	0.03	0.19	0.02	0.006	0.05	0.20	6242	6230	7.31	7.56	-3.50	1187
13:13:06	112.4	108.4	80.8	96.8	24	0.44	1.98	5.53	12.58	0.02	0.02	0.44	0.02	0.007	0.05	0.22	6242	6201	7.31	7.21	1.29	1225
13:14:06	112.4	108.4	80.9	96.8	25	0.44	2.00	5.54	12.58	0.01	0.02	0.19	0.01	0.007	0.05	0.23	6242	6232	7.31	7.21	1.40	1229
13:15:06	112.4	108.4	80.2	96.8	26	0.44	1.98	5.52	12.58	0.01	0.02	0.12	0.02	0.006	0.04	0.22	6242	6201	7.31	7.48	-2.39	1189
13:16:06	112.4	108.4	80.5	96.8	27	0.44	2.00	5.51	12.58	0.02	0.02	0.39	0.02	0.005	0.04	0.21	6242	6232	7.31	7.39	-1.06	1204
13:17:06	112.4	108.5	80.8	96.9	28	0.44	1.99	5.53	12.58	0.02	0.02	0.24	0.02	0.006	0.04	0.21	6242	6215	7.13	7.28	-2.12	1176
13:18:06	112.5	108.5	80.2	96.9	29	0.44	2.00	5.53	12.58	0.01	0.02	0.41	0.02	0.006	0.04	0.22	6242	6230	7.31	7.56	-3.51	1181
13:19:06	112.5	108.5	80.9	97.0	30	0.44	1.99	5.52	12.58	0.01	0.03	0.11	0.03	0.006	0.05	0.22	6242	6213	7.31	7.28	0.45	1224
13:20:06	112.6	108.6	81.2	97.0	31	0.44	1.99	5.54	12.58	0.02	0.02	0.20	0.02	0.006	0.04	0.23	6241	6213	7.31	7.14	2.29	1237
13:21:06	112.6	108.6	80.9	97.0	32	0.44	1.99	5.52	12.58	0.02	0.02	0.28	0.01	0.006	0.04	0.21	6241	6213	7.31	7.28	0.44	1218
13:22:06	112.5	108.5	80.9	96.9	33	0.44	1.98	5.52	12.58	0.01	0.03	0.24	0.04	0.007	0.05	0.23	6242	6199	7.31	7.21	1.30	1225
13:23:06	112.6	108.6	81.0	97.0	34	0.44	1.98	5.52	12.56	0.02	0.02	0.06	0.02	0.006	0.05	0.23	6232	6198	7.30	7.21	1.15	1223
13:24:06	112.6	108.6	81.2	97.1	35	0.44	1.98	5.53	12.58	0.02	0.02	0.14	0.02	0.006	0.05	0.23	6241	6196	7.31	7.17	1.93	1238
13:25:06	112.6	108.6	81.1	97.1	36	0.44	1.99	5.52	12.56	0.02	0.01	0.17	0.02	0.006	0.04	0.23	6232	6212	7.30	7.23	0.91	1227
13:26:06	112.6	108.6	80.5	97.1	37	0.44	1.97	5.52	12.58	0.03	0.02	0.15	0.02	0.006	0.04	0.21	6241	6181	7.31	7.46	-2.09	1197
13:27:06	112.7	108.7	80.7	97.2	38	0.44	1.99	5.52	12.58	0.02	0.02	0.16	0.02	0.005	0.04	0.21	6241	6210	7.31	7.45	-1.98	1200
13:28:06	112.8	108.8	81.3	97.2	39	0.44	1.99	5.52	12.56	0.03	0.03	0.13	0.03	0.006	0.05	0.23	6231	6210	7.30	7.18	1.54	1227
13:29:06	112.8	108.8	80.6	97.3	40	0.44	1.99	5.53	12.58	0.02	0.02	0.30	0.03	0.007	0.05	0.20	6241	6209	7.31	7.54	-3.20	1188
13:30:06	112.9	108.9	80.7	97.4	41	0.44	1.99	5.53	12.58	0.02	0.02	0.18	0.01	0.005	0.04	0.20	6241	6208	7.31	7.54	-3.19	1188
13:31:06	113.0	109.0	80.9	97.5	42	0.44	1.98	5.54	12.58	0.03	0.03	0.20	0.04	0.007	0.05	0.22	6241	6190	7.31	7.48	-2.31	1196
13:32:06	113.0	109.0	80.7	97.5	43	0.44	1.99	5.53	12.58	0.01	0.03	0.13	0.04	0.006	0.05	0.19	6241	6206	7.31	7.58	-3.79	1182
13:33:06	113.1	109.1	81.0	97.6	44	0.44	1.98	5.53	12.58	0.01	0.03	0.30	0.03	0.006	0.04	0.24	6241	6189	7.31	7.47	-2.29	1196
13:34:06	113.0	109.0	81.3	97.5	45	0.44	1.98	5.52	12.58	0.03	0.01	0.23	0.02	0.005	0.04	0.21	6241	6190	7.31	7.30	0.14	1220
13:35:06	113.1	109.1	81.0	97.6	46	0.44	1.98	5.53	12.56	0.02	0.02	0.28	0.04	0.005	0.04	0.22	6231	6189	7.30	7.47	-2.46	1193
13:36:06	113.2	109.2	81.3	97.7	47	0.44	1.98	5.52	12.58	0.02	0.01	0.17	0.02	0.006	0.04	0.23	6241	6188	7.31	7.38	-1.06	1207
13:37:06	113.2	109.2	81.0	97.7	48	0.44	1.98	5.52	12.61	0.02	0.01	0.08	0.03	0.007	0.05	0.25	6255	6188	7.32	7.52	-2.65	1194

NTU	ε	Var Win	Var Wout	Var Ain	Var Aout	Win Min	Win Max	TR Win	TR Wout	TR Ain	TR Aout	TR UA	Min D TRUA	Max D TRUA	Δ TRUA	Win AVG	Wout AVG	Ain AVG	Aout AVG	m H20 AVG	m Air AVG	DP AVG
0.75	0.4951	0.1	0.1	0.3	0.1	113.2	113.3	0.0	0.0	0.0	0.0	0.0										
0.73	0.4861	0.0	0.0	0.4	0.0	113.0	113.0	0.0	0.0	0.0	0.0	0.0										
0.76	0.499	0.1	0.1	0.2	0.1	112.9	112.9	0.0	0.0	0.0	0.0	0.0										
0.77	0.5005	0.1	0.1	0.9	0.1	112.7	112.9	0.0	0.0	0.0	0.0	0.0										
0.77	0.5005	0.1	0.1	0.8	0.1	112.8	112.9	0.0	0.0	0.0	0.0	0.0										
0.77	0.5003	0.1	0.1	0.7	0.1	112.8	112.9	0.0	0.0	0.0	0.0	0.0										
0.78	0.5055	0.1	0.1	0.7	0.1	112.8	112.9	0.0	0.0	0.0	0.0	0.0										
0.75	0.4954	0.1	0.1	0.5	0.1	112.7	112.8	0.0	0.0	0.0	0.0	0.0										
0.77	0.5036	0.1	0.1	0.9	0.1	112.7	112.8	0.0	0.0	0.0	0.0	0.0										
0.73	0.4866	0.1	0.1	0.3	0.1	112.8	112.9	0.0	0.0	0.0	0.0	0.0										
0.76	0.497	0.1	0.1	0.3	0.1	112.8	112.9	111.8	107.8	79.6	96.1	1174.5										
0.77	0.5025	0.1	0.0	1.4	0.0	112.8	112.9	111.8	107.8	79.8	96.1	1179.9										
0.75	0.4939	0.0	0.0	0.9	0.1	112.9	113.0	111.8	107.8	79.8	96.2	1177.7										
0.77	0.5038	0.0	0.1	0.9	0.1	113.0	113.0	111.8	107.9	79.9	96.2	1178.9										
0.76	0.4986	0.0	0.1	0.8	0.1	113.0	113.1	111.8	107.9	80.0	96.2	1177.9										
0.78	0.5052	0.0	0.0	1.0	0.0	113.1	113.1	111.9	107.9	80.0	96.3	1179.7										
0.74	0.4896	0.1	0.0	0.7	0.0	113.0	113.1	111.9	107.9	80.0	96.3	1173.1										
0.81	0.5163	0.1	0.1	0.6	0.1	113.1	113.2	111.9	108.0	80.1	96.4	1181.0										
0.78	0.5068	0.1	0.1	0.6	0.1	113.2	113.2	112.0	108.0	80.1	96.4	1181.8										
0.79	0.5105	0.1	0.1	0.3	0.1	113.2	113.3	112.0	108.1	80.2	96.5	1189.9										
0.77	0.5005	0.0	0.0	0.6	0.1	113.3	113.3	112.1	108.1	80.2	96.5	1190.7										
0.77	0.502	0.0	0.1	0.7	0.1	113.4	113.4	112.1	108.2	80.3	96.6	1190.4										
0.77	0.5011	0.1	0.1	0.6	0.0	113.4	113.5	112.2	108.2	80.3	96.6	1193.3										
0.80	0.5129	0.0	0.0	1.1	0.1	113.4	113.4	112.2	108.2	80.4	96.7	1196.0										
0.79	0.5119	0.1	0.1	0.6	0.0	113.4	113.5	112.2	108.3	80.4	96.7	1201.3										
0.77	0.5035	0.0	0.1	0.4	0.0	113.4	113.4	112.3	108.3	80.4	96.7	1200.2										
0.78	0.5056	0.0	0.1	1.0	0.0	113.4	113.5	112.3	108.3	80.5	96.7	1206.4										
0.76	0.4989	0.1	0.0	0.8	0.0	113.4	113.5	112.3	108.4	80.5	96.8	1199.7										
0.76	0.4995	0.0	0.0	1.1	0.0	113.5	113.5	112.4	108.4	80.5	96.8	1197.2										
0.79	0.5118	0.0	0.1	0.4	0.1	113.5	113.6	112.4	108.4	80.5	96.9	1198.0										
0.80	0.5149	0.0	0.0	0.6	0.1	113.6	113.7	112.4	108.5	80.7	96.9	1203.9	-1.28	1.19	2.47	112.1	108.1	80.2	96.5	6241.63	6227.37	0.44
0.79	0.5102	0.1	0.1	0.7	0.0	113.6	113.7	112.5	108.5	80.7	96.9	1207.0	-1.05	1.22	2.27	112.1	108.2	80.3	96.5	6241.60	6225.93	0.44
0.80	0.513	0.0	0.1	0.7	0.1	113.6	113.6	112.5	108.5	80.7	96.9	1210.8	-1.36	1.41	2.77	112.1	108.2	80.3	96.6	6241.57	6224.53	0.44
0.79	0.5122	0.1	0.1	0.2	0.1	113.6	113.7	112.5	108.5	80.8	96.9	1210.6	-1.36	1.29	2.65	112.2	108.2	80.3	96.6	6241.57	6223.10	0.44
0.81	0.5163	0.0	0.1	0.5	0.1	113.6	113.7	112.5	108.5	80.8	97.0	1211.5	-1.59	1.22	2.81	112.2	108.2	80.4	96.6	6241.20	6221.57	0.44
0.80	0.5126	0.1	0.0	0.7	0.0	113.6	113.6	112.5	108.6	80.9	97.0	1215.3	-1.56	1.41	2.97	112.2	108.3	80.4	96.7	6241.13	6219.97	0.44
0.78	0.5065	0.1	0.1	0.6	0.1	113.6	113.7	112.6	108.6	80.9	97.0	1214.6	-2.08	1.38	3.46	112.3	108.3	80.5	96.7	6240.77	6219.50	0.44
0.78	0.5056	0.0	0.0	0.5	0.0	113.8	113.8	112.6	108.6	80.9	97.0	1217.0	-1.52	1.48	3.00	112.3	108.3	80.5	96.7	6240.70	6216.93	0.44
0.80	0.5126	0.1	0.1	0.4	0.1	113.8	113.9	112.6	108.6	81.0	97.1	1221.6	-1.53	1.78	3.32	112.3	108.4	80.5	96.8	6240.63	6216.40	0.44
0.77	0.5026	0.1	0.1	0.9	0.1	113.8	113.9	112.6	108.7	80.9	97.1	1218.0	-1.00	1.33	2.34	112.4	108.4	80.6	96.8	6240.23	6215.33	0.44
0.77	0.5026	0.0	0.1	0.5	0.0	113.9	114.0	112.7	108.7	80.9	97.1	1213.1	-0.99	0.88	1.86	112.4	108.4	80.6	96.8	6240.17	6214.27	0.44
0.78	0.5055	0.1	0.1	0.6	0.1	114.0	114.1	112.7	108.7	80.9	97.2	1210.9	-1.03	0.68	1.70	112.4	108.5	80.6	96.9	6240.10	6213.73	0.44
0.77	0.5011	0.0	0.1	0.4	0.1	114.1	114.1	112.8	108.8	80.9	97.2	1206.6	-0.85	0.60	1.45	112.5	108.5	80.6	96.9	6240.37	6212.60	0.44
0.78	0.5055	0.0	0.1	1.0	0.1	114.1	114.1	112.8	108.8	80.9	97.3	1203.9	-0.62	0.59	1.21	112.5	108.5	80.7	97.0	6240.33	6212.00	0.44
0.79	0.5118	0.1	0.0	0.7	0.1	114.0	114.1	112.8	108.9	80.9	97.3	1202.1	-0.30	0.54	0.85	112.5	108.6	80.7	97.0	6240.30	6210.37	0.44
0.78	0.5047	0.0	0.1	0.7	0.1	114.2	114.2	112.9	108.9	80.9	97.4	1198.7	-0.50	0.88	1.38	112.6	108.6	80.7	97.0	6240.27	6209.30	0.44
0.79	0.5087	0.1	0.1	0.5	0.1	114.2	114.3	113.0	109.0	80.9	97.4	1199.7	-0.60	0.64	1.23	112.6	108.6	80.8	97.1	6239.90	6208.23	0.44
0.78	0.5052	0.1	0.0	0.3	0.1	114.2	114.3	113.0	109.0	81.0	97.5	1199.1	-0.51	0.97	1.49	112.6	108.7	80.8	97.1	6239.87	6207.13	0.44

REFERENCES

ACEEE, 2004. American Council for an Energy-Efficient Economy, http://www.aceee.org/press/0404seer13.htm

ARI. 2001. ARI Standard 410-2001, Forced-circulation Air cooling and Air Heating coils. Arlington, VA. Air-Conditioning and Refrigeration Institute.

ASHRAE. 1987. *ANSI/ASHRAE Standard 41.2-1987, Standard methods for laboratory air-flow measurement.* Atlanta: American Society of Heating, Refrigeration and Air-Conditioning Engineers, Inc.

Energy Information Administration (EIA), AEO2004 (Annual Energy Outlook) February 2004 pg 80.

ESDU, 1991. Effectiveness-NTU Relationships for the Design and Performance Evaluation of Two-Stream Heat Exchangers. Engineering Science Data Unit86018 with Amendment A, July 1991, pp.920107, ESDU International plc, London.

Garimella, S., Coleman, J.W., Wicht, A., 1997. Tube and Fin Geometry Alternatives for the Design of Absorption-Heat-Pump Heat Exchangers. Enhanced Heat Transfer, Vol. 4, pp. 217-235.

Incropera, F.P. and DeWitt, D.P., 1996. Fundamentals of Heat and Mass Transfer, 4th Edition, John Wiley & Sons, New York, N.Y..

Kays, W. M. and London, A.L. 1984. Compact Heat Exchangers, 3rd Edition. McGraw Hill, New York, N.Y.

Klein, S.A. (2003). Engineering Equation Solver, F-Chart Software, Professional Version 6.811.

McAdams, W. H., 1954. Heat Transmission, 3rd Edition. McGraw Hill, New York, N.Y.

McQuiston, F.C., 1978. Correlation of heat, mass and momentum transport coefficients for plate-fin-tube heat transfer surfaces with staggered tubes. ASHRAE Transactions, Vol. 84, No. 1, pp. 294-309.

McQuiston, F.C., 1981. Finned Tube Heat Exchangers: State of the Art for the Airside. ASHRAE Transactions, Vol. 87, pp. 1077-1085.

Perrotin, T. and Clodic, D., 2003. Fin efficency calculation in enhanced fin-and-tube heat exchangers in dry conditions. Proceedings of the 21st International Congress of Refrigeration, Paper #ICR0026, August 2003.

Rich, D.G. 1973. The effect of fin spacing on the heat transfer and friction performance of multi-row, smooth plate fin-and-tube heat exchangers. ASHRAE Transactions, Vol. 79, No.2, pp.135-145.

Rich, D.G. 1975. The effect of the number of tube rows on heat transfer performance of smooth plate fin-and-tube heat exchangers. ASHRAE Transactions, Vol. 81, pp. 307-317.

Sheffield J. W., Wood, R. A., Sauer Jr., H. J., 1989. Experimental investigation of thermal conductance of finned tube contacts. Experimental Thermal and Fluid Science, Vol. 2, Issue 1, pp. 107-121.

Stewart, S.W., 2003. Enhanced Finned-Tube Condenser Design and Optimization. PhD. Dissertation.

Wang, C.C. 2000a. Recent Progress on the Air-side Performance of fin-and-tube heat exchangers. Int. J. of Heat Exchangers, Vol. 1, pp. 49-76.

Wang, C.C., Chi, K.Y., Chang, C.J., 1999. Heat transfer and friction characteristics of plain fin-and-tube heat exchangers, part II: Correlation. Int. J. of Heat and Mass Transfer, Vol. 43, pp. 2693-2700.

Wang, C.C., Chi, K.Y., Chang, C.J., 1998a. Some aspects of plate fin-and-tube heat exchangers: with and without louvers. Enhanced Heat Transfer, Vol. 6, pp. 357-368.

Wang, C.C., Chi, K.Y., Chang, Y.J., Chang, Y.P., 1998c. A comparison study of compact plate fin-and-tube heat exchangers. ASHRAE Transactions, #TO-98-3-3.

Wang, C.C., Lee, C.J., Chang, C.T., Lin, S.P., 1998b. Heat transfer and friction correlation for compact louvered fin-and-tube heat exchangers. . Int. J. of Heat and Mass Transfer, Vol. 42, pp. 1945-1956.

Wang, C.C., Webb, R.L., Chi, K.Y., 2000b. Data reduction for air-side performance of Fin-and-Tube Heat Exchangers. Experimental Thermal and Fluid Science, Vol. 21, pp. 218-226.

Webb, R.L. and Gray, D.L., 1986. Heat transfer and friction correlations for plate finned-tube heat exchangers having plain fins. Proceedings of 8th Heat transfer Conference, 1986, pp. 2745-2750.

Webb, R.L. and Kang, H.C., 1998. Performance comparison of enhanced fin geometries used in fin-and-tube heat exchangers. Heat Transfer 1998, Proceedings of the 11th IHTC, Vol. 6, pp.273-278.

Wilson, E.E., 1915. A Basis for Rational Design of Heat Transfer Apparatus. ASME Transactions, Vol. 37, pp 47-69.

Zukauskas, A. and Ulinskas, R., 1998. Banks of plain and finned tubes, Heat Exchanger Design Handbook, G.F. Hewitt Edition, Begell House, Inc., New York, pp. 2.2.4-1 – 2.2.4-17.